ADDIS ABABA UNIVERSITY

ADDIS ABABA INSTITUTE OF TECHNOLOGY

SCHOOL OF CIVIL AND ENVIRONMENTAL ENGINEERING

A NONLINEAR INELASTIC NUMERICAL ANALYSIS TOOL for CIRCULAR CONCRETE-FILLED STEEL TUBULAR COLUMNS and BEAM-COLUMNS

A Thesis in Structural Engineering

By Kusse Gelebo

July 2019

Addis Ababa, Ethiopia

A Thesis

Submitted in Partial Fulfillment of the Requirements for the Degree of Master of Science

The undersigned have examined the thesis entitled '**A Nonlinear Inelastic Numerical Analysis Tool for Circular Concrete-Filled Steel Tubular Columns and Beam-Columns**' presented by **Kusse Gelebo**, a candidate for the degree of **Master of Science** and hereby certify that it is worthy of acceptance.

Dr. Ing. Adil Zekaria		
Advisor	Signature	Date
Dr. Ing. Girma Zerayohannes		
Internal Examiner	Signature	Date
Dr. Abraham Gebre		
External Examiner	Signature	Date
Dr. Henok Fikre		
Chair person	Signature	Date

UNDERTAKING

I certify that research work titled "**A Nonlinear Inelastic Numerical Analysis Tool for Circular Concrete-Filled Steel Tubular Columns and Beam-Columns**" is my own work. The work has not been presented elsewhere for assessment. Where material has been used from other sources it has been properly acknowledged/referred.

_____

Kusse Gelebo

ABSTRACT

The overall objective of this study is to develop fast, simple and accurate numerical analysis tool to investigate the non-linear inelastic response of circular CFT columns and beam-columns subjected to eccentric compressive loading. This thesis presents a systematic development of new numerical models for the nonlinear inelastic analysis of circular CFT columns and slender beam-columns. In the proposed numerical model, the inelastic behavior of column cross-sections is simulated using the accurate fiber element method. Accurate constitutive laws for confined concrete are implemented in the models. The effects of steel tube local buckling are taken into account in the models. Axial load-moment-curvature relationships computed from the fiber analysis of sections are used in the column stability analysis to determine equilibrium states. Efficient computational algorithms based on Secant's method are developed to obtain nonlinear solutions. Analysis procedures are proposed for predicting load-deflection and axial load-moment interaction curves for circular CFT columns and slender beam-columns under eccentric compression. The numerical model was used to develop fast, easy and user-friendly MS Excel spreadsheet analysis tool using visual basic programmed Macros to enhance the applicability of the study. A total of more than 200 experimental tests of circular concrete-filled steel tube columns and beam-columns have been used to validate the developed numerical approach by comparing the maximum load capacity, axial load-axial strain/shortening, and axial load- deflection response curves. The developed tool was utilized to undertake extensive parametric studies on the fundamental behavior of circular CFT slender columns covering a wide range of parameters. The proposed numerical approach is capable of tracing the complete circular CFT columns performance including the challenging post-peak inelastic softening response. Despite rich features of the proposed numerical scheme, the computational time is highly efficient and suitable for practical design and analysis of circular concrete-filled steel tube columns and beam-columns using the tool. Good agreements between the numerical results with experiments have proved that the proposed numerical scheme is very efficient for predicting both the maximum load capacity and the axial load - deflection response of the stub and slender circular concrete-filled steel tube composite columns and beam-columns. The numerical model analysis has successfully captured the axial load-strain and axial load-deflection response along with important features.

Keywords: *Nonlinear, Inelastic, Numerical, Circular CFT, Confinement, Local Buckling, Slender, Beam-Column, Eccentric Compression*

ACKNOWLEDGMENTS

First of all, I would like to express my deep gratitude and sincere appreciation to my instructor and thesis advisor, Dr.-Ing Adil Zekaria, for his productive academic guidance, very kind assistance and strong support. I am truly thankful for his invaluable time, encouragement and attention to listen and discuss issues with me. In addition to his great academic contribution, his positive personalities exceptionally inspire my life as well as my future academic profession. I am very thankful for the unique opportunity and the privilege of working on this remarkable thesis project that has become one of the best experiences in my professional career and my personal life.

My profound thanks and grateful gratitude go to my instructor, Dr.-Ing Girma Zerayohannes, for his support, constructive advice and valuable time. His insight and fruitful discussion have given me a better understanding of the basic concepts of the course matter.

I would like to extend my appreciation to all committee members for reviewing and giving constructive comments to qualify this thesis; lecturers and instructors at Institute of Technology of Addis Ababa University for providing me engineering knowledge to conduct my researches.

The MSc program supported by the ministry of education is gratefully acknowledged. I wish to thank all coordinators and administrative staffs at Madda Walabu University for their kind facilitation and friendly environment. I extend my sincere appreciation to my colleagues in the Department of Civil and Environmental Engineering at the Addis Ababa Institute of Technology who have made my time in Addis Ababa memorable at a personal level. I am convinced that the experience I had with the Addis Ababa Technology Institute and fellow students will result in many futures and productive academic interactions.

My special appreciation was to Birhan Assefa, for her remarkable patience, sweet encouragement, unwavering support, unconditional love, and warming care. Undoubtedly, none of this would have been possible without her. I also would like to thank my brothers, sisters, and friends for their prayers and encouragement.

It is my great honor to specially dedicate my MSc thesis to my beloved parents, Gelebo Bancho and Roppa Karafo, who always love, advice, encourage and support me. They own my endless gratitude and deepest love.

Above all, I would like to thank the living God, Jesus Christ, with all my heart and soul for being my Lord and Savior, and for every blessing He has given me. He granted my prayers and never let me down in all circumstances I have been through.

TABLE OF CONTENTS

ABSTRACT ..... **iii**
ACKNOWLEDGMENTS ..... **iv**
TABLE OF CONTENTS ..... **v**
LIST OF TABLES ..... **viii**
LIST OF FIGURES ..... **ix**
ABBREVIATIONS ..... **xi**
NOTATION ..... **xii**
CHAPTER ONE **1**
INTRODUCTION **1**
1.1 General background 1
1.1.1 Classification of composite columns 2
1.1.2 Advantages of composite columns 3
1.1.3 Concrete-filled steel tubes (CFT) 4
1.1.4 Advantages of using CFT columns 5
1.2 Statement of the problem 5
1.3 Objectives 6
1.4 Methodology 6
1.5 Scope of the study 7
1.5.1 Basic assumptions 7
1.6 Significance of the study 7
1.7 Thesis outlines 8
CHAPTER TWO **9**
LITERATURE REVIEW **9**
2.1 Introduction 9
2.1.1 Typical CFT cross sections 9
2.1.2 Applications of CFT members in the construction industry 11
2.2 The behavior of Concrete-Filled Steel Tubes 14
2.2.1 Component behavior 15
2.2.2 Axially Loaded CFT Columns 17
2.2.3 Combined Axial Load and Bending (CFT Beam-Columns) 22
2.3 Summary of Previous Researches on CFT Members 24
2.3.1 Experimental Research 24

2.3.2 Analytical Research 25
CHAPTER THREE 26
ANALYSIS AND DESIGN OF CFT MEMBERS with BC4 and AISC CODES 26
3.1 Analysis and Design of CFT Members According to BC4: 2015 (an Extension to EC4 Method for CFT with High Strength Materials) 26
3.1.1 About BC4: 2015 26
3.1.2 General limitations of the guide 26
3.1.3 Material Compatibility between Steel Grade and Concrete Class 28
3.1.4 Local Buckling 29
3.1.5 The resistance of Cross Section to Compression 30
3.1.6 The resistance of Cross Section to Combined Compression and Bending 31
3.1.7 The resistance of Members *to Compression* 35
3.1.8 The resistance of Members to Combined Compression and Uniaxial Bending 39
3.1.9 The resistance of Members to Combined Compression and Biaxial Bending 41
3.2 Analysis and Design of CFT Members According to AISC 42
3.2.1 Buckling load by the AISC Specifications 42
3.2.2 P-M interaction diagram by the AISC Specifications 48
CHAPTER FOUR 53
NONLINEAR INELASTIC NUMERICAL ANALYSIS of CIRCULAR CFT COLUMNS and BEAM-COLUMNS 53
4.1 Introduction 53
4.2 Material constitutive models 54
4.2.1 Stress-strain relation for confined concrete in CFT 54
4.2.2 The behavior of concrete in tension 57
4.2.3 Stress-strain relation for steel 58
4.3 Analysis of cross-sections 60
4.3.1 Fiber - Section based analysis 60
4.3.2 Strain and stress distributions 61
4.3.3 Cross-section Discretisation 62
4.3.4 Cross-section capacities 63
4.3.5 Secant's method algorithms 64
4.3.6 Cross-section’s axial load–moment-curvature relationships 64

4.4 Structural system (Beam-Column member analysis) 67
4.4.1 Member Load–deflection analysis 68
4.4.2 Axial load–moment interaction strength analysis 72
4.5 Developing the MS Excel spreadsheet analysis tool 72
4.6 Verification of the numerical model 73
4.6.1 Short Column ultimate strength capacity and axial load-strain curves 74
4.6.2 Beam-column ultimate strength and Load- Deflection curves 76
4.6.3 Evaluation of various numerical models 80
4.7 Parametric studies 81
4.7.1 Effects of D/t ratio 81
4.7.2 Effects of concrete compressive strengths 83
4.7.3 Effects of steel yield strengths 84
4.7.4 Effects of L/D ratio 86
4.7.5 Effects of eccentricity ratio 87
4.8 Concluding Remarks 88
CHAPTER FIVE 89
CONCLUSIONS AND RECOMMENDATIONS 89
5.1 Summary 89
5.2 Concluding Remarks 89
5.3 Recommendations for Future Research 90
REFERENCES 92
APPENDICES 97
APPENDIX A: VERIFICATION RESULTS 97
APPENDIX B: Visual Basic for Application (VBA): User defined function Codes 115
APPENDIX C: Worked Example 125

LIST OF TABLES

Table 3-1: Compatibility of steel and concrete materials for CFT columns 29
Table 3-2: Maximum values (d/t), (h/t) for local buckling.....30
Table 3-3: Imperfect factors for buckling curves 35
Table 3-4: Buckling curves and member imperfections for CFT composite columns.....36
Table 3-5: Buckling lengths for composite columns.....37
Table 3-6: Equivalent moment factor β.....41
Table A-1: Material and Geometric Properties – CCFT Validation Set – Short Colum..97
Table A-2: Comparison – CCFT Validation Set – Short Column.....100
Table A-3: Material and Geometric Properties – CCFT Validation Set – Beam-Column 104
Table A-4: Comparison – CCFT Validation Set –Beam-Column.....108
Table A-5: Material and Geometric Properties – for various CCFT models Evaluation112
Table A-6: Comparison between the proposed model and various CCFT numerical models.....113

LIST OF FIGURES

Figure 1-1: Some possible cross-sections configurations in composite columns.....2
Figure 1-2: Types of concrete-filled steel tubular cross sections 4
Figure 2-1: Typical concrete-filled steel tubular cross sections 9
Figure 2-2: Inclined, tapered and curved CFT columns 10
Figure 2-3: CFT hybrid structural systems for high-rise buildings 11
Figure 2-4: CFT used in bridges 12
Figure 2-5: Subway stations using CFT columns 13
Figure 2-6: A CFDST pole 14
Figure 2-7: Schematic failure modes of hollow steel tube, concrete and CFT stub columns 15
Figure 2-8: Axial compressive behavior of CFT stub column 16
Figure 2-9: Longitudinal and circumferential stresses in the steel tubes.....17
Figure 3-1: Types of double symmetric CFT sections 27
Figure 3-2: Prevention of local buckling of the outer tube of CFT columns using plate stiffeners 30
Figure 3-3: Interaction curve for combined compression and bending 32
Figure 3-4: Simplified interaction curve and corresponding stress distributions 32
Figure 3-5: Buckling lengths for composite columns.....37
Figure 3-6: Amplifications for moments from first-order analysis and member imperfection 40
Figure 3-7: Interaction curves for the design of combined compression and biaxial bending 42
Figure 3-8: Theoretical and suggested K factors for different BCs (AISC Commentary, 2005) 46
Figure 3-9: column curve by the AISC (2010) Specifications 47
Figure 3-10: plastic stress distribution method.....48
Figure 3-11: strain compatibility method 49
Figure 3-12: P-M interaction diagrams obtained with the plastic stress method and strain compatibility method 49
Figure 3-13: Reduction by the AISC (2005) Specifications on the P-M cross-section by the stability effects factor χ to get the P-M strength on composite beam-columns 52
Figure 3-14: P-M interaction diagram for composite cross-sections (stocky columns) and beam-columns (reduced by stability effects) by the AISC (2005) Specifications.....52
Figure 4-1: General stress-strain curve model for confined concrete in Circular CFT columns 58
Figure 4-2: Typical stress-strain curve model for steel in CFT columns with local buckling and residual stress effects 59
Figure 4-3: Cross-section strain and stress distributions under axial compression, uni-axial bending and combined axial compression and uni-axial bending 62
Figure 4-4: Cross-section Discretization 63
Figure 4-5: Flowchart for determining the Axial load-Moment-Curvature curve for circular CFT columns 66

Figure 4-6: Pin-ended and concentrically loaded imperfect column 67
Figure 4-7: Pin-ended beam–column model 69
Figure 4-8: Flowchart for determining the Axial load-Deflection curve for circular CFT columns 71
Figure 4-9: The input-output user-friendly interface of the developed tool 73
Figure 4-10: Comparison of predicted and experimental axial load-strain curves for some samples of circular CFT short columns 76
Figure 4-11: Comparison of predicted and experimental load-deflection curves for some samples of circular CFT columns and beam-columns 80
Figure 4-12: Effects of D/t ratio on the axial load-strain behavior of circular CFT columns 81
Figure 4-13: Effects of D/t ratio on the axial load-deflection and axial load-moment interaction curves for circular CFT beam-columns 82
Figure 4-14: Effects of concrete compressive strength on the axial load-strain behavior of circular CFT columns 83
Figure 4-15: Effects of concrete compressive strength on the axial load-deflection and axial load-moment interaction curves for circular CFT beam-columns 84
Figure 4-16: Effects of steel yield strength on the axial load-strain behavior of circular CFT columns 85
Figure 4-17: Effects of steel yield strength on the axial load-deflection and axial load-moment interaction curves for circular CFT beam-columns 85
Figure 4-18: Effects of L/D ratio on the axial load-deflection and axial load-moment interaction curves for circular CFT beam-columns 87
Figure 4-19: Effects of eccentricity ratio on the axial load-deflection curves for circular CFT beam-columns 87

ABBREVIATIONS

AISC	American Institute of the Steel Construction
ACI	American Concrete Institute
EC	Eurocode
AIJ	Architectural Institute of Japan
RC	Reinforced concrete
SRC	Steel reinforced concrete, encased steel by concrete or embedded steel into concrete
CFT	Concrete-filled steel tube
CCFT	Circular CFT
CFDST	Concrete-filled Double skin steel tubes
RCFT	Rectangular CFT
HSS	Hollow structural section
FEA	Finite element analysis
FEM	Finite element method
PNA	Plastic neutral axis
ENA	Elastic neutral axis
LRFD	Load and resistance factor design
ASD	Allowable Strength Design
ULS	Ultimate limit state
SCM	Strain Compatibility Method
DAM	Direct Analysis Method
VBA	Visual Basic for Application

NOTATION

χ	P_n/P_o ratio
δ	Small or local deflections
Δ	Large or global deflections
ε	Strain
ε_c	Concrete strain
ε_{co}	Concrete strain at f_c'
ε_{cc}	Confined concrete strain at f_{cc}'
ε_{cu}	Ultimate concrete strain
ε_{lb}	Compressive strain related to the initiation of the steel local buckling
ϕ	Cross-section curvature
Φ	Strength reduction factor by AISC or ACI
λ	Slenderness parameter related to flexural buckling
ρ	Total steel ratio in the cross-section
ρ_s	Structural steel ratio in the cross-section
σ	Normal stress
f_c	Concrete strength as a function of the strain (ε)
f_c'	Compressive strength of a 28 days concrete cylinder
f_{cc}'	Compressive strength of confined concrete
f_{cu}	Ultimate concrete strength linked to ε_{cu}
t	Thickness of steel plate or tube
A	Gross cross-section area
A_c	Concrete cross-section area
A_s	Steel cross-section area
A_λ	Point A on the P- M diagram reduced by χ
C_λ	Point C on the P-M diagram reduced by χ
D	External diameter of a circular tubular cross-section

E_c	Concrete modulus of elasticity
E_s	Steel modulus of elasticity
E_{eff}	Effective modulus of elasticity on a composite element
E_m	Modified or effective flexural stiffness of a composite element
EI_c	Concrete contribution to the flexural stiffness of a composite element
EI_s	Steel contribution to the flexural stiffness of a composite element
EI_{eff}	Effective flexural stiffness of a composite element
F_c	Block stress for the concrete in compression
F_y	Yield stress of the steel
F_r	Residual stress in the steel
I_c	Concrete cross-section moment of inertia
I_s	Steel cross-section moment of inertia
I_{eff}	Effective composite cross-section moment of inertia
K	Effective length coefficient
KL	Effective length of an element
L	Length of an element
M	Bending moment
M_o	Pure bending strength of the composite cross-section (equal M_B)
M_u	Ultimate flexural demand
M_B	Flexural strength at the point B on the P-M interaction diagram (equal to M_o)
M_C	Flexural strength at the point C on the P-M interaction diagram
M_D	Flexural strength at the point D on the P-M interaction diagram
M_E	Flexural strength at the point E on the P-M interaction diagram
M_1	Moment from a first order analysis
M_2	Moment from a second order analysis
P	Axial force in compression (negative value if tension)

P_e	Euler or elastic critical load
P_{cr}	Critical load
P_n	Nominal compressive strength of the element
P_{exp}	Experimental compressive strength
P_{num}	Numerical compressive strength
P_o	Nominal compressive strength of the cross-section or a short element
P_u	Ultimate compressive demand
P_A	Compressive strength at the point A of the P-M interaction diagram (equal to P_o)
$P_{A\lambda}$	Compressive strength at the point A_λ of the P-M interaction diagram (equal to χP_A)
P_C	Compressive strength at the point C of the P-M interaction diagram
$P_{C\lambda}$	Compressive strength at the point C_λ of the P-M interaction diagram (equal to χP_C)
P_D	Compressive strength at the point D of the P-M interaction diagram
P_E	Compressive strength at the point E of the P-M interaction diagram
Z_c	Plastic section modulus of concrete (W_{pc} in EC4)
Z_s	Plastic section modulus of steel (W_{pa} in EC4)
$W_{pc,n}$	Plastic section moduli of concrete within the region of $2h_n$ from the centre-line of the composite cross-section
$W_{pa,n}$	Plastic section moduli of steel within the region of $2h_n$ from the centre-line of the composite cross-section

CHAPTER ONE

INTRODUCTION

1.1 General background

One of the critical decisions that face the structural designer is the selection of materials to be used in civil construction. This decision is frequently based on structural and economic reasons, and it is supported by the designer's judgment and experience. The central goal is to achieve an economic structure with good performance (Perea T. 2010).

Steel and concrete are the two most commonly used constructional materials in the building, bridge and civil engineering construction. Steel is characterized by its high tensile strength, excellent ductility, and greater elastic modulus, resulting in smaller cross-section and slender member of which the buckling behavior often needs to be considered in the design. On the other hand, concrete is characterized by high compressive but low tensile strength, relatively lower material cost per unit weight and lower thermal conductivity as compared to steel, which often results in bulky members where brittle tensile cracking, creep and shrinkage properties may affect their long term structural performance. The advantages of both materials are well known. Concrete is very stiff, inexpensive and has good fire resistance; meanwhile, steel is strong, ductile and lightweight. The "smart" combination of these two materials, or synergy, results in a system with much higher efficiency than that of the individual components combining the advantages of steel and concrete materials to achieve an overall enhancement in strength and stiffness.

The use of composite columns in many structural systems is increasing worldwide due to the intrinsic synergy when these materials are designed and detailed properly together. Composite columns provide not only many advantages in construction (i.e. speed and economy), but also a substantial improvement of the mechanical properties of structural members when compared to either steel or reinforced concrete elements. A composite column, if designed and detailed properly, will result in a synergistic behavior that highlights the best of the concrete properties (stiffness, high compressive strength, fireproofing) and the best of the steel properties (ductility, high tensile strength, lightweight).

Additional advantages of composite columns can be achieved if they are detailed as part of a mixed structural system. For example, if they are properly connected with the floor system (beams and slab), higher strength and a better behavior can be achieved in the beam-column connection, thus increasing the redundancy and toughness. Once the construction complexities are overcome (i.e. the interdisciplinary coordination between steel and concrete workers, and forming of the beam-column connection), more advantages will be obtained in the construction process (i.e. speed construction, formwork savings, reduced loads on foundation, increased useful space, lower construction and maintenance costs, etc.). Moreover, for areas with higher seismic design accelerations as the need to limit non-structural damage becomes more important,

replacement of either congested concrete columns or flexible steel columns with composite columns is a clear solution for brand-new and existing structures.

1.1.1 Classification of composite columns

Composite columns can be made up of different configurations as shown in Figure below.

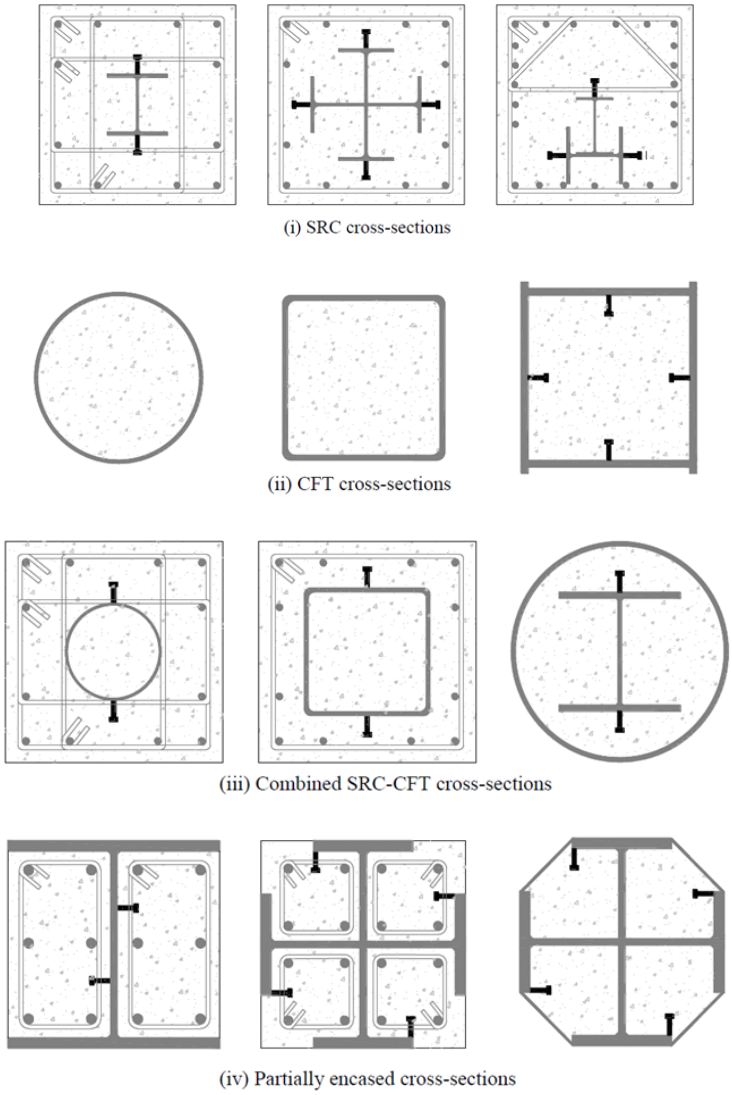

Figure 1-1: Some possible cross-sections configurations in composite columns

While there is great variety in these configurations, composite columns have been classified into two general types in terms of the position of steel and concrete. These are:

1. **Encased or Steel Reinforced Concrete (SRC) Elements:** where the steel section is embedded in or encased by the concrete; in other words, the concrete section is reinforced by a rolled or a built-up steel section. It can be fully or partially encased.

2. **Concrete-Filled Steel Tubes (CFT):** where the steel is a rolled or built-up hollow section filled with concrete. It can be with or without longitudinal bars.

1.1.2 Advantages of composite columns

Composite columns, either as SRCs or as CFTs, offer different advantages to the structural engineer. Some of these advantages include:

- ***Optimal location of steel section:*** Due to its location at the periphery of the cross-section, the steel in CFTs has an optimal distribution that increases the strength and stiffness of the element. In SRC configurations, the column is ideally located for fast erection.
- ***Fast construction of the structure*****:** The steel columns are erected and connected to the floor system to support the construction loads (beams, girders, metal deck, etc.). This is followed by the casting of the concrete slabs and columns in the lower levels, while the steel structure erection may continue in upper levels. Once the concrete has hardened, and thus the composite action has been developed, the system can achieve its final strength and stiffness to support the designated gravity and lateral loads.
- ***Higher flexural strength in embedded beam-column connections of SRCs*****:** Since the steel beam-steel column connection in SRC elements are embedded in a massive reinforced concrete section, the rotational stiffness of the steel connection is increased by the loads transferred between the beam and concrete in the embedded zone. In addition, the bending moment that can be sustained by the connection is higher than that capacity given by the initial steel connection or beam section alone.
- ***Delay of the steel local buckling*****:** In composite cross-sections, the steel column (as compact, non-compact or slender section) is stiffened by the contact with the hardened concrete, delaying or avoiding local buckling of the steel. Thus, the local buckling is delayed until the steel-concrete contact is lost (i.e. if the concrete cracks or separation of concrete-steel occurs). Even if the concrete cracks, the delay of local buckling in CFT sections will still occur since the concrete expands and bears against the steel tube, maintaining the concrete-steel contact. Since the concrete core forces all local buckling modes outward, thinner steel sections may be used that still ensure the yield strength to be reached in the tube before buckling occurs.
- ***Higher confinement in the concrete*****:** The steel column section adds confinement to the concrete core, which induces an increment in strength and ductility in the concrete. Due to the shape of the section and the higher hoop stresses that can be achieved, circular CFT cross-sections provide higher confinement than either rectangular CFT and SRC cross-sections. This confinement is also influenced by the diameter-to-thickness (*D/t*) ratio of the tubes.
- ***Savings in the construction costs*****:** Constructions costs may be reduced due to the fast erection and optimal design. Because of its higher strength, a composite column is lighter than a typical RC column with a similar strength, which reduces the loads on and cost of the foundation, the cost and amount of reinforcement bars, and thus the cost of

construction. The steel section, which acts as formwork and is stiffened by the concrete in CFT columns, is much lighter than a conventional steel column, which also reduces substantially the steel costs. Finally, the beam-column connections can be designed as efficiently (or even better) as a conventional steel or concrete column.

- ***Fireproofing*:** In SRC cross-sections, the concrete works as a fireproofing to the steel section.

Among the composite structural members, concrete-filled steel tubular (CFT) columns have attracted special attention. This is partly due to their excellent earthquakes resistant properties such as high strength, high ductility, and large energy absorption capacity.

1.1.3 Concrete-filled steel tubes (CFT)

Concrete filled steel tubular (CFT) column, comprising a hollow steel tube infilled with concrete with or without additional reinforcements or steel section, has been widely used in high rise building construction. The local buckling of the outer steel tube is delayed or even prevented by the concrete core while the inner concrete core is confined by the steel tube providing an enhancement in strength and ductility under high compressive load. The steel tube can serve as permanent formwork for concrete casting and thus it eliminates the need for additional work and leads to fast track construction.

CFT columns have various composite cross-sections as shown in Figure below. Circular, square and rectangular sections are commonly adopted while polygonal or elliptical sections also may be used for architectural and functional requirements. Conventionally, only plain concrete is filled into the hollow steel sections. Nowadays, the concrete core may be reinforced by fibers or steel bars to enhance ductility and fire resistance of the column. For convenience, the reinforcements can be replaced by an internal steel tube which can provide higher confinement to the concrete core. Other steel sections, such as solid steel section or H-section, can be inserted into the concrete core to further enhance the compression resistance and thus reduce the column size. For columns subjected to high flexural loading, concrete filled double-tube sections can be used to increase the flexural stiffness using less material.

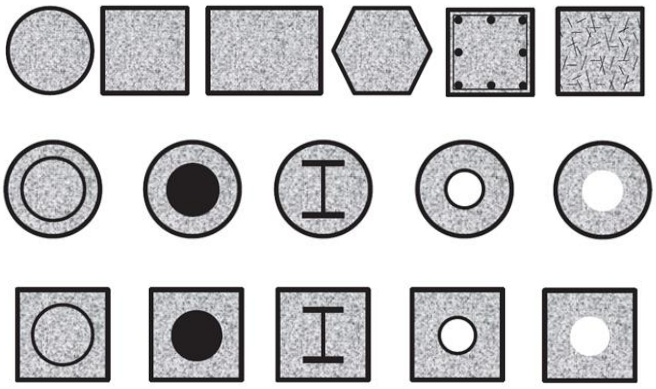

Figure 1-2: Types of concrete-filled steel tubular cross sections

1.1.4 Advantages of using CFT columns

The concrete-filled steel tubular (CFT) structure offers numerous structural benefits, including high strength, favorable ductility and large energy absorption capacities. There is also no need for the use of shuttering during concrete construction; hence, the construction cost and time are reduced. These advantages have been widely exploited and have led to the extensive use of concrete-filled tubular structures in civil engineering structures. The use of concrete-filled tubular columns provides a large saving in cost by increasing the floor area by a reduction in the required cross-section size. This is very important in the design of tall buildings in cities where the cost of letting spaces are extremely high. Concrete filled tubular columns can provide an excellent monotonic and seismic resistance in two orthogonal directions. Using multiples bays of composite concrete-filled tubular column framing in each primary direction of a low-to medium-rise building provides seismic redundancy while taking full advantage of the two-way framing capabilities of concrete filled tubular columns. As a typical composite structural system, due to the composite effects, the advantages of the two materials can be utilized and their disadvantages can be avoided, thus forming a more rational system. The steel tubes can be used as the formwork for casting concrete and the shoring system in construction, thus concrete-filled tubular column structures have much better constructability than concrete structures.

1.2 Statement of the problem

The behavior of CFT columns and slender beam-columns depends on many parameters such as the depth-to-thickness ratio, loading eccentricity ratio, column slenderness ratio, concrete compressive strengths, and steel yield strengths. It is highly expensive and time-consuming to conduct tests to study the effects of every parameter on the behavior of CFT columns and slender beam-columns. Additionally, the dimensions of the columns are usually very large; hence it is impractical to experimentally investigate the effects of every parameter on the behavior of CFT columns and slender beam-columns under various loading conditions.

Furthermore, it is not rational to derive a theory for the design of CFT columns and beam-columns from limited test data. Experiments should be used to verify a theory for the design of CFT columns and beam-columns rather than to derive the theory (Liang 2009a). On the other hand, numerical modeling can compensate for the drawbacks of experiments and can be used to investigate the behavior of full-scale normal and high strength CFT columns and beam-columns. In such cases, verified nonlinear inelastic analysis techniques may be the cost-effective methods for determination of the behavior of full-scale CFT columns and slender beam-columns.

Despite the widespread use of steel-concrete composite systems, accurate numerical procedures for their analysis and design have not evolved in the same way as for steel frames and as a consequence it is recognized widely that prescriptive codes of practice possess many shortcomings when applied to the safe and economical design of composite structures as they use simplified analytical formulas which cannot predict the accurate behavior of these elements.

Problems in the analysis and design of slender composite steel-reinforced concrete elements are quite actual today.

When considering the nonlinear behavior of structures, the approaches proposed by design codes become less realistic as the structural elements become slender. In the current context, the use of high-strength materials in construction gives rise to less rigid structures that are susceptible to large displacements. Accurate analysis of such structures requires the use of computational tools that take into account both the nonlinear behavior of the geometry of the structure and the bearing capacity of its structural elements. Major work is done on slender CFT is experimental. Experimental studies have provided sufficient information to develop analytical models. Such models can be very useful tools for detailed analysis and parametric studies to aid engineers in more efficient design of CFT columns. Since experimental programs are expensive, time-consuming and limited to small ranges of parameters, there is a need for numerical study needed to check the parameters which affect the ultimate strength and it is important to develop accurate numerical analysis tools and procedures for CFT columns and beam-column members.

1.3 Objectives

The main objective of this paper was to develop an accurate Nonlinear Inelastic Numerical Analysis Tool and procedure for Circular Concrete-Filled Steel Tubular Slender Columns and Beam-Columns under static eccentric compression load taking into account the effects of material and geometric non-linearity, geometric imperfection, second-order effects, concrete confinement, tension stiffening and local buckling of steel tubes.

In brief, the following points will be believed to be addressed:

- Develop a clear and accurate non-linear inelastic numerical analysis approach to investigate the behaviors of the circular CFT columns and beam-columns.
- Take into account the effects of material nonlinearity, geometric imperfection, geometric nonlinearity, concrete confinements, local buckling of structural steel, tension stiffening of concrete and slenderness.
- Use the numerical model to develop fast, easy and user-friendly MS Excel spreadsheet analysis tool using visual basic programmed Macros that generates axial load-strain, axial load-deflection, axial load-moment-curvature, and P-M interaction diagrams to enhance the applicability of the study.
- Use the analysis tool to conduct sensitive parametric analysis to study various effects on the behaviors of circular CFT columns and beam-columns under eccentric compression.

1.4 Methodology

Below are the procedures to achieve the mentioned objectives and scopes:

- Develop an efficient numerical method to rapidly converge the solutions of nonlinear inelastic analysis.
- Develop a nonlinear inelastic fiber element analysis method to map out the complete responses of the circular CFT columns and beam-columns, i.e. axial load and strain response, load and deflection response, axial force-bending moment interaction diagram, moment-curvature diagram, and maximum load-carrying capacity.
- Develop fast, easy and user-friendly MS Excel spreadsheet analysis tool using visual basic programmed Macros that generates axial load-strain, axial load-deflection, axial load-moment-curvature, and P-M interaction diagrams.
- Validate the proposed approach by comparing the analysis results with the previous experimental tests and researches.
- Use the validated approach to study various effects on the behaviors of circular CFT columns and beam-columns.
- Draw conclusions and recommend guidelines for future research.

1.5 Scope of the study

This paper only addresses the nonlinear inelastic numerical analysis of circular CFT Slender Columns and Beam-Columns under static eccentric compression including the effects of concrete confinement, tension stiffening of concrete and local buckling of the steel tubes. Furthermore, the study was also limited to the following:

- Slender pin ended circular CFT Columns and Beam-Columns subjected to actions of static eccentric compression under single curvature.

1.5.1 Basic assumptions

In this study, the following assumptions have been made:

1) The plane section remains plane after loading;
2) A perfect bond exists between the concrete core and the steel shell at the material interface;
3) Monotonic loading;
4) Effect of creep and shrinkage is neglected; and
5) The shear deformation and torsional effect are all neglected.

1.6 Significance of the study

This paper is going to present an accurate and clear numerical solutions procedure for Nonlinear Inelastic Analysis of Circular Concrete-Filled Steel Tubular Slender Columns and Beam-Columns under static eccentric compression. The numerical analysis tool that was developed can be used for generating more data under various loading and parametric conditions and also for evaluating both the ultimate strength and load-deflection relation of CFT slender columns and Beam-Columns under static eccentric compression. Hence this research is believed to assist the

students, designers, and researchers by providing clear and accurate numerical analysis procedures and tool for CFT slender columns and Beam-columns under static eccentric compression for data simulation, checking and also ultimate strength evaluation purposes under various parametric conditions.

1.7 Thesis outlines

This thesis is organized into five chapters.

This chapter presents a general background of composite columns and followed by concrete-filled steel tubular columns. Then the problem statement, objectives of the research, methodology, scope, and research significance are presented.

Chapter two presents an extensive literature review on different steel tube section columns filled with concrete. It describes briefly a review of the previous investigation on composite CFT columns and beam-columns. Then, it presents previous experimental and analytical investigations of concrete-filled steel tube columns filled with concrete.

Chapter three presents a review of the analysis and design of slender CFT columns and beam-columns according to two design codes i.e. BC4: 2015 (an extension to EC4 for CFT columns with high strength materials) and AISC specifications.

A numerical model based on the fiber element analysis method for determining the axial load-deflection curves and axial load-moment interaction diagrams of circular CFT columns and beam-columns under static eccentric compression is developed and presented in *Chapter Four*. The effects of geometric and material nonlinearity, local buckling of steel tubes, concrete confinement and tension stiffening, slenderness and initial geometric imperfections are considered in the fiber element analysis program. Computational algorithms based on the Secant method are developed to iterate the neutral axis depth to satisfy equilibrium conditions.

Chapter Four also discusses the model verification and comparison results of columns and beam-columns, which include cross-sectional load capacity, axial load-deflection curves and axial load-moment interaction diagrams for beam-columns. Moreover, parametric study to investigate the behavior of CFT columns and beam-columns under static eccentric compression for variation in geometric arrangements and material properties were presented as well using the tool.

Finally, *Chapter Five* summarizes the main conclusions from the work undertaken for this thesis and gives recommendations for future research.

CHAPTER TWO

LITERATURE REVIEW

2.1 Introduction

Two types of composite columns, those with steel section encased in concrete and those with steel section in-filled with concrete are commonly used in buildings. Concrete-filled steel tubular columns have been used for earthquake-resistant structures, bridge piers subject to impact from traffic, columns to support storage tanks, decks of railways, columns in high-rise buildings and as piles. Concrete-filled steel tubes require additional fire-resistant insulation if fire protection of the structure is necessary. Because of the increased use of composite columns, a great deal of analytical and experimental work has been carried out.

2.1.1 Typical CFT cross sections

Fig 2-1(a) below depicts three typical column cross-sections, where the concrete is filled in a circular hollow section (CHS), a square hollow section (SHS) or a rectangular hollow section (RHS), where *D* and *B* are the outer dimensions of the steel tube and *t* is the wall thickness of the tube. It is noted that the circular cross section provides the strongest confinement to the core concrete, and the local buckling is more likely to occur in square or rectangular cross-sections. However, the concrete-filled steel tubes with SHS and RHS are still increasingly used in construction, for the reasons of being easier in beam-to-column connection design, high cross-sectional bending stiffness and for aesthetic reasons. Other cross-sectional shapes have also been used for aesthetical purposes, such as polygon, round-ended rectangular and elliptical shapes, as shown in Fig 2-1(b) below.

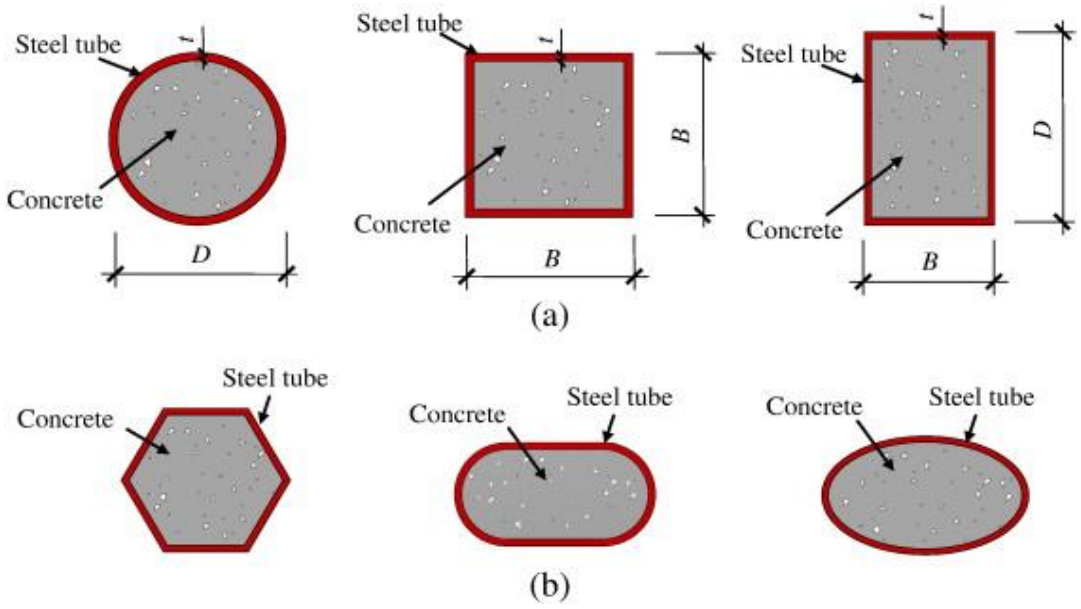

Figure 2-1: Typical concrete-filled steel tubular cross sections

Most concrete-filled steel tubular members used in constructions are prismatic. However, due to architectural or structural requirements, inclined or non-prismatic members were used [L.H. Han, Q.X. Ren, W. Li (2010)]. The inclined column could serve as a load transfer member in the structure with irregular architectural style, as illustrated in Fig. 2-2(a). The tapered members could be used for aesthetic or economic purposes, as shown in Fig. 2-2(b). In some large-span structures or bridges, curved members could be used, as shown in Fig. 2-2(c) [L.H. Han, L.Q. Zheng, S.H. He, Z. Tao (2011)]. The research results from short column tests have shown that the steel tube and the concrete can work together well despite the inclined or tapered angle. The failure mode of the non-prismatic inclined and tapered members under compression is similar to that of the prismatic member, which is the outward buckling of the steel tube and the crushing of the concrete. The failure location is perpendicular to the longitudinal direction of members. For the curved members, their failure modes are similar to that of the corresponding CFT under bending. The axial compressive strength of the curved member could be reduced when the curvature is increased, while ductility is enhanced [L. H. Han, W. Li and R. Bjorhovde, 2014].

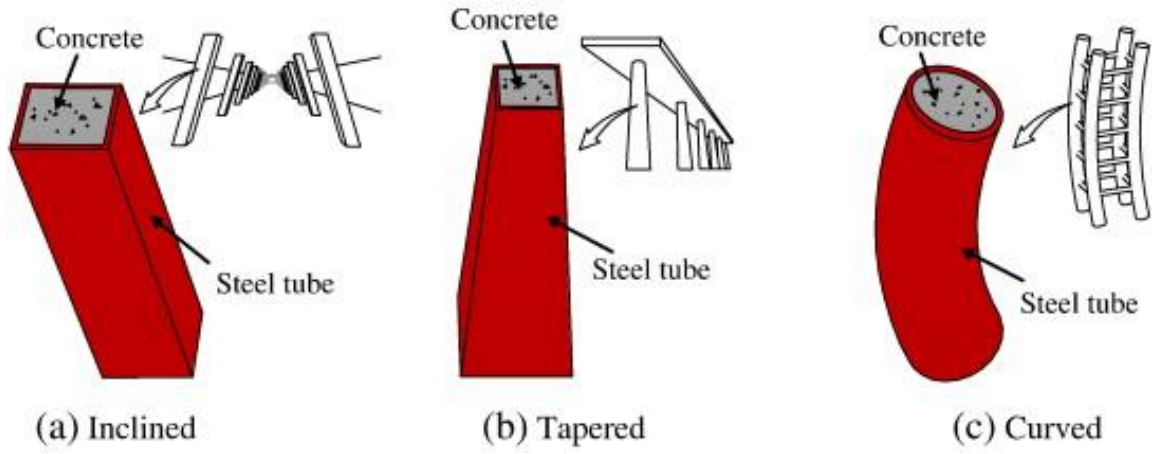

Figure 2-2: Inclined, tapered and curved CFT columns [Han et al. 2014b]

Much research work has been done to understand the "composite action" between the steel and the concrete for these composite sections under axial compression. It has been confirmed that the circular steel tubes can provide much more effective confinement to their core concrete than other types of tubular sections. It is believed that the confinement effect is related to the cross-sectional properties as well as the material properties. A confinement factor (ξ) thus had been introduced to describe this effect [L.H. Han (2007), L.H. Han (2002)]:

$$\xi = A_s f_y / A_c f_{ck} \qquad (2\text{-}1)$$

Where $\mathbf{A_s}$ and $\mathbf{A_c}$ are the cross-sectional areas of the steel tube and the concrete, respectively; $\mathbf{f_y}$ is the yield strength of the steel; $\mathbf{f_{ck}}$ is the characteristic compressive strength of the concrete cube, and can be taken as $\mathbf{0.67\ f_{cu}}$ for normal strength concrete.

It was found that the confinement provided by the steel tube to its core concrete can be increased with the increase of the confinement factor (**ξ**). It is also noted that this factor can describe the confinement effect qualitatively for different kinds of cross-sectional shapes, such as circular, square and rectangular [L.H. Han (2007)].

2.1.2 Applications of CFT members in the construction industry

Concrete-filled steel tubes have been used in different parts of the world for almost 50 years. It was used as the main columns in subway stations in Beijing since 1966 and also in workshops and power plant buildings since the 1970s. In recent decades, the pace of the concrete-filled steel tube construction has increased rapidly. The concrete-filled steel tubes are used as major compressive components or key members under various loading conditions in buildings, bridges and other structures. Several examples are presented below.

2.1.2.1 In Buildings

In the 1980s, the concrete-filled steel tube was used in buildings to avoid having a very large size column. The concrete-filled steel tube usually served as the member resisting compressive load and is usually connected to steel or reinforced concrete beams to form a composite frame system. In high-rise buildings or super high-rise buildings, the CFT composite frame structures are often combined with other lateral load resisting systems such as RC core tubes or steel shear walls. The frame using concrete-filled steel tubular columns integrates the high stiffness and the high ductility and works well with the core tubes or shear walls in hybrid structural systems. The figure below shows another composite structural system with the CFT frame and RC shear walls.

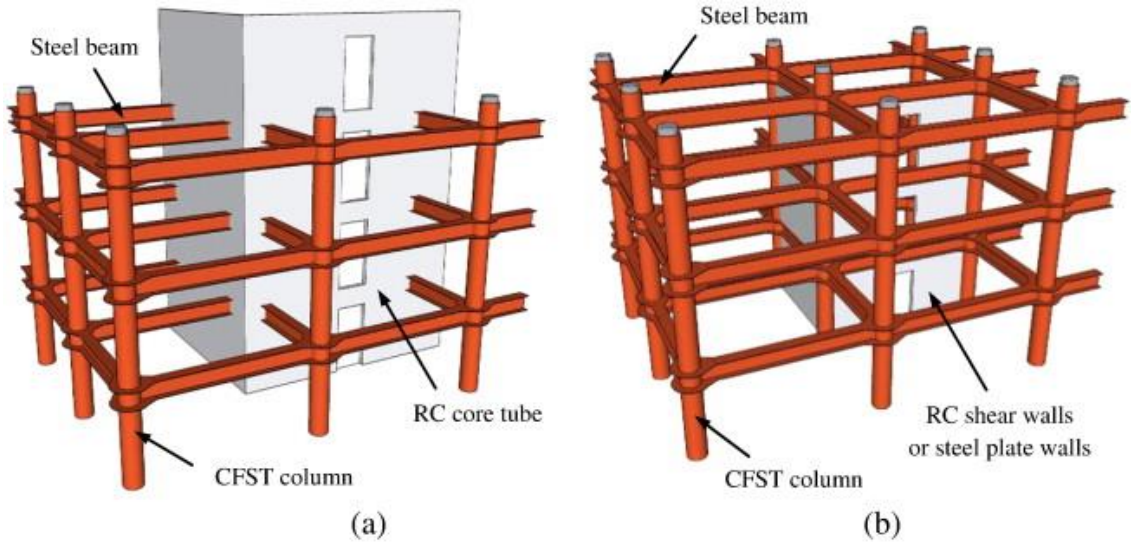

Figure 2-3: CFT hybrid structural systems for high-rise buildings [Han et al. 2014b]

As an innovative and efficient structural component, CFT members are used widely around the world in various types of structures. For example, CFT members are used as columns in composite braced frames in: (i) the Two Union Square building in Seattle, Washington, (ii)

Casselden Place project in Melbourne, Australia, (iii) Taipei 101 tower in Taipei, Taiwan, and (iv) Kommerz bank in Frankfort, Germany.

CFT members are also used as columns in composite moment frames, for example in (i) 3 Houston Center in Houston, Texas, (ii) Postal Office building in Quanzhou, China, (iii) Wuhan International Financial Center in Wuhan, China, and iv) Shimizu Super High Rise in Tokyo, Japan (This is a 121-story building with a height of 550 m).

2.1.2.2 In Bridges

Concrete-filled steel tubular members have been applied in many types of bridges, such as arch bridges; cable-stayed bridges, suspension bridges, and truss bridges. CFT members can serve as piers, bridge towers, and arches, and they can also be used in the bridge deck system. Fig. 2-4 below depicts the usage of CFT members in various bridge structures.

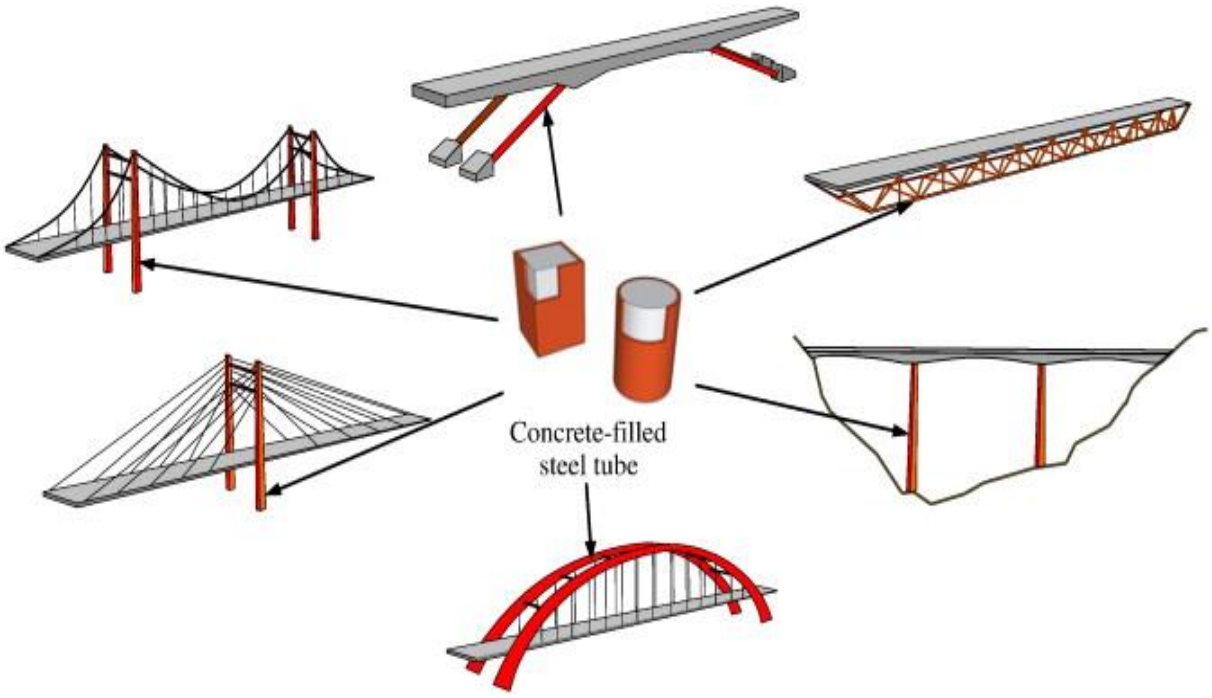

Figure 2-4: CFT used in bridges [Han et al. 2014b]

CFT members are used as compression chords in composite bridges, for example, in: (i) the Yajisha bridge in Guangzhou, China, (ii) Chunnan Napu bridge in Zhejiang, China, (iii) Pudong Canal bridge in Shanghai, China, (iv) Wuxia Changjiang bridge in Chongqing, China, and (v) Shinsaikai bridge in Sasebo, Japan. In China, CFT members are used in more than three hundred composite bridges. The chords, webs, and bracings of the four-pipe truss are all made of CFT members. CFT members are also used as piles, transmission towers, and bracing members in buckling.

An important advantage of using CFT in an arch bridge is that, during the stage of erection, the hollow steel tubes can serve as the formwork for casting the concrete, which significantly reduces the construction cost. Furthermore, the composite arch can be erected without the aid of a temporary bridging due to the inherent stability of the tubular structure. The hollow steel tubes can be filled with concrete to convert the system into a composite structure. Since the weight of the hollow steel tubes is comparatively small, relatively simple construction technology can be used for the erection. The most common methods include cantilever launching methods, and either horizontal or vertical "swing" methods, whereby each half-arch can be rotated horizontally into position.

2.1.2.3 In other structures

Concrete-filled steel tubular columns have also been used in various structures such as subway stations, workshops, electricity pylons, transmission towers, and poles. It is well known that the columns in subway stations are usually subjected to large axial compressive loads. The concrete-filled steel tubular member is suitable for being used as the supporting column.

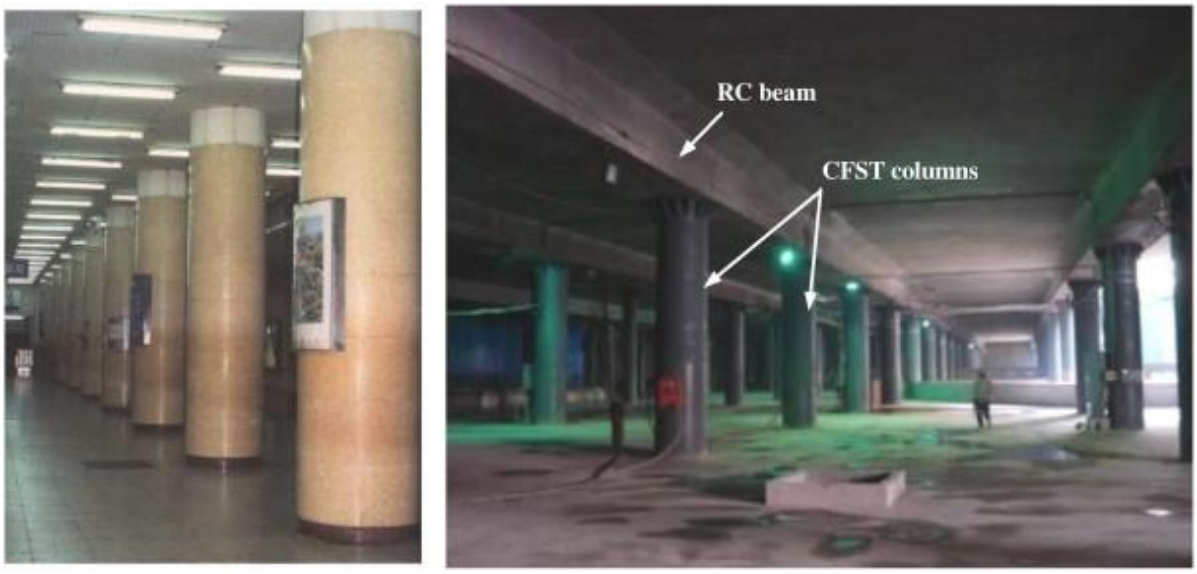

Figure 2-5: Subway stations using CFT columns [Han et al. 2014b]

The concrete-filled steel tubes can be used in the construction and the upgrade of poles and transmission towers as well. Concrete-filled double skin steel tubes are being used in electrical grid infrastructures in recent years. This composite section has high bending stiffness, and the self-weight is lighter when compared with the fully filled CFT section. A photo of the CFDST pole is shown in Fig. 2-6 below. The bearing capacity of the pole is enhanced when compared to the traditional steel lattice tower, while the occupied land area is reduced and the total cost is not raised.

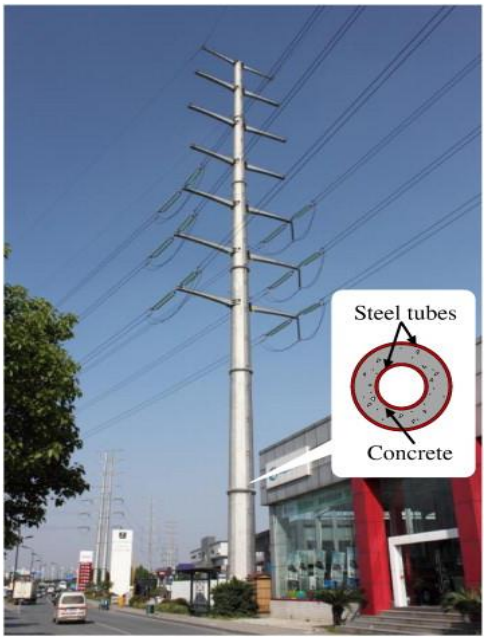

Figure 2-6: A CFDST pole [Han et al. 2014b]

2.2 The behavior of Concrete-Filled Steel Tubes

In current international practice, concrete-filled steel tube (CFT) columns are used in the primary lateral resistance systems of both braced and unbraced building structures. There exist applications in Japan and Europe where CFTs are also used as bridge piers. Moreover, CFTs may be utilized for retrofitting purposes for strengthening concrete columns in earthquake zones.

A primary deterrent to the widespread use of CFTs is the limited knowledge regarding their behavior. A number of factors complicate the analysis and design of concrete-filled steel tubes. A CFT member contains two materials with different stress-strain curves and distinctly different behavior. The interaction of the two materials poses a difficult problem in the determination of combined properties such as the moment of inertia and modulus of elasticity. The failure mechanism depends largely on the shape, length, diameter, steel tube thickness, and concrete and steel strengths. Parameters such as a bond, concrete confinement, residual stresses, creep, shrinkage, and type of loading also have an effect on the CFT's behavior. Axially loaded columns and, in more recent years, CFT beam-columns and connections, have been studied worldwide and to some extent, many of the aforementioned issues have been reconciled for these types of members. However, researchers are still studying topics such as the effect of bond, confinement, local buckling, scale effect, and fire on CFT member strength, load transfer mechanisms and economical detailing strategies at beam-to-CFT column connections, and categorization of response in CFTs and their connections at all levels of loading so as to facilitate the development of performance-based seismic design provisions. It should also be noted that, despite a recent increase in the number of full-scale experiments, the majority of the tests to date have been conducted on relatively small specimens, often 150mm in diameter or smaller. This is

due to the load limits of the testing apparatus and the need to run the tests economically (Morino et al., 1996). Whether these results can be accurately extrapolated to the typically larger columns used in practice remains a pertinent and debatable question.

2.2.1 Component behavior

It is well known that the compressive strength of concrete is much higher than its tensile strength. Furthermore, the compressive strength is enhanced under bi-axial or tri-axial restraint. For the structural steel, the tensile strength is high while the shape may buckle locally under compression. In concrete-filled steel tubular members, steel and concrete are used such that their natural and most prominent characteristics are taken advantage of. The confinement of concrete is provided by the steel tube, and the local buckling of the steel tube is improved due to the support of the concrete core. Fig. 2-7 below shows schematic failure modes for the stub concrete-filled steel tubular column and the corresponding steel tube and concrete. It can be seen that both inward and outward buckling is found in the steel tube, and shear failure is exhibited for the plain concrete stub column. For the concrete-filled steel tube, only outward buckling is found in the tube, and the inner concrete fails in a more ductile fashion. Fig. 2-8(a) shows a comparison of the measured results between a steel stub column, a reinforced concrete stub column and a concrete-filled steel tubular stub column without steel reinforcement, where *D* and *t* are the outer diameter and the wall thickness of the circular steel tube, respectively; f_y is the yield strength of the steel; f_{cu} is the compressive strength of the concrete cube. The geometric dimension of the circular hollow steel section is the same as in both steel column and composite column, and also the same for the concrete parts in both the reinforced concrete column and the composite column. The term "steel tube + RC" in Fig, indicates the summation of the ultimate strength of the steel tube and the reinforced concrete (RC) specimens. It clearly shows that the ultimate strength for a concrete-filled steel tube is even larger than the summation of the strength of the steel tube and the RC column, which is described as "(steel tube) + (concrete core) greater than (simple summation of the two materials)" [L. H. Han, 2007]. Fig. 2-8(b) shows a schematic view of the load versus deformation relationship of the hollow steel tube, the concrete stub column by itself and the concrete-filled steel tube. It can be seen that the ductility of the concrete-filled steel tube is significantly enhanced, when compared to those of the steel tube and the concrete alone.

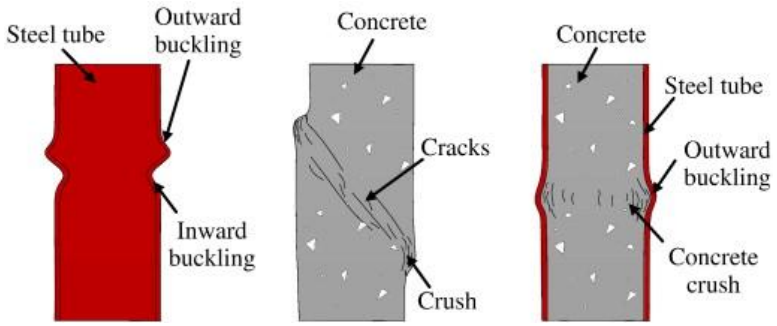

Figure 2-7: Schematic failure modes of hollow steel tube, concrete and CFT stub columns

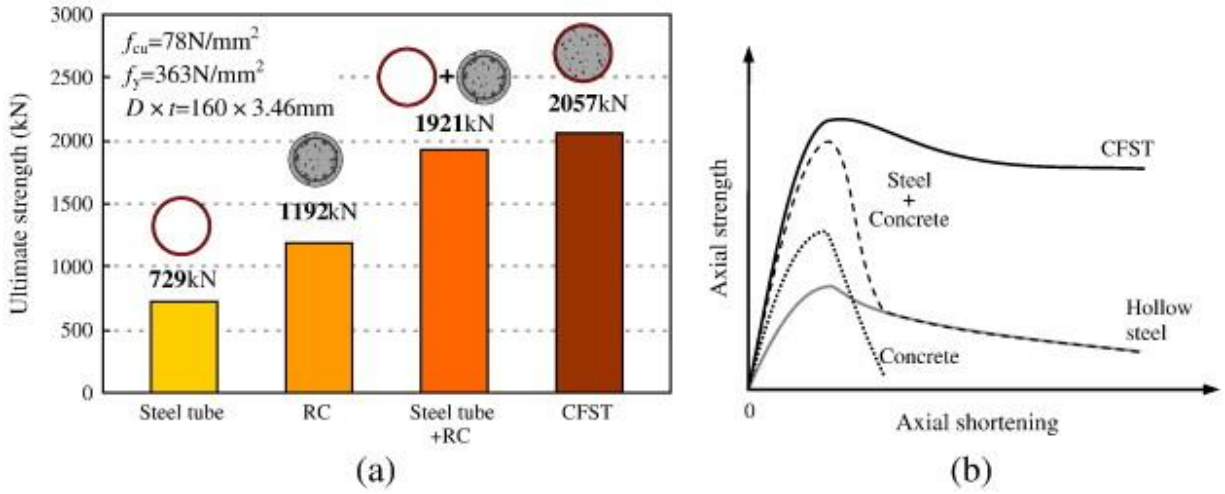

Figure 2-8: Axial compressive behavior of CFT stub column [L. H. Han, 2007]

2.2.1.1 Effect of confinement

Circular hollow sections provide a significant amount of confinement while this effect is negligible in the case of rectangular sections. Additional strength occurs because of the increase in compressive strength of the concrete core that is restrained laterally by the surrounding steel tube. This increase in concrete strength outweighs the reduction in the yield strength of steel in vertical compression due to the confinement tension needed to contain the concrete. The confinement effect is not present in concrete-filled rectangular hollow sections, except in the corner regions, as the hoop tension developed along the side walls is not constant [Matsui C, Tsuda K, Ishibashi Y (1995)].

In the concrete-filled circular sections, the influence of confinement is reduced as bending moments are applied. This is due to the mean compressive strain in the concrete (and the associated lateral expansion) is then reduced. It also diminishes with increasing slenderness of the column, since the lateral deflection prior to failure increases the bending moment and reduces the mean compressive strain in the concrete.

The confinement may occur for columns where concrete is crushed prior to local buckling of steel and this would generally be true for columns where the plate slenderness limit is small. The effect of confinement was calculated in terms of confining pressure as circumferential stress f_l [Brauns J (1999)]. Steel jacket would be subjected to a bi-axial state of stress as shown in Fig below. Longitudinal stress f_s develops due to axial load and bending moment whereas a circumferential stress f_l develops due to concrete confinement. The two stresses define the yield criteria as outlined by von Mises' yield criteria.

$$f_s^2 + f_l^2 + f_l f_s = F_y \qquad (2\text{-}2)$$

Where, F_y is the yield stress of the steel jacket

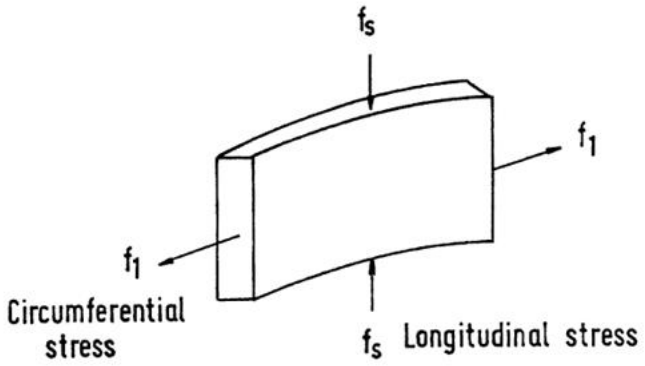

Figure 2-9: Longitudinal and circumferential stresses in the steel tubes

2.2.1.2 Effect of local buckling

Thin-walled circular composite columns used in many constructions have to be designed to account for the confinement effect of concrete restraint against local buckling of steel tube. Design of the steel casing using a rational analysis for local buckling would lead to a considerable saving on material cost. A concrete-filled tube has a local buckling capacity of about 50% more than that for unfilled tube since the steel tube is restrained against buckling inwards by the concrete infill [Matsui C (1993)]. Effect of local buckling on the axial compressive strength of circular steel tubes is a function of the plate diameter to thickness ratio (D/t) and is accounted in a number of design standards through the use of an effective diameter or an effective area.

A model for local buckling of steel plates when in contact with a rigid medium was developed by Wright [1993]. His theoretical model is based on the energy method but is applicable to uniform compression only. A semi-analytical procedure to incorporate the elastic and in-elastic local buckling of plates with clamped loaded edges was proposed using cubic polynomial [Uy B, Bradford MA (1994), Cheung YK (1976)]. A post-local buckling model based on the effective width principle was established [Uy B (1998)]. The local buckling stress was set equal to the yield stress for columns that buckled in-elastically. Local buckling strain was determined as the point at which a significant change occurs in the average load-strain relationship. The model seems to be very accurate in the elastic region with residual stresses in the order of 30%. However, the finite strip analysis does not incorporate initial imperfections which play a significant role in reducing the local-buckling load in thin-walled structures.

2.2.2 Axially Loaded CFT Columns

Columns loaded axially in compression (either concentrically or eccentrically) will behave in one of two distinct ways. Columns with a small L/D ratio (short columns) are governed by cross-section strength. These types of columns reach their ultimate capacity when both the steel and the concrete reach their strength limit point, i.e., yielding of the steel and crushing of the concrete. Eccentric loading will have little effect on this type of column. The second type of

behavior pertains to columns with a larger L/D ratio intermediate or long (slender) columns. These columns are governed by stability and fail by either elastic or inelastic column buckling.

A load applied eccentrically will tend to cause buckling to occur earlier than an equal load applied concentrically (concentric also implies that the column is perfectly straight). Straight columns under purely concentric axial loading rarely, if ever, exist in practice. Therefore, a more realistic approach to examining CFT column behavior incorporates the bending moment caused by geometric imperfections or eccentricities.

2.2.2.1 Short CFT Columns

General Behavior

When a concentric axial load is applied to a short concrete-filled steel tube column (assuming the load is applied uniformly across both materials), the steel and the concrete will both begin to deform longitudinally. At these initial strains, Poisson's ratio of the steel exceeds Poisson's ratio of the concrete (0.28 versus 0.15 to 0.25) (Gardner and Jacobson, 1967). This results in a greater lateral expansion of the steel, and little interaction between the two materials occurs. During this stage of loading, the steel and the concrete sustain load independently of one another. Thus, the longitudinal stress along the steel tube remains approximately constant. At a strain of approximately 0.001, micro-cracking in the concrete begins to occur and the lateral expansion of the concrete increases and begins to approach the constant lateral expansion of the steel. The concrete expansion reinitiates interactive contact between the two materials, which induces bond stresses to develop, and results in biaxial stresses in the steel and triaxial stresses in the concrete. This causes the longitudinal stresses in the steel tube to change as a function of the transfer of force between the steel and concrete. The strain at which interaction and subsequent confinement occur varies typically from 0.001 to 0.002. Knowles and Park (1970) state that confinement occurs suddenly at a strain of about 0.002 (about $0.95f_c'$, after the concrete begins a rapid volumetric expansion (dilation). Other authors suggest a more gradual increase in confinement beginning shortly after micro-cracking at a strain of 0.001, and reaching full confinement at 0.002 (Tsuji et al., 1991; Zhang et al., 1991).

Once confinement occurs; the steel tube experiences circumferential stresses from the lateral pressure of the expanding concrete in addition to the longitudinal stresses. If the steel tube has not yet yielded, this biaxial state of stress effectively decreases the amount of additional axial load the steel can sustain before yielding occurs. If, on the other hand, the steel tube is in a state of yielding when the biaxial stress state initiates, the steel will be unable to sustain the longitudinal yield stress. In either case, the effective elastic stiffness of the steel tube decreases and the tube sheds some of its axial load to the concrete. While the rapid expansion of concrete has a deleterious effect on the longitudinal steel capacity, the load-carrying capacity of the concrete component of the CFT is enhanced. The confinement of the steel tube augments the axial strength of the concrete core. For circular sections, in particular, this increase in axial

strength of the concrete actually outweighs the corresponding decrease in steel strength, resulting in an overall increase in the capacity of the CFT section (Shanmugam, N. E., and Lakshmi, B. 2001).

While circular sections can effectively develop circumferential tension to exert lateral pressure on the concrete, the flat sides of rectangular sections provide little perpendicular pressure to restrain the expanding concrete (Furlong, 1967). Only the corners of rectangular tubes can exert confinement and this effect is negligible. Therefore, the strength of the rectangular CFTs in excess of its nominal axial load capacity is attributed primarily to the strain hardening of the steel tube.

When high strength concrete is utilized, the low dilatation of concrete prevents any significant confinement effect. Thus in most experimental studies, the axial load capacity of short columns with high strength concrete was often less than their nominal cross section strengths, unless the D/t ratio was small.

The load-deflection behavior of short columns exhibits different trends depending on their post-peak response. Circular CFT columns generally show strain-hardening or elastic-perfectly plastic type of load-deflection curves. For rectangular columns, a degrading (i.e., softening) load-deflection curve is commonly observed. The degradation of the load-deflection curves is also typical for stub columns with high strength concrete.

Failure Mechanism: CFTs with Thick-Walled Tubes

Short columns can be further subdivided into two categories based on the D/t ratio (the ratio of the tube diameter to the tube thickness). Concrete-filled steel tubes with "thick" walls will exhibit the more standard mechanism of failure. The concrete becomes confined at a strain of approximately 0.002 and additional axial strength is achieved. However, if the strength of the steel exceeds approximately 375MPa (the stress corresponding to a longitudinal strain of approximately 0.002), the concrete will likely reach its compressive strength limit and may crush before the steel yields, which is an undesirable mode of failure (Furlong, 1967). In addition, this might cause elastic local buckling of the steel tube. SSRC (1979) thus specifies a steel yield strength limit of 375MPa for composite columns. For lower strength steels, the failure of thick-walled short columns begins with the yielding of the steel. As the yielding of the cross-section of the tube proceeds, the concrete begins to fail by crushing. With confinement, the concrete can continue to sustain additional load until the steel tube fails (usually by extensive local buckling or full plastification of the cross-section) marking the ultimate strength of the section. The location of the failure is usually mid-height for square and rectangular CFT specimens. For square CFTs, local buckling generally spreads to all four flanges. However, for rectangular CFTs, the longer flanges are more susceptible to local buckling. This causes steel yielding in the transverse direction along the shorter sides (Shakir-Khalil, 1991). The failure of circular CFTs

also may take place at the mid-height with extensive local buckling, and local buckling then spreads to the ends (Schneider, 1998).

Failure Mechanism: CFTs with Thin-Walled Tubes

Thin-walled specimens fail either by elastic or inelastic local buckling of the steel tube or by a shear failure in the concrete (at a strain of approximately 0.005) followed by local buckling of the steel tube, which is in a state of yielding. In either case, the longitudinal strains in the member are not large enough to allow significant confinement of the concrete core to occur. The local buckling of the steel is, however, delayed by the influence of the concrete core. The concrete forces the steel to buckle in an outward mode, which provides three advantages. First, when buckling occurs, the distance between the top and bottom flanges of the steel tube increases rather than decreases (as it would without the concrete core), which prevents the section modulus from decreasing significantly. The second advantage is that the concrete tends to spread the local buckling over a larger region, mitigating severe strain concentrations which tend to cause cracking. Third, delaying the local buckling effectively stabilizes the tube wall in the elastic range and often enables full development of the yield stress prior to buckling. In their tests for thin-walled high strength CFT columns, O'Shea and Bridge (1997c, 1997d) observed two types of failure patterns. The columns failed either by local buckling combined with concrete crushing or by sudden failure without any local buckling. Concrete crushing took place beyond an axial strain of 0.003. Prion and Boehme (1989) found, in their tests of thin-walled CFTs using high strength concrete, that the steel yielded, then the concrete failed by shearing, after which the capacity of the section fell off considerably, and local buckling occurred in the steel tube at the location of the shear failure in the concrete. Luksha and Nesterovich (1991) noticed a similar type of failure in their tests of large diameter tubes. Tubes with D/t ranging from 54 to 104 began failing at 90% of ultimate with the formation of buckles along the tube. At incipient failure, the concrete sheared causing the steel to buckle completely. This shearing or local buckling type of failure is undesirable because it is often sudden and could be catastrophic (Knowles and Park, 1969). A limiting value of D/t should be adhered to in order to prevent such failures.

Eccentric Loading of Short CFT Columns

Short columns subjected to eccentric loading or having initial out-of-straightness show insignificant lateral displacement for a given applied moment. These columns are essentially governed by the axial load effects alone. In their eccentric axial tests on thin-walled circular high strength concrete CFT stub columns, O'Shea and Bridge (1997c, 1997d) found that ductility improves with increasing eccentricity. Bridge (1976) also found that square CFT columns with larger eccentricity have a more stable post-peak response. This is because, for small eccentricities, more concrete is effective in resisting the loads. Thus, softening exhibited in the post-peak response of concrete is reflected in the overall response of the column. Confinement

has been shown to be negligible in both circular and rectangular tubes for e/D (eccentricity to diameter) ratios greater than 0.125 (Neogi et al., 1969; Bridge, 1976).

2.2.2.2 Long CFT Columns

General Behavior

If the CFT column is sufficiently slender, stability rather than strength will govern the ultimate load capacity and second-order effects become more critical. Overall column buckling will precede strains of sufficient magnitude to allow large volumetric expansion of the concrete to occur. Hence, for overall buckling failures, there is little confinement of the concrete and thus little additional strength gain. Many authors have agreed that a slenderness ratio (L/D) equal to 15 generally marks a rough boundary between short and long column behavior. Neogi et al. (1969) originally proposed this value for eccentrically loaded columns (eccentrically loaded columns, rather than concentrically loaded columns, are the case of interest since this type of loading will cause an earlier buckling of the member). Chen and Chen (1973), Bridge (1976), and Prion and Boehme (1989) confirmed the L/D value of 15. Knowles and Park (1969) proposed a KL/r_c value of 44 (approximately equal to an L/D of 12), above which confinement does not occur. In addition, the AIJ (1990) specification also has a minimum L/D ratio of 12 for long columns. However, Zhong et al. (1991) specified a lower value of L/D equal to 5 above which confinement does not occur.

Both elastic and inelastic flexural buckling can occur in CFT columns. CFTs that fail by inelastic buckling are referred to here as intermediate CFT columns and CFTs that fail by elastic buckling are referred to as long or slender CFT columns.

Failure Mechanism: Intermediate CFT Columns

Intermediate columns will undergo some steel yielding and/or concrete crushing before buckling occurs. As the steel yields and the concrete crushes, the stiffness of the member decreases and its capacity to withstand buckling decreases. Rectangular tubes tested in biaxial bending by Shakir-Khalil and Mouli (1990) yielded first in the compression corner of the tube at approximately 90% of the failure load, followed by tensile yielding of the opposite corner, leading to an overall buckling failure. By increasing the size of the tube or the strength of the concrete, additional strength may be attained. Conversely, increasing the yield strength of the steel tube or increasing the length has detrimental effects. Both of these factors will increase the relative contribution of the steel and decrease the concrete contribution, which begins to negate the benefits of filling the tube with concrete.

Failure Mechanism: Slender CFT Columns

The method of failure of long concrete-filled steel tube columns is characterized by an overall elastic buckling of the member (Shakir-Khalil and Zeghiche, 1989). This type of column has a

sufficiently large L/D ratio to cause buckling before any significant yielding occurs in the column. Tsuda et al. (1996) observed the same type of failure in their tests of slender concentrically loaded columns. The columns with an L/D greater than 18 did not reach their plastic axial strength and failed by flexural buckling.

Eccentric Loading of Long CFT Columns

As the length of a column increases, it becomes more sensitive to eccentric loading effects and initial out-of-straightness. Lateral deflections of the column increase the likelihood of a buckling failure rather than a cross-section strength failure. Eccentric loading will impart external and internal moments on the section. The eccentricity of the load itself produces a primary moment. Bending of the member chord (P - δ effect) induces secondary moments in the cross section due to the lateral deflection of the column. The failure mechanism of long columns due to eccentric loading will be similar to the concentric case, except that failure will occur at a smaller load and the failure load will decrease with an increase in eccentricity. Shakir-Khalil (1991) tested long CFT columns under eccentric loading and observed that CFT columns become more sensitive to initial imperfections when the eccentricity is low. However, Tsuda et al. (1996) found that as the L/D ratio increases, the behavior of both circular and square columns is less affected by eccentricity. In the same experimental study, CFT columns with an L/D ratio greater than 18 did not attain their full plastic moment capacity, and they failed due to flexural buckling. This indicates that slender CFT columns under eccentric axial loading are susceptible to elastic flexural buckling.

2.2.2.3 Stiffness of Axially Loaded CFT Columns

The stiffness of concrete-filled steel tubes is complicated by the concrete core and the interaction between the two materials. The modulus of elasticity, the moment of inertia, and the effective area for tensile loading are well known for steel, but these properties are difficult to predict for concrete because of its in-homogeneity. They vary depending on the concrete strength, the occurrence of tensile cracking, and long-term load effects, among other things. SSRC (1979) has proposed a modified elastic modulus that is the sum of the moduli of elasticity for the steel and concrete, with a reduction factor of 0.4 imposed on the initial stiffness of the concrete to account for creep and tensile cracking. Other authors have proposed summing the individual rigidities of each component (Hajjar et al., 1997a). The overall stiffness of the CFT, though, will be mostly influenced by the steel tube, since the steel has a much higher modulus of elasticity than the concrete.

2.2.3 Combined Axial Load and Bending (CFT Beam-Columns)

Typically, beam-column tests are differentiated from eccentric loading tests by the magnitude of the induced moment and the type of failure. Eccentric load tests refer to tests where a moment was introduced to accentuate initial out-of-straightness, or tests in which the moment was of relatively small magnitude (e.g., less than 20% of the ultimate moment capacity). The eccentricity hastens the onset of buckling in a typical failure. Beam-column tests, on the other

hand, have moments of significantly larger magnitude, warranting careful consideration of the interactive failure due to combined moment and axial load. These moments may be introduced transversely, via loading of a connected member, or by a number of other methods.

General Behavior

Several key parameters influence the behavior of beam-columns. Among them are the D/t ratio, the axial load ratio (P/P_o), and the L/D ratio or the slenderness of the member. The D/t ratio determines the point of local buckling, and it affects the ductility of the section. A smaller D/t ratio will delay the onset of local buckling of the steel tube. Tubes with high D/t ratios (above approximately 50) will often exhibit local buckling even before yielding of the section occurs. A low D/t will provide greater ductility, illustrated by the long plateau in the moment-curvature diagrams for such columns (Tomii and Sakino, 1979a). Tomii and Sakino (1979a) also showed that beam-columns with low D/t ratios can sustain the maximum moment after local buckling. Beam-columns with higher D/t ratios began to lose capacity as the curvature increased, although only under large axial loads did the capacity drop significantly. Ichinohe et al. (1991) determined that for circular CFT specimens with a D/t less than 53, the moment increases after local buckling without strength degradation.

The axial load ratio is a second important parameter in CFT beam-column behavior. The relationship between the moment and axial load, as illustrated by interaction diagrams, is typically a curve that bulges outward for low axial compressive loads (i.e., with the maximum moments exceeding M_o) and then approaches P_o approximately linearly, showing a rapid decrease in the moment capacity for high axial compressive load ratios. As axial compression is added to a CFT member in bending, the contribution of the concrete begins to increase, utilizing the composite action of the section to a greater extent. The axial load increases the strength of the concrete in a manner similar to the confinement effect discussed above. As with the D/t ratio, the axial load ratio has an effect on ductility. Large values of P/P_o lead to rapid moment capacity deterioration and brittle failures. If the steel on the compression side has buckled (which is more likely as the D/t ratio increases), a more brittle failure typically ensues. It can be seen that a combination of a high D/t and high P/P_o leads to undesirable modes of failure. Because of this, Tomii and Sakino (1979a), for example, limited their studies to beam-columns with P/P_o less than or equal to 0.5.

Finally, the L/D ratio will have a significant effect on the performance of the member. A number of authors (e.g., Chen and Chen, 1973; Bridge, 1976; Tomii and Sakino, 1979a; Fujimoto et al., 1996; Tsuda et al., 1996) have presented interaction diagrams (both from experimental and analytical research) that show the moment-axial load relationship for different L/D ratios. For a given cross section, the maximum moment (M_o) will remain approximately the same with an increase in length, but the maximum compressive axial force (P_o) will drop markedly.

With respect to material strength, Varma et al. (2000) conducted beam-column tests on square CFTs with high strength materials. He observed a reduction of initial stiffness and moment capacity with an increase in D/t ratio. The yield strength of the steel and the axial load ratio did not have any significant influence on the initial stiffness. However, when the yield strength of the steel increased, the moment capacity was enhanced. The amount of improvement was larger for low D/t ratios due to better resistance to local buckling. The steel strength also had little influence on the ductility seen in the CFT beam-columns. However, both high axial load levels and large D/t ratios caused a reduction in ductility, often more severe than is seen with normal strength materials. Failure took place due to local buckling of the flanges and extensive concrete crushing. In most of the cases, yielding of steel tube occurred prior to the specimen achieving its peak load. In the post-peak region, local buckling moved to the webs and tension cracking of the corners took place. Nakahara and Sakino (1998) also determined that, compared to using normal strength concrete, the introduction of high strength concrete reduces ductility.

2.3 Summary of Previous Researches on CFT Members

2.3.1 Experimental Research

Since the first documented experimental research on CFT columns by Klöppel and Goder (1957), significant research has been conducted to investigate the behavior of CFT members under various loading conditions. For example:

1) Axial compression tests have been conducted by Furlong (1967), Knowles and Park (1969), Anslijin and Janss (1974), Bridge (1976), Lin (1988), Sakino and Hayashi (1991), Bridge and Webb (1993), Bergmann (1994), Fujimoto et al. (1995), Yoshioka et al. (1995), O'Shea and Bridge (1996), Song and Kwon (1997), Schneider (1998), Han and Yan (2000), Uy (1998, 2001), Kang et al. (2001), Mursi and Uy (2004), and Guo et al. (2007) among others.
2) Flexural tests have been conducted by Ichinohe et al. (1991), Lu and Kennedy (1994), Elchalakani et al. (2001, 2004, 2008), Uy (2000), Ichinohe et al. (1991), Han (2004), Wheeler and Bridge (2004), Han et al. (2006), Lennie et al. (2008), and Jiang et al. (2013) among others.
3) Combined axial force and flexure (beam-column) tests have been conducted by Bridge (1976), Cai (1991), Prion and Boehme (1994), O'Shea and Bridge (1997a, 1997b, 1997c, 2000), Bridge and O'Shea (1998), Nakahara and Sakino (2000), Sakino and Nakahara (2000), Uy (2001), Mursi and Uy (2004), Varma et al. (2002, 2004), Soundararajan and Shanmugasundaram (2008), and Huang et al. (2011) among others.

Nishiyama et al. (2002), Kim (2005), Gourley et al. (2008), and Hajjar et al. (2013) have independently compiled comprehensive databases of experimental research conducted on rectangular and circular CFTs. The database compiled by Hajjar et al. (2013) (previously, Gourley et al., 2008) is the most comprehensive database of experimental and numerical research performed on CFT members, frames, and systems. The database includes all the tests conducted

on compact, non-compact, and slender CFT members with a wide range of material, geometric, and loading parameters. Experimental research shows that the strength of CFT members depends on several parameters, namely, the steel yield stress F_y, concrete compressive strength f_c', tube wall slenderness (b/t or D/t) ratio, column lengthto- depth ratio (L/B or L/D) and composite interaction between the steel tube and concrete infill, etc.

2.3.2 Analytical Research

Significant analytical research has also been conducted to investigate the behavior of CFT members, as can be placed in four general categories:

1) Three-dimensional (3-D) finite element method (FEM) models, as have been developed by Yonezawa et al. (1996), Goto et al. (1998, 2010, 2011), Schneider (1998), Varma et al. (2002b), Lu et al. (2009), Moon et al. (2012), Tao et al. (2013) among others.
2) Fiber analysis based macro models, as have been developed by Tomii and Sakino (1979a, 1979b), Hajjar and Gourley (1996), Inai and Sakino (1996), Morino et al. (1996), Zhang and Shahrooz (1997), Varma et al. (2005) and Liang (2008, 2009, 2010, 2011) among others.
3) Concentrated-plasticity based FEM models, as have been developed by Hajjar and Gourley (1996, 1997).
4) Distributed-plasticity based FEM models for CFT columns, as have been developed by Hajjar et al. (1998a, 1998b).

CHAPTER THREE

ANALYSIS AND DESIGN OF CFT MEMBERS with BC4 and AISC CODES

3.1 Analysis and Design of CFT Members According to BC4: 2015 (an Extension to EC4 Method for CFT with High Strength Materials)

EC4 covers concrete encased and partially encased steel sections and concrete filled sections with or without reinforcement. This code uses limit state concepts to achieve the aims of serviceability and safety by applying a partial safety factor to loads and material properties. This is the only code that treats the effect of long-term loading separately.

3.1.1 About BC4: 2015

This design guide entitled **"*Design Guide for Concrete Filled Tubular Members with High Strength Materials - An Extension of Eurocode 4 Method to C90/105 Concrete and S550 Steel*"** is based on Eurocode 4 (EN 1994-1-1, 2004) for the design of concrete filled steel tubular members with special considerations for higher concrete strength with cylinder compressive strength up to 90N/mm^2 and higher grade of steel with yield strength up to 550N/mm^2. According to the guide, more than 2000 test data collected from the literature on concrete filled steel tubes with normal and high strength materials have been analyzed to formulate the design method proposed in it. The Guidebook is a concise version of the book on design guide for Concrete Filled Tubular Members with High Strength Materials by Liew and Xiong (2015) including detailed guides on the use of high strength steel and high strength concrete materials, test database and work examples.

3.1.2 General limitations of the guide

The following are points under the Section-1 (General) of the guide:

1) The design guide is applicable for design of concrete filled steel tubular members with concrete cylinder strength up to 90N/mm2 and steel of yield strength up to 550N/mm2.

2) The design guide is based on EN 1994-1-1 and EN 1994-1-2 for the design of concrete filled steel tubular members with special considerations for the high strength concrete and the high tensile steel.

3) The design guide should be limited to the types of concrete filled tubular members of doubly symmetrical and uniform cross-section over the member length, as shown in Figure 3-1.

4) The design guide is not applicable to composite members with concrete encased sections and partially encased sections.

5) The design guide does not apply to laced or battened concrete filled steel tubular members which consist of two or more discontinuously connected sections. In which case the specialist advices should be consulted.

6) The partial factors for concrete, steel and reinforcement are according to (EN 1992-1-1, 2004; EN 1993-1-1, 2005; EN 1993-1-8, 2005; EN 1994-1-1, 2004).

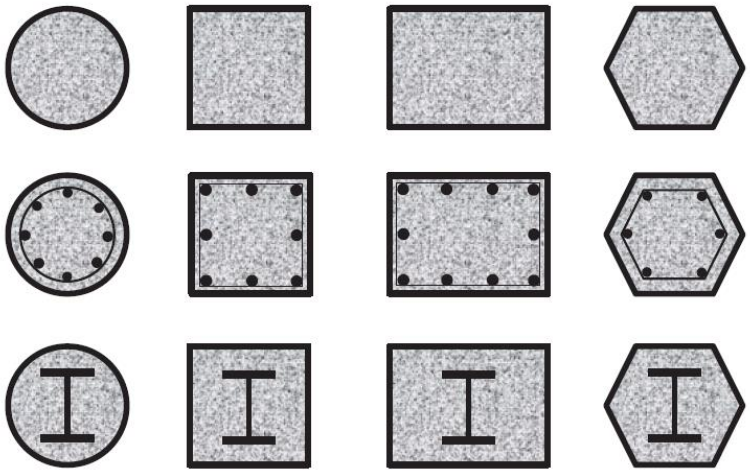

Figure 3-1: Types of double symmetric CFT sections

7) The ratio of the depth to the width of the composite cross-section should be within the limits of 0.2 and 5.0.
8) The longitudinal reinforcement that may be used in the calculation should not exceed 6% of the concrete area. Longitudinal reinforcement in the concrete filled tube may not be necessary if it is not required for fire resistance.

9) The steel contribution ratio, defined in Eq. (3-1), should fulfill the condition in Eq. (3-2).

$$\delta = \left(A_a f_{yd} + A_e f_{ed}\right)/N_{pl,Rd} \quad (3\text{-}1)$$

$\boldsymbol{A_a}$, $\boldsymbol{A_e}$ are the cross-sectional area of steel tube and encased steel section if any respectively

$\boldsymbol{f_{yd}}$, $\boldsymbol{f_{ed}}$ are the design strength of steel tube and encased steel section if any respectively

$\boldsymbol{N_{pl,Rd}}$ is the axial resistance of the composite section

The steel contribution ratio δ should fulfill the following condition:

$$0.2 \leq \delta \leq 0.9 \quad (3\text{-}2)$$

10) The general method given in EN 1994-1-1 (2004) is applicable to the concrete filled steel tubular members with high strength materials. The general method may be implemented by means of advanced finite element analysis.

3.1.3 Material Compatibility between Steel Grade and Concrete Class

For high strength concrete-filled steel tubular columns subjected to compression, it is necessary to ensure that yielding of the steel section occurs before the concrete core reaches its maximum stress. Otherwise, the full plastic resistance of the composite section cannot be achieved due to brittle failure of high strength concrete after reaching the maximum stress. Hence, the selections of steel grade and concrete class have to ensure that the yield strain of steel is smaller than the compressive strain of concrete at the peak stress. The yield strain of steel and the strain of concrete at peak stress may be calculated in accordance with EN 1992-1-1 (2004) and EN 1993-1-1 (2005) as:

Steel yield strain:

$$\varepsilon_y = f_y / E_a \tag{3-3}$$

Concrete strain at peak stress (‰):

$$\varepsilon_{c1} = 0.7(f_{cm})^{0.31} < 2.8 \tag{3-4}$$

Where $\boldsymbol{f_{cm} = f_{ck} + 8}$ is the mean compressive strength of concrete at 28 days, in $\mathrm{N/mm^2}$.

$\boldsymbol{E_a = 210GPa}$ is the elastic modulus of steel tube.

It is noted that the calculation for the strain of concrete at peak stress ignores the confinement effect from the steel tubes. If the increase of strain by confinement is taken into account, higher steel grade could be used.

The table below gives recommendation on the matching grades of steel and concrete suitable for use in CFT columns such that $\boldsymbol{\varepsilon_y < \varepsilon_{c1}}$. It is recommended that the steel tubular sections up to Grade S550 may be used with concrete grade up to C90/105; although test evidence by Liew *et al.* (2013) shows that the strain of concrete at peak stress of CFT is very much higher than the concrete without any confinement. In the case where higher strength concrete and high tensile steel not shown in Table should be used in CFT columns, specialist advices should be sought.

Alternatively, the maximum steel strength can be determined according to the concrete characteristic strength with strength class up to C90/105 using the following expression:

$$f_y \leq 0.7E_a(f_{ck} + 8)^{0.31} \tag{3-5}$$

Where

$\boldsymbol{f_y}$ is the characteristic yield strength of steel

$\boldsymbol{f_{ck}}$ is the characteristic cylinder compressive strength of concrete

$\boldsymbol{E_a}$ is the modulus of Elasticity of steel

Table 3-1: Compatibility of steel and concrete materials for CFT columns (BC4: 2015)

	S235	S275	S355	S420	S460	S500	S550	S620	S690
C12/15	√	√	√	×	×	×	×	×	×
C16/20	√	√	√	×	×	×	×	×	×
C20/25	√	√	√	×	×	×	×	×	×
C25/30	√	√	√	√	×	×	×	×	×
C30/37	√	√	√	√	×	×	×	×	×
C35/45	√	√	√	√	√	×	×	×	×
C40/50	√	√	√	√	√	×	×	×	×
C45/55	√	√	√	√	√	√	×	×	×
C50/60	√	√	√	√	√	√	×	×	×
C55/67	√	√	√	√	√	√	×	×	×
C60/75	√	√	√	√	√	√	×	×	×
C70/85	√	√	√	√	√	√	√	×	×
C80/95	√	√	√	√	√	√	√	×	×
C90/105	√	√	√	√	√	√	√	×	×

Notes: "√"indicates compatible materials and "×" is not recommended.

3.1.4 Local Buckling

The effects of local buckling may be neglected for a steel section fully encased in concrete of CFT columns. For outer tubes, the maximum values of the Table below should not be exceeded. The local buckling of the outer tube could be prevented by increasing the plate thickness. Alternatively, stiffener plates to be welded on the steel plate in the longitudinal direction of the column, as shown in Figure, may be used to reduce the effective width of the steel plates.

Table 3-2: Maximum values (d/t), (h/t) for local buckling

Concrete filled Cross-section	Maximum value in expressions	Maximum values according to steel grades						
		S275	S355	S460	S500	S550	S620	S690
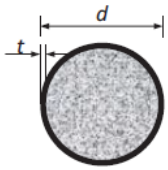	$\left(d/t\right)_{max} = 90\frac{235}{f_y}$	77	60	46	42	38	34	30
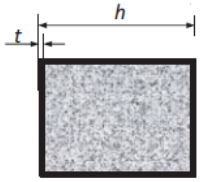	$\left(h/t\right)_{max} = 52\sqrt{\frac{235}{f_y}}$	48	42	37	35	34	32	30

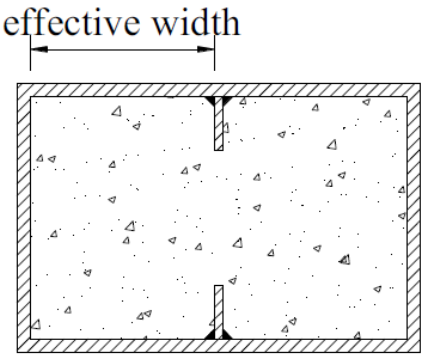

Figure 3-2: Prevention of local buckling of the outer tube of CFT columns using plate stiffeners

3.1.5 The resistance of Cross Section to Compression

The plastic design resistance to compression of a CFT column cross-section $\boldsymbol{N_{pl,Rd}}$ is calculated by adding the plastic resistances of its components:

$$N_{pl,Rd} = A_a f_{yd} + A_c f_{cd} + A_s f_{sd} + A_e f_{ed} \tag{3-6}$$

Where

$\boldsymbol{A_a}$, $\boldsymbol{A_c}$, $\boldsymbol{A_s}$, $\boldsymbol{A_e}$ are the cross-sectional area of steel tube, concrete, reinforcements and encased steel section if any respectively

$\boldsymbol{f_{yd}}$, $\boldsymbol{f_{cd}}$, $\boldsymbol{f_{sd}}$, $\boldsymbol{f_{ed}}$ are the design strength of steel tube, concrete, reinforcements, and encased steel section if any respectively

For circular CFT columns, the increase of concrete strength due to confinement effect may be allowed provided that the relative slenderness $\bar{\lambda}$ of the member does not exceed 0.5 and $e/D < 0.1$, where e is the eccentricity of loading given by M_{ED}/N_{ED} and D is the external dimension of the column section. The plastic resistance to axial compression considering the confinement effect may then be calculated as:

$$N_{pl,Rd} = \eta_a A_a f_{yd} + A_c f_{cd}\left(1 + \eta_c t f_y / d f_{ck}\right) + A_s f_{sd} + A_e f_{ed} \quad (3\text{-}7)$$

Where

$\boldsymbol{f_y}$, $\boldsymbol{f_{ck}}$ = the characteristic strength of steel tube and concrete, respectively

t = the thickness of the steel tube

$$\eta_a = \eta_{ao} + (1 - \eta_{ao})(10\, e/D) \quad \text{For } e/D \le 0.1 \quad (3\text{-}8)$$
$$= 1.0 \quad \text{for } e/D > 0.1$$
$$\eta_{ao} = 0.25\left(3 + 2\bar{\lambda}\right) \quad \text{but} \le 1.0 \quad (3\text{-}9)$$
$$\eta_c = \eta_{co}(1 - 10\, e/D) \quad \text{For } e/D \le 0.1 \quad (3\text{-}10)$$
$$= 0 \quad \text{for } e/D > 0.1$$
$$\eta_{co} = 4.9 - 18.5\bar{\lambda} + 17\bar{\lambda}^2 \quad \text{but} \le 0 \quad (3\text{-}11)$$

For high strength concrete ($\boldsymbol{f_{ck} > 50\, N/mm^2}$), the compressive strength $\boldsymbol{f_{ck}}$ or $\boldsymbol{f_{cd}}$ should be reduced by the reduction factor of $\boldsymbol{\eta}$ given as

$$\eta = 1.0 - (f_{ck} - 50)/200 \quad \text{for} \quad 50\, N/mm^2 < f_{ck} \le 90\, N/mm^2 \quad (3.12)$$
$$= 0.8 \quad \text{for} \quad f_{ck} > 90\, N/mm^2$$

3.1.6 The resistance of Cross Section to Combined Compression and Bending

The resistance of a cross-section to combined compression and moments may be calculated based on the interaction curve assuming rectangular stress blocks as shown in Figure below.

The tensile strength of the concrete may be neglected. As a simplification, the interaction curve is a polygonal diagram as shown in Figure. The plastic stress distributions of a CFT cross section for the points A, B, C and D are also shown in Figure.

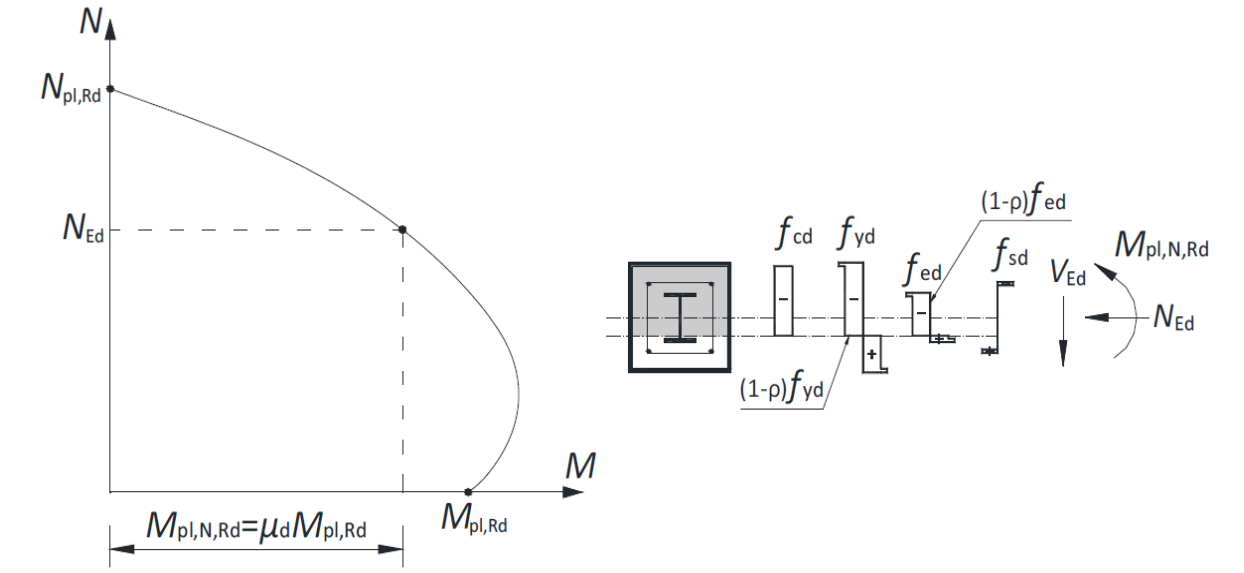

Figure 3-3: Interaction curve for combined compression and bending

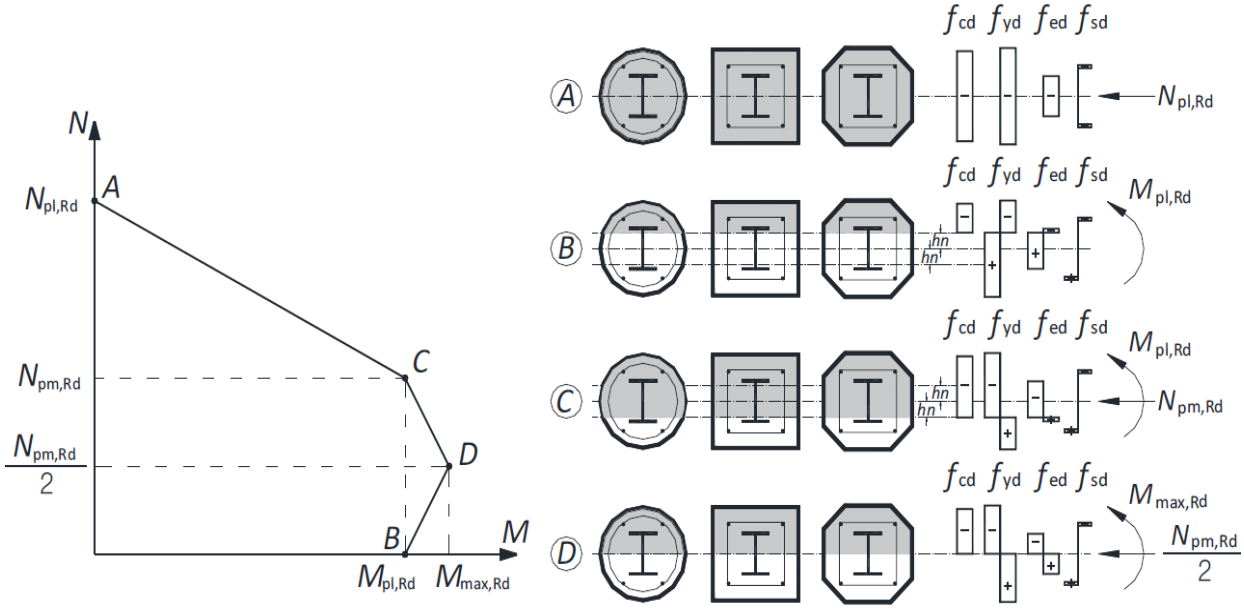

Figure 3-4: Simplified interaction curve and corresponding stress distributions

3.1.6.1 Section analysis of circular CFT column

Point	Defining equations

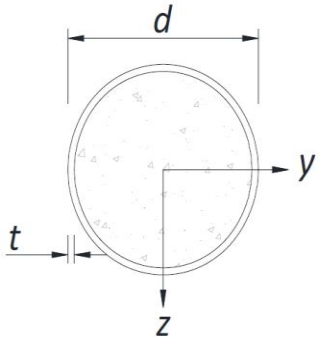

A $$N_{pl,Rd} = \eta_a A_a f_{yd} + A_c f_{cd}\left(1 + \eta_c \frac{t}{d}\frac{f_y}{f_{ck}}\right)$$

B $$h_n = \frac{A_c f_{cd}}{2d f_{cd} + 4t\left(2f_{yd} - f_{cd}\right)}$$

$$W_{pc} = \frac{(d-2t)^3}{6}$$

$$W_{pc,n} = (d-2t)\,h_n^2$$

$$W_{pa} = \frac{d^3}{6} - W_{pc}$$

$$W_{pa,n} = d h_n^2 - W_{pc,n}$$

$$M_{pl,Rd} = \left(W_{pa} - W_{pa,n}\right) f_{yd} + 0.5\left(W_{pc} - W_{pc,n}\right) f_{cd}$$

C $$N_{pm,Rd} = A_c f_{cd}\left(1 + \eta_c \frac{t}{d}\frac{f_y}{f_{ck}}\right)$$

D $$M_{pl,Rd} = W_{pa} f_{yd} + 0.5 W_{pc} f_{cd}$$

Note:

- For high strength concrete ($\boldsymbol{f_{ck} > 50\,N/mm^2}$), the compressive strength $\boldsymbol{f_{ck}}$ or $\boldsymbol{f_{cd}}$ should be reduced by the reduction factor of $\boldsymbol{\eta}$ given in above.

3.1.6.2 Section analysis of rectangular CFT column

Point Defining equations

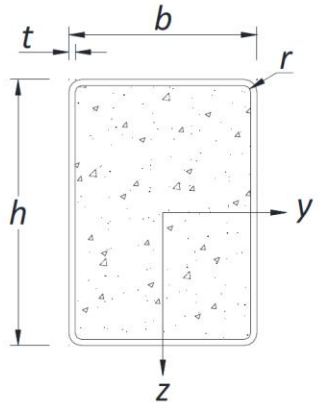

A $N_{pl,Rd} = A_a f_{yd} + A_c f_{cd}$

B $h_n = \frac{A_c f_{cd}}{2bf_{cd} + 4t(2f_{yd} - f_{cd})}$

$W_{pc} = \frac{(b-2t)(h-2t)^2}{4} - \frac{2}{3}r^3 - r^2(4-\pi)\left(\frac{h}{2} - t - r\right)$

$W_{pc,n} = (b-2t)\,h_n^2$

$W_{pa} = \frac{bh^2}{4} - \frac{2}{3}(r+t)^3 - (r+t)^2(4-\pi)\left(\frac{h}{2} - t - r\right) - W_{pc}$

$W_{pa,n} = bh_n^2 - W_{pc,n}$

$M_{pl,Rd} = (W_{pa} - W_{pa,n})\,f_{yd} + 0.5\,(W_{pc} - W_{pc,n})\,f_{cd}$

C $N_{pm,Rd} = A_c f_{cd}$

D $M_{pl,Rd} = W_{pa} f_{yd} + 0.5 W_{pc} f_{cd}$

Note:

- For high strength concrete ($\boldsymbol{f_{ck} > 50\,N/mm^2}$), the compressive strength $\boldsymbol{f_{ck}}$ or $\boldsymbol{f_{cd}}$ should be reduced by the reduction factor of $\boldsymbol{\eta}$ given above.
- For bending about the weak axis, the dimensions **b** and **h** are to be exchanged.

3.1.7 The resistance of Members *to Compression*

For a member subject only to axial compression, Clause 6.7.3.5(2) in EN 1994-1-1 enables buckling curves to be used. This is a useful simplification because these curves allow for member initial imperfections. The design effect due to axial compression N_{ED} in a member should satisfy:

$$N_{ED}/\chi N_{pl,Rd} \leq 1 \tag{3-13}$$

For axial compression in members the value of $\boldsymbol{\chi}$ for the appropriate non dimensional slenderness $\bar{\boldsymbol{\lambda}}$ should be determined from the relevant buckling curve according to:

$$\chi = \frac{1}{\Phi+\sqrt{\Phi^2-\bar{\lambda}^2}} \qquad but\ \chi \leq 1 \tag{3-14}$$

Where

$$\Phi = 0.5\left[1 + \alpha\left(\bar{\lambda} - 0.2\right) + \bar{\lambda}^2\right] \tag{3-15}$$

$\boldsymbol{\alpha}$ = the imperfection factor

$\bar{\boldsymbol{\lambda}}$ = the relative slenderness for the plane of bending and equal to $\sqrt{\boldsymbol{N_{pl,Rk}/N_{cr}}}$

$\boldsymbol{N_{pl,Rk}}$ = the characteristic value of the plastic resistance to compression $\boldsymbol{N_{pl,Rd}}$ in which the material characteristic strengths rather than the design strength should be used.

$\boldsymbol{N_{cr}}$ = the elastic critical normal force for the relevant buckling mode

The imperfection factor $\boldsymbol{\alpha}$ corresponding to an appropriate buckling curve should be obtained from Table below.

The buckling curves and member imperfections for CFT composite columns can be determined from the Table that follows.

Table 3-3: Imperfection factors for buckling curves (BC4: 2015)

Buckling curve	a_0	a	b	c	d
Imperfection factor	0.13	0.21	0.34	0.49	0.76

Table 3-4: Buckling curves and member imperfections for CFT composite columns

Cross section	Limits	Axis of buckling	Buckling curve	Member imperfection
	$\rho_s \leq 3\%$	any	a	$L/300$
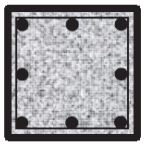	$\rho_s \leq 3\%$	any	b	$L/200$
	-	any	b	$L/200$
	-	any	b	$L/200$

Note:

- $\boldsymbol{\rho_s}$ is the area ratio of reinforcements relative to the concrete area.

The elastic critical normal force $\boldsymbol{N_{cr}}$ for the relevant buckling mode is determined by:

$$N_{cr} = \frac{\pi^2 (EI)_{eff}}{L_{eff}^2} \tag{3-16}$$

$\boldsymbol{L_{eff}}$ is the buckling length of a composite column for the relevant buckling mode. In the absence of Eurocode guidance, buckling lengths given in BS 5950: Part 1(2000) are therefore recommended as shown in Table below, where *L* is the system length of the composite column.

The boundary conditions and corresponding buckling lengths are illustrated in Figure. The effective flexural stiffness of a CFT column $\boldsymbol{(EI)_{eff}}$ may be calculated as:

$$(EI)_{eff} = E_a I_a + E_s I_s + E_e I_e + 0.6 E_{cm} I_c \tag{3-17}$$

Table 3-5: Buckling lengths for composite columns

Non-sway mode			
End restraint in the plane under consideration by other parts of the structure			L_{eff}
Effectively held in position at both ends	1) Effectively restrained in direction at both ends		$0.7L$
	2) Partially restrained in direction at both ends		$0.85L$
	3) Restrained in direction at one end		$0.85L$
	4) Not restrained in direction at either end		1.0
Sway mode			
One end		Other end	L_{eff}
Effectively held in position and restrained in direction	Not held in position	5) Effectively restrained indirection	$1.2L$
		6) Partially restrained indirection	$1.5L$
		7) Not restrained in direction	$2.0L$

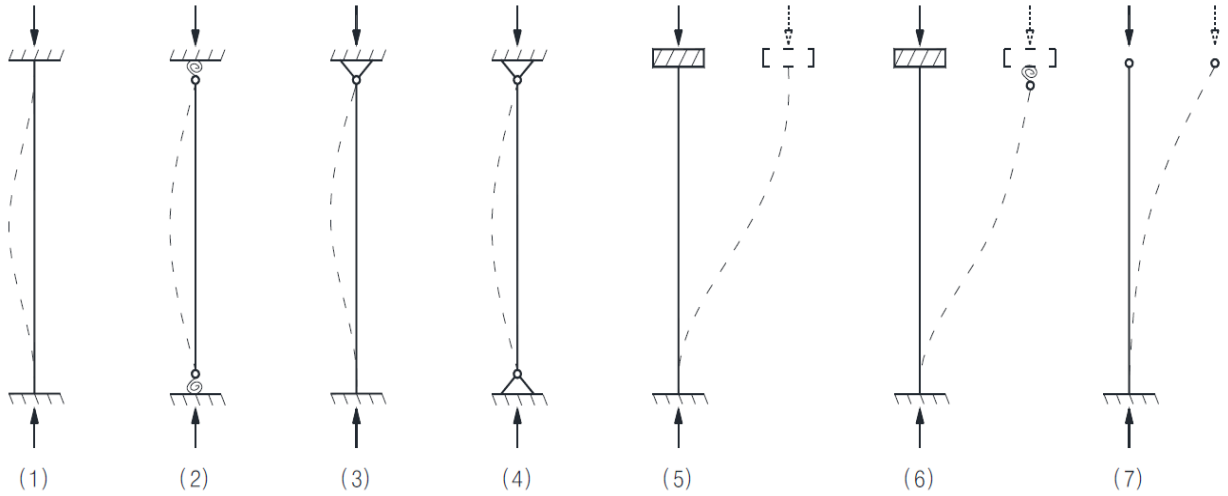

Figure 3-5: Buckling lengths for composite columns

Where

$\boldsymbol{I_a}$, $\boldsymbol{I_c}$, $\boldsymbol{I_s}$, $\boldsymbol{I_e}$ are the second moments of area of the steel tube, the un-cracked concrete, the reinforcements and the encased steel section for the bending plane being considered

$\boldsymbol{E_a}$, $\boldsymbol{E_{cm}}$, $\boldsymbol{E_s}$, $\boldsymbol{E_e}$ are the modulus of elasticity of the steel tube, the un-cracked concrete, the reinforcements and the encased steel section.

The influence of long-term effects on the effective flexural stiffness $(\boldsymbol{EI})_{\boldsymbol{eff}}$ should be accounted for. The modulus of elasticity of concrete $\boldsymbol{E_{cm}}$ should be reduced to the value $\boldsymbol{E_{c,eff}}$ in accordance with the following equation:

$$E_{c,eff} = E_{cm}\frac{1}{1+(N_{G,Ed}/N_{Ed})\varphi_t} \tag{3-18}$$

Where

$\boldsymbol{N_{G,Ed}}$ is the part of the normal force that is permanent

$\boldsymbol{\varphi_t}$ is the creep coefficient

It should be noted that for high strength concrete ($f_{ck} > 50\,N/mm^2$), a reduced $\boldsymbol{E_{cm}}$ value should be used.

BC2 (2008) allows for reduced creep effects with increasing concrete strength. Thus, the creep coefficient $\boldsymbol{\varphi_t}$ is conservatively taken as that for normal strength concrete when high strength concrete is used. The creep coefficient $\boldsymbol{\varphi_t}$ may be calculated from (EN 1992-1-1, 2004):

$$\varphi_t = \varphi_0\beta_c^{(t,t_o)} \tag{3-19}$$

Where

$$\varphi_0 = \varphi_{RH}\beta^{(f_{cm})}\beta^{(t_0)} \tag{3-20}$$

$$\varphi_{RH} = 1 + \frac{1-RH/100}{0.1\sqrt[3]{h_0}} \qquad for \;\; f_{cm} \le 35MPa \tag{3-21}$$

$$\varphi_{RH} = \left[1 + \frac{1-RH/100}{0.1\sqrt[3]{h_0}}\alpha_1\right]\alpha_2 \quad for \quad f_{cm} > 35MPa \tag{3-22}$$

$$\beta^{(f_{cm})} = \frac{16.8}{\sqrt{f_{cm}}} \tag{3-23}$$

$$\beta^{(t_0)} = \frac{1}{0.1+t_0^{0.2}} \tag{3-24}$$

$$h_0 = \frac{2A_c}{u} \tag{3-25}$$

$$\beta_c^{(t,t_o)} = \left(\frac{t-t_0}{\beta_H+t-t_0}\right)^{0.3} \tag{3-26}$$

$$\beta_c^{(t,t_o)} = 1.0 \quad when \;\; t \to \infty \tag{3-27}$$

$$\beta_H = 1.5[1 + (0.012RH)^{18}]h_0 + 250 \quad \le 1500 \quad for\; f_{cm} \le 35MPa \tag{3-28}$$

$$\beta_H = 1.5[1 + (0.012RH)^{18}]h_0 + 250\alpha_3 \;\; 1500\alpha_3 \quad for\; f_{cm} > 35MPa \tag{3-29}$$

$$\alpha_1 = \left[\frac{35}{f_{cm}}\right]^{0.7} \quad (3\text{-}30)$$

$$\alpha_2 = \left[\frac{35}{f_{cm}}\right]^{0.2} \quad (3\text{-}31)$$

$$\alpha_3 = \left[\frac{35}{f_{cm}}\right]^{0.5} \quad (3\text{-}32)$$

$\boldsymbol{RH}$ = the relative humidity of the ambient environmental in %

$\boldsymbol{f_{cm}}$ = the mean compressive strength of concrete at the age of 28 days and equal to $(\boldsymbol{f_{ck}} + \mathbf{8})$ $\mathrm{N/mm^2}$

A_c = the cross-sectional area of concrete

u = the perimeter of the concrete section

t = the age of concrete in days at the moment considered

t_0 = the age of concrete in days at first loading in days

In practice, the age of concrete at the moment considered t can be conservatively taken as infinity. For the age of concrete on first loading by effects of creep, although EN 1994-1-1 (2004) recommends $t_0 = 1$ day, it is actually the judgment of the designer to determine t_0 since it makes quite a difference whether this age is assumed to be 1 day or 1 month. When $t_0 > 100$, its effect on creep coefficient is not significant and it is sufficiently accurate to assume t_0 = 100. For concrete in-filled in steel tubes, the relative humidity *RH* can be assumed to be 50% conforming to EN 1992-1-1 (2004) regarding the condition of concrete inside the steel tube.

3.1.8 The resistance of Members to Combined Compression and Uniaxial Bending

The following expression based on the interaction curve determined according to Section above should be satisfied:

$$\frac{M_{Ed}}{M_{pl,N,Rd}} = \frac{M_{Ed}}{\mu_d M_{pl,Rd}} \leq \alpha_M \quad (3\text{-}33)$$

Where

$\boldsymbol{M_{Ed}}$ is the greatest of the end moments and the maximum bending moment within the column length, including imperfections and second order effects

$\boldsymbol{M_{pl,N,Rd}}$ is the plastic bending resistance taking into account the normal force $\boldsymbol{N_{Ed}}$, given by $\boldsymbol{\mu_d M_{pl,Rd}}$

$\boldsymbol{M_{pl,Rd}}$ is the plastic bending resistance given by Point B in Section above

$\boldsymbol{\alpha_M}$ = 0.9 for *S*235, *S*275, *S*355

= 0.8 for other steel grades

Within the column length, second-order effects may be allowed for by multiplying the greatest first-order design bending moment by a factor *k* given by:

$$k = \frac{\beta}{1-N_{Ed}/N_{cr,eff}} \tag{3-34}$$

The second-order effect should be considered for both moments from initial member imperfection and from first-order analysis, as illustrated in Figure 3.7 (Johnson and Anderson, 2004).

Thus, the design moment, considering the second-order effect, is calculated as:

$$M_{Ed} = k_0 N_{Ed} e_0 + k_1 M_{Ed,1} \quad \geq M_{Ed,1} \tag{3-35}$$

Where, $\boldsymbol{k_0}$ *and* $\boldsymbol{k_1}$ are magnification factors for imperfection moment and first order equivalent moment respectively, $\boldsymbol{M_{Ed,1}}$ is the maximum first-order design moment in column length and $\boldsymbol{e_0}$ is the member imperfection, given by Table 3-4 above.

The equivalent moment factor $\boldsymbol{\beta}$ can be determined as given in the Table below.

$\boldsymbol{N_{cr,eff}}$ is the critical normal force for the relevant axis and corresponding to the effective flexural stiffness with the effective length taken as the column length. It can be calculated as:

$$N_{cr,eff} = \frac{\pi^2 (EI)_{eff,II}}{L^2} \tag{3-36}$$

The design value of effective flexural stiffness $(\boldsymbol{EI})_{\boldsymbol{eff,II}}$ should be determined from the following expression:

$$(EI)_{eff,II} = 0.9\left(E_a I_a + E_s I_s + E_e I_e + 0.5 E_{c,eff} I_c\right) \tag{3-37}$$

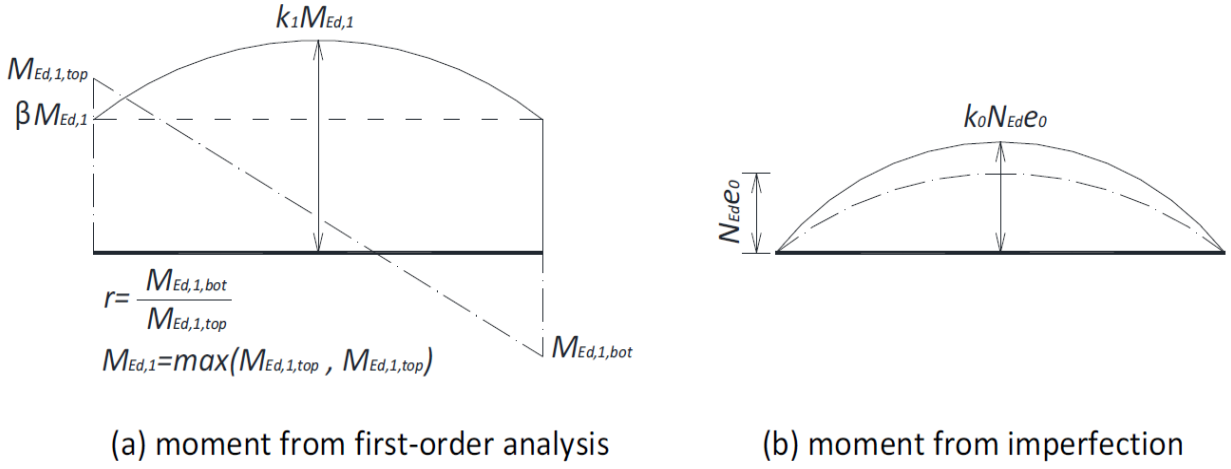

Figure 3-6: Amplifications for moments from first-order analysis and member imperfection (BC4:2015)

Table 3-6: Equivalent moment factor β

Moment distribution	Moment factors β	Comment
	First-order bending moment from member imperfection or lateral load: $\beta = 1.0$	M_{Ed} is the maximum bending moment within the column length ignoring second-order effects
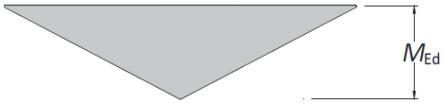		
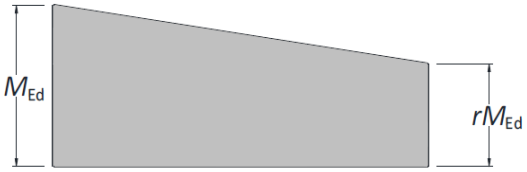	End moments: $\beta = max\,(0.44,\ 0.66 + 0.44r)$	M_{Ed} and rM_{Ed} are the end moments from first-order or second-order global effects

3.1.9 The resistance of Members to Combined Compression and Biaxial Bending

For combined compression and biaxial bending, the following conditions should be satisfied for the stability check within the column length and for the check at the column ends:

$$\frac{M_{y,Ed}}{\mu_{dy} M_{pl,y,Rd}} \leq \alpha_{M,y} \tag{3-38}$$

$$\frac{M_{z,Ed}}{\mu_{dz} M_{pl,z,Rd}} \leq \alpha_{M,z} \tag{3-39}$$

$$\frac{M_{y,Ed}}{\mu_{dy} M_{pl,y,Rd}} + \frac{M_{z,Ed}}{\mu_{dz} M_{pl,z,Rd}} \leq 1 \tag{3-40}$$

$\boldsymbol{M_{y,Ed}}$, $\boldsymbol{M_{z,Ed}}$ = the design bending moments around $y-y$ or $z-z$ axis including second-order effects and imperfects

$\boldsymbol{M_{pl,y,Rd}}$, $\boldsymbol{M_{pl,z,Rd}}$ = the plastic bending resistances around $y-y$ or $z-z$ axis

$\boldsymbol{\alpha_{M,y}}$, $\boldsymbol{\alpha_{M,z}}$ = 0.9 for *S*235, *S*275, *S*355

= 0.8 for other steel grades

The value $\boldsymbol{\mu_d}$ = $\boldsymbol{\mu_{dy}}$ *or* $\boldsymbol{\mu_{dz}}$ as shown Figure below, refers to the design plastic resistance moment $\boldsymbol{M_{pl,Rd}}$ for the plane of bending being considered. Values $\boldsymbol{\mu_d}$ greater than 1.0 should

only be used where the bending moment $\boldsymbol{M_{Ed}}$ depends directly on the compression force $\boldsymbol{N_{Ed}}$, for example where the moment $\boldsymbol{M_{Ed}}$ results from an eccentricity of the normal force $\boldsymbol{N_{Ed}}$.

For composite columns and compression members with biaxial bending the values $\boldsymbol{\mu_{dy}}$ *and* $\boldsymbol{\mu_{dz}}$ as shown in Figure below may be calculated separately for each axis. Imperfections should be considered only in the plane in which failure is expected to occur. If it is not evident which plane is the more critical, checks should be made for both planes. Irrespective of the axis, the value $\boldsymbol{\mu_d}$ can be interpolated according to Figure.

$\boldsymbol{N_{Ed} \leq N_{pm,Rd}/2}$:

$$\mu_d = 1 + \frac{2\,N_{Ed}}{N_{pm,Rd}} \left(\frac{M_{max,Rd}}{M_{pl,Rd}} - 1 \right) \tag{3-41}$$

$\boldsymbol{N_{pm,Rd}/2 < N_{Ed} \leq N_{pm,Rd}}$:

$$\mu_d = 1 + \frac{2(N_{pm,Rd} - N_{Ed})}{N_{pm,Rd}} \left(\frac{M_{max,Rd}}{M_{pl,Rd}} - 1 \right) \tag{3-42}$$

$\boldsymbol{N_{Ed} > N_{pm,Rd}}$:

$$\mu_d = 1 + \frac{N_{pl,Rd} - N_{Ed}}{N_{pl,Rd} - N_{pm,Rd}} \tag{3-43}$$

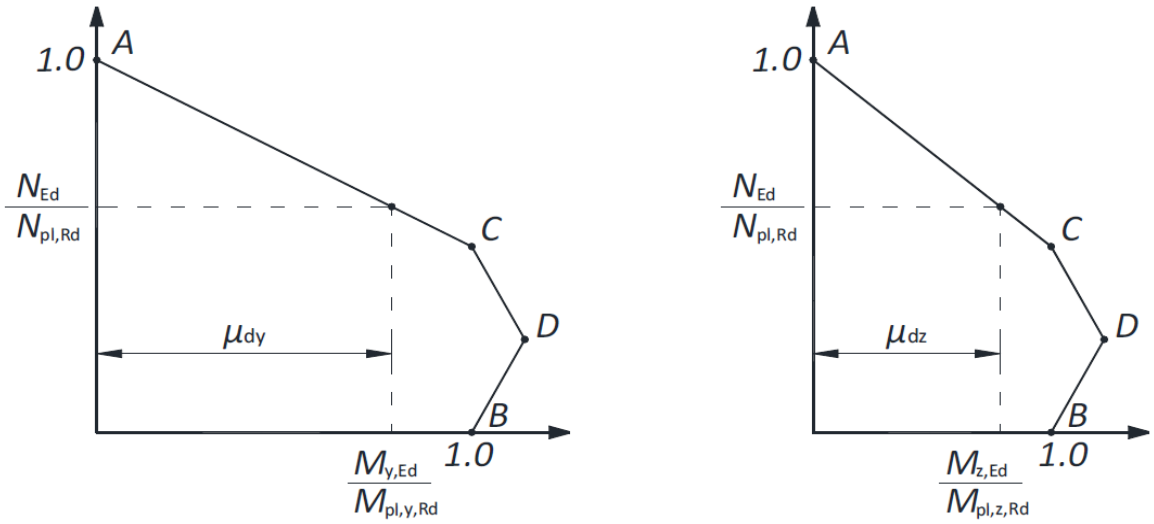

Figure 3-7: Interaction curves for the design of combined compression and biaxial bending

3.2 Analysis and Design of CFT Members According to AISC

3.2.1 Buckling load by the AISC Specifications

In late 2005, the American Institute of Steel Construction issued its most recent Specification for Structural Steel Buildings ANSI/AISC 360-05 (AISC, 2005) and its Seismic Provisions

ANSI/AISC 340-05 (AISC, 2005b). The changes for 2005 included the unification of both allowable strength design (ASD) and load and resistance factor design methods (LRFD) for steel (rolled and hollow structural sections), composite members (columns, beams, slabs), and connections. The recent revisions to those editions (AISC, 2010; AISC, 2010b) include a complete revamping of the methodologies for assessing the stability of framed structures that include the use of the nominal load approach, new provisions for composite structures (i.e. updated material requirements), and new design provisions for fire.

This section presents a brief summary of Chapter I.2.2 (Design of Composite Members, Axially Loaded Members, and Filled Composite Columns) of the AISC (2010) Specifications.

Analytical computation of the critical load, as recommended by the AISC (2010), assumes the following:

- The compressive capacity of the CFT column shall be determined by the limit state of flexural buckling governing by either inelastic or elastic buckling for short and slender columns, respectively.
- Some cross-section limitations shall be satisfied, such as:

1. The cross-sectional area of the HSS tube shall comprise at least 1 percent of the total composite cross-section; previous specifications did not address sections with 1 to 4 percent steel.
2. The maximum width-thickness ratio shall not exceed for RCFTs

$$h/t \leq 2.26\sqrt{E/F_y} \tag{3-44}$$

And for CCFTs

$$D/t \leq 0.15\,E/F_y \tag{3-45}$$

These limits are higher than those for conventional HSS steel-only columns (by 61% and 36%, respectively), and recognize the delay in local buckling due to the steel-concrete contact interaction.

In addition, some material limitations shall be satisfied. The concrete compressive strength must be higher than 20MPa and lower than 40MPa for lightweight concrete and 70MPa for normal concrete, respectively. The lower limit of 20MPa and the upper limit for lightweight concrete (40MPa) encourage the use of good quality concrete, while the upper limit of 70MPa was imposed to restrict the strength calculations related to brittle failure modes. Higher strength concrete is permitted if appropriate testing and analyses are conducted (Commentary AISC, 2005c). These material limitations reflect the range of material properties available from experimental testing (Commentary AISC, 2005c; Ziemian, 2010; Hajjar, 2000; Shanmugam and Lakshmi, 2001; Leon *et al.*, 2005; Goode, 2007).

The compression capacity also includes the effects of some initial residual stresses in the steel members resulting from the manufacturing or the welding process. The amount of the

accumulated initial residual stresses and its distribution in the steel member may have a wide dispersion. Previous studies, including different cross-section shapes and sizes, different steel types, and different manufacturing process, have confirmed a small reduction on the critical load due to residual stresses (Bjorhovde, 1972; Ziemian, 2010).

Last but not least, the element shall not exceed the allowable fabrication and erection tolerances given by the *Standard ASTM A6* (2009) or the *AISC Code of Standard Practice* (AISC, 2005d) for the steel components, and the *Specifications for Tolerances for Concrete Construction and Materials ACI-117* (2006) for the concrete components.

- The maximum initial out-of-straightness (δ_0) by the Standard ASTM A6 (2009) is limited for hot-rolled W shapes to 1/8"(3.175mm) for each 10 feet(3048mm) of length (L/960 exactly or L/1000 nominally), or 1 mm for each meter of length (L/1000), and 1/8"(3.175mm) for each 5 feet(1524mm) of length (L/480 or L/500 nominally) or 2 mm for each meter of length (L/500) for S, M, C, MC, L, T, Z and HSS shapes.
- The AISC Code of Standard Practice (AISC, 2005d) allows
    - A maximum out-of-plumbness $\Delta_0 = L/500$ (section 7.13.1.1 in AISC, 2005d), and
    - A maximum out-of-straightness $\delta_0 = L/1000$ (section 6.4.2 in AISC, 2005d).

All these Specifications are consequently applicable to composite members and, in particular for CFTs elements. The final initial imperfections are limited by the imperfection of the steel component plus some possible deformations during the erection and the concrete pouring processes.

Several previous research studies have proved the high influence of the initial imperfection on the buckling load capacity (Timoshenko and Gere, 1972; Bjorhovde, 1972; White and Hajjar, 1997; Ziemian, 2010). Thus, AISC equations E3-2 and E3-3 for the flexural buckling stress on steel members were established (since AISC, 1999) based on the SSRC-P2 column curve (Ziemian, 2010) that accounted for an average initial out-of-straightness of L/1470 observed statistically by Bjorhovde (1972) or L/1500 observed by Fukumoto *et al.* (1983). These design equations were also adapted for composite members since the AISC Specification published in 1999. Thus, imperfections higher than the limits adopted in the AISC Specifications will result in lower capacities of the flexural buckling load.

Unfortunately, there are no analytical equations where the value for the initial imperfection is explicitly expressed. Some Specifications or guidelines have suggested the use of multiple column curves (i.e. EC3 2005, EC4 2004 and CSA 2009) so the dispersion due to the initial imperfection and the manufacturing process can be implicitly accounted in the statistical analysis. A previous methodology that accounted for initial imperfection effects proposed reducing the strength with either a reduction strength factor (ϕ) or a safety factor (Ω). An example of the latter is the CRC column curve (Ziemian, 2010) for steel columns, which has its

basis in the tangent modulus theory with a safety factor that depends on the slenderness. Since in practice the straightness and plumpness are controlled and limited by the Standards (i.e. ASTM A6, 2009; AISC, 2005d; ACI-117, 2006), developments of analytical equations with geometric imperfections explicitly expressed are not practical for design purposes.

Thus, the nominal compression capacity of a CFT column (P_n) can be calculated as:

$$P_n = \begin{cases} P_o\left(0.658^{\frac{P_o}{P_e}}\right) & if \quad P_o/P_e \leq 2.25 \\ 0.877P_e & if \quad P_o/P_e > 2.25 \end{cases} \tag{3-46}$$

The cross-section compressive strength ($\boldsymbol{P_o}$) and the Euler load ($\boldsymbol{P_e}$) are computed by:

$$P_o = \begin{cases} A_s F_y + A_r F_{yr} + C_2 A_c f_c' & for\ compact\ sections \\ A_s F_{cr} + 0.7 f_c'(A_c + A_{sr} E_s/E_c) & for\ non-compact\ sections \end{cases} \tag{3-47}$$

$$P_e = \frac{\pi^2 E I_{eff}}{(KL)^2} \tag{3-48}$$

The concrete contribution ($\boldsymbol{A_c f_c'}$) to the compressive strength is affected by the effectiveness coefficient $\boldsymbol{C_2}$, classically assumed by the ACI as 0.85 for reinforced concrete members (Section 10.2.7 in ACI-318, 2008). This value was taken by the AISC (2010) for RCFTs but increased to 0.95 for CCFTs, recognizing the higher confinement in circular shapes (Commentary AISC, 2005c; Leon and Aho, 2002). Some research studies (i.e. Sakino *et al*., 2004; Chang and Mander, 1994, etc) or other specifications (i.e. Eurocode EC-4, 2004; AIJ, 2000) suggest a higher effectiveness for the confined concrete, especially for short columns with low $\mathrm{D/t}$ ratios. AISC chose to ignore this effect for simplicity.

Both the critical load and the Euler load depend on the given boundary conditions in the column. For ideal boundary conditions (i.e. "fixed" or "pinned" support), Table below has been commonly used to get both the theoretical and suggested values of the effective length factor (*K*), even when in practice these support types are developed only under idealized conditions. The AISC (2005) Specifications has proposed alternative approaches, such as the *direct analysis method (DAM)*, to avoid the use of effective length. However, such an approach has not been explored extensively in composite columns in general.

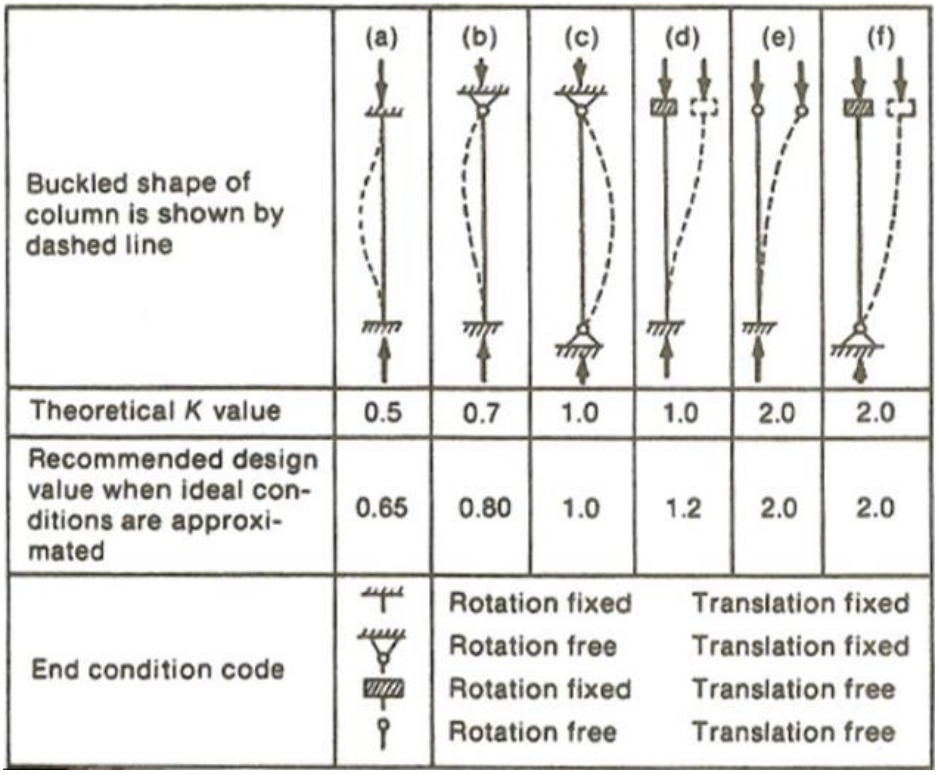

Figure 3-8: Theoretical and suggested K factors for different BCs (AISC Commentary, 2005)

The flexural effective stiffness ($\boldsymbol{EI_{eff}}$) in the above Equation also accounts for the contribution of the component materials (steel, reinforcement and concrete). The concrete contribution to the effective stiffness is given by a $\boldsymbol{C_3}$ the coefficient that depends on the structural steel ratio and is related to the influence of cracking and creep on the lateral buckling resistance (Commentary AISC, 2005c; Viest et al., 1997). Thus:

$$EI_{eff} = E_s I_s + E_s I_{sr} + C_3 E_c I_c \tag{3-49}$$

$$C_3 = 0.6 + 2\left(\frac{A_s}{A_c + A_s}\right) \leq 0.9 \tag{3-50}$$

As described in the AISC Commentary (AISC, 2005c), these design equations were calibrated with the available experimental data and adapted to provide a smooth transition from and to steel-only and concrete-only elements.

Concerning the flexural effective stiffness ($\boldsymbol{EI_{eff}}$), most specifications concur that this is the summation of the stiffness of each component, with a reduction mostly in the concrete component to account for cracking. Thus, ACI-318 (2008) accounts for the stiffness of steel and 20% of the concrete and a reductive factor $\boldsymbol{\beta_d}$ for sustained axial loads (Equation below).

$$EI = E_s I_s + \frac{0.2 E_c I_c}{1 + \beta_d} \tag{3-51}$$

In turn, the Eurocode EC4 (2004) provides two equations. The first Equation below is given for the determination of the slenderness (λ) and the elastic critical force (P_n). The second Equation, instead, is given for the determination of internal forces on second order analysis; the factor of 0.9 in the second Equation is roughly equivalent to that in the calculation of the effective stiffness used on the Direct Analysis Method (DAM) in the AISC (2010) Specifications for steel members.

$$EI_{eff,I} = E_s I_s + E_s I_{sr} + 0.6 E_c I_c \tag{3-52}$$

$$EI_{eff,II} = 0.9(E_s I_s + E_s I_{sr} + 0.5 E_c I_c) \tag{3-53}$$

The above Equation for P_n, which is similar to the one used for steel members in the AISC (2010) Spec., is valid in the inelastic buckling range (when $P_o/P_e \leq 2.25$ or $\lambda = \sqrt{P_o/P_e} = 1.5$), and for a second interval in the elastic buckling range where a reduced Euler load is used. The reductive factor 0.877 in the Euler load for the elastic buckling interval was proposed to account for geometric imperfection effects (White and Hajjar, 1997; Ziemian, 2010). On the other hand, the expression for the inelastic buckling range was obtained by curve fitting experimental data (Bjorhovde, 1972; Ziemian, 2010). Thus, the total reduction factor ($\chi = P_n/P_o$) on a column that accounts for initial imperfection, residual stresses, geometric and material non-linearities and stability effects is illustrated in Figure below.

$$\chi = \frac{P_n}{P_o} = \begin{cases} 0.658^{\lambda^2} & if\ \ \lambda = \sqrt{P_o/P_e} \leq 1.5 \\ 0.877/\lambda^2 & if\ \ \lambda = \sqrt{P_o/P_e} > 1.5 \end{cases} \tag{3.54}$$

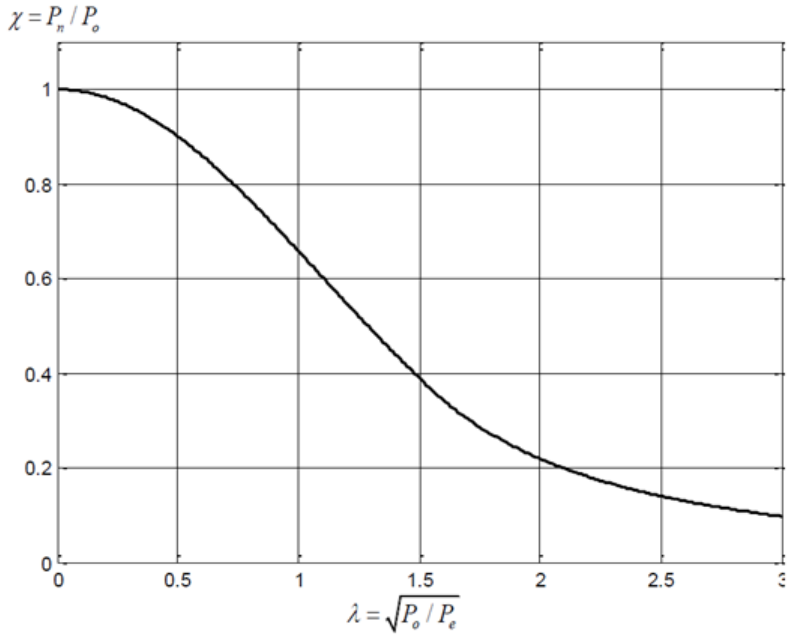

Figure 3-9: column curve by the AISC (2010) Specifications

3.2.2 P-M interaction diagram by the AISC Specifications

There are two methods allowed in the AISC Specifications (2010) for the determination of the interaction diagrams of composite cross-sections. These methods, first introduced in the 2005 version (AISC 2005a), have been widely used for reinforced concrete sections in the USA, and the ACI-318 code has allowed their use since 1963. These methods are:

(1) ***Plastic stress distribution method***: This method, illustrated in Figure below, aims to obtain the ultimate capacity of the cross-section assuming that both steel and concrete have reached their nominal plastic capacity, as there is little remaining strength in the section beyond this point. This method is a simplification of the *strain compatibility method* and assumes either an elastic-perfectly-plastic or fully plastic stress-strain (σ-ε) relationship as a material constitutive model for both the steel and concrete. No strain hardening or degradation either in strength or in stiffness is contemplated in this method. The yield stress of the steel in both compression and tension is the nominal F_y. The rectangular compressive block stress assumed for the concrete is taken as having an equivalent stress equal to $0.85f_c'$ (the same that has been given by ACI-318 for reinforced concrete cross-sections) for SRCs and RCFTs. This value is increased to $0.95f_c'$ in CCFTs to account for the superior confinement effect by the circular tube. The contribution of the concrete in tension is neglected. The current AISC procedure does not reduce the size of the compression block to that of an equivalent one as the ACI procedures do (β_1 factor).

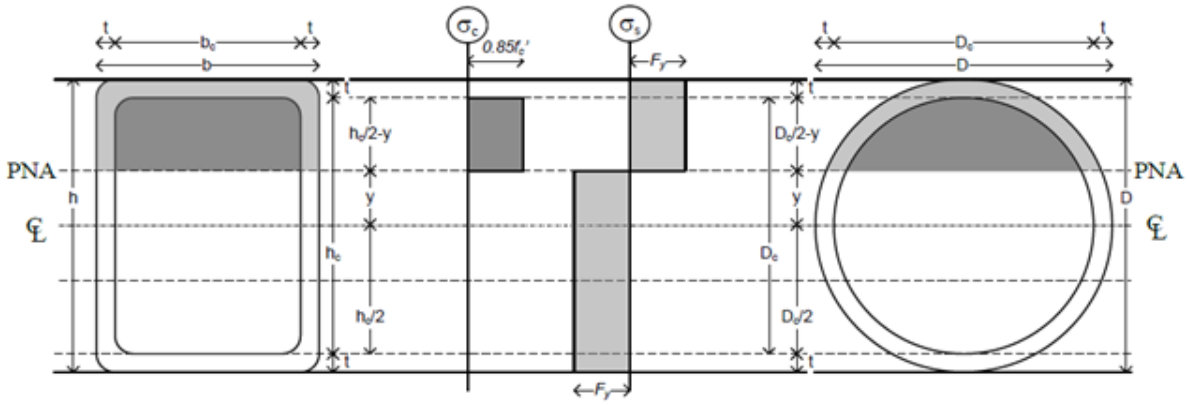

Figure 3-10: plastic stress distribution method

(2) ***Strain compatibility method***: In contrast to the plastic stress distribution method, this approach allows the constitutive material σ-ε models for both the concrete and the steel to be assumed in a more generalized form, as long as they represent the material behavior as supported by experimental tests. The stresses in the cross-section then are defined by the σ-ε model used under the assumption that plane sections remain plane, as shown in Figure below, with an ultimate strain in the concrete of $\varepsilon_c = 0.003$. Since any constitutive σ-ε material models validated by tests and analytical investigations are allowed, including models that allow higher ductility due to the confinement effects, the usual strain limit of 0.003 of compression in concrete (ε_c) may be adjusted.

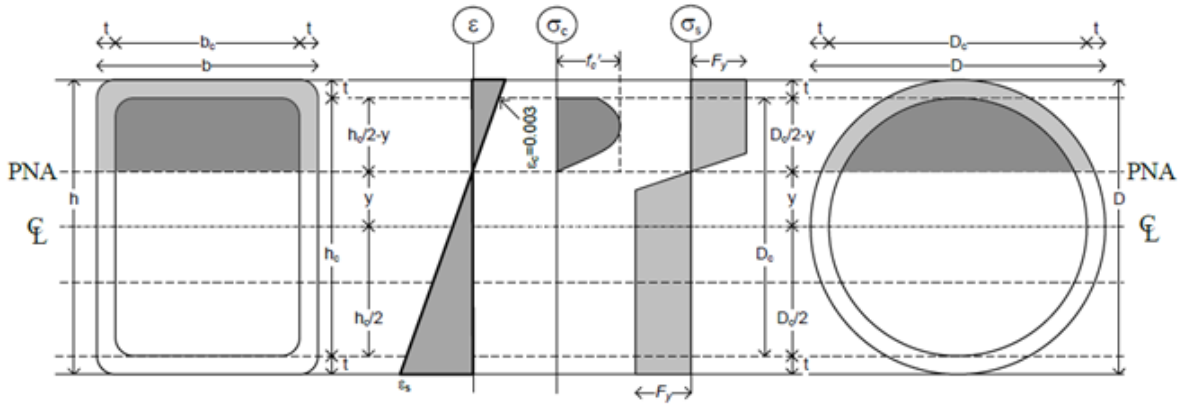

Figure 3-11: strain compatibility method

A single combination of P and M can be calculated by taking the maximum concrete strain (ε_c), linear distribution of strains across the section, and the corresponding stresses from the σ-ε material model. By sweeping the position of the neutral axis through the cross-section, a set of continuous points of resultant forces and moments (*P-M*) can be calculated. This set of points are illustrated in Figure below by the continuous curve, which defines the P-M interaction diagram obtained for the cross-section with the *strain compatibility method* for the case where $\varepsilon_c = 0.003$. If elastic-perfectly-plastic or fully-plastic σ-ε behavior is chosen as constitutive material models for both the steel (with F_y as plastic stress) and concrete (with plastic stress of $0.85f_c'$, or $0.95f_c'$ for CCFTs), the continuous curve obtained with the *strain compatibility method* passes over the AISC (2005) anchor points A-E-C-D-B obtained with the *plastic stress distribution method* assuming key positions of the neutral axis.

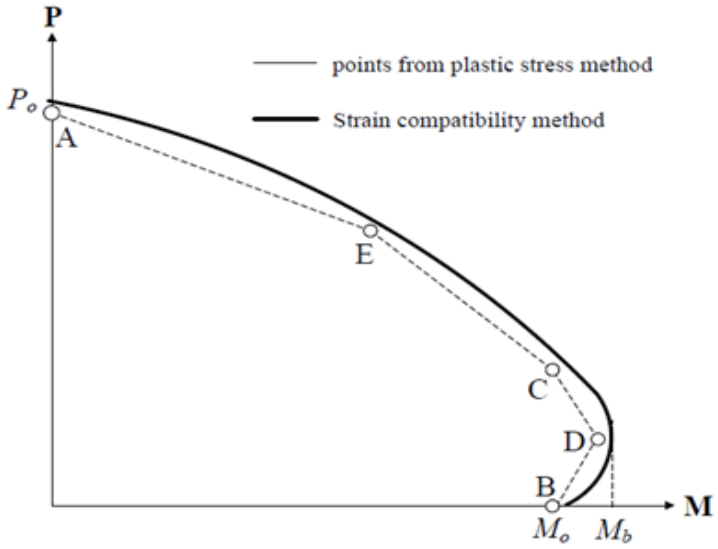

Figure 3-12: P-M interaction diagrams obtained with the plastic stress method and strain compatibility method

Based on the *plastic stress distribution method*, simplified equations for characteristic cases on simple cross-sections (symmetric and simple reinforcement distribution) are available in the *AISC Design Examples (2005)*. The characteristic or anchor points for conventional composite cross-sections evaluated by AISC include the following cases:

Point A is the column case when there is no bending, and so the cross section is in pure compression. The value of compression P_A is equal to the squash load P_o. For CFTs with no longitudinal reinforcement, this capacity is equal to the superposition of the steel and the concrete capacities.

$$P_A = P_o = P_s + P_c = A_s F_y + C_2 A_c f_c' \tag{3-55}$$

The coefficient $\boldsymbol{C_2}$ proposed in AISC (2005) is 0.85 for RCFTs and 0.95 for CCFTs.

Point B is the beam case when contrary to the previous case, there is no axial force and the cross-section is in pure bending. The pure bending moment (M_B) is the plastic moment of the cross-section (also referred to as M_o).

Point D is the balanced case for the beam-column when both the steel yields and the concrete crushes simultaneously. This point (P_D, M_D) corresponds to the highest plastic bending capacity (M_D) of the cross-section, which occurs when the plastic neutral axis (PNA) is located at the centroidal axis. The strength for CFTs (with no reinforcement) is equal to the concrete capacity axially and the superposition of steel and concrete flexural capacity for flexure.

$$P_D = \frac{P_c}{2} = \frac{C_2 A_c f_c'}{2} \tag{3-56}$$

$$M_D = M_s + M_c = Z_s F_y + \frac{1}{2} Z_c f_c' \tag{3-57}$$

As illustrated in Figure above, **Point C** has mirrored stresses to those of the pure bending point where, after some algebraic operations, it can be shown that this point (P_C, M_C) is defined for CFTs with no reinforcement by the concrete capacity ($\boldsymbol{P_c}$) and the moment of pure bending capacity (M_B).

$$P_C = P_c = C_2 A_c f_c' \tag{3-58}$$

$$M_C = M_B \tag{3-59}$$

Point E is an optional intermediate case between points A and C. For some cross-sections with certain geometries, the point E is very close (but always above) the straight line between the points A and C. This point E is useful mainly for SRC under weak axis bending and CFTs dominated by the steel contribution, where there is a non-linear transition between the points A and C.

Thus, the union of those characteristic neutral axis locations, or anchor points, by straight lines, as illustrated in Figures below by the dash-dot multiline A-E-C-D-B or A-C-D-B, defines the P-M interaction diagram obtained for the cross-section with the plastic stress distribution method. For asymmetric or more complex cross-sections, the *strain compatibility method* should be used. Even for that case, however, the overall shape of the interaction diagram does not change significantly from those shown in these figures.

Using either the *plastic stress distribution* or the *strain compatibility* method for the P-M interaction diagram of the cross-section, the axial capacity should be multiplied by a reduction factor (χ) that accounts for the stability effects (i.e. the geometric and material non-linearities, the initial imperfection and the steel residual stresses) on the P-M interaction diagrams of beam columns. The stability reduction factor ($\chi = P_n/P_o$) is calculated for the pure compression condition (Figure 3-13), where the squash load (P_o) at point A is reduced to the critical load (P_n) at the point A_λ by equations given in AISC. As illustrated in Figure 3-13, the point C obtained with the stress distribution method is also reduced by χ to the points C_λ. In addition, all the calculated points from A to C should be also reduced by the χ factor. Since the reduced balance point D drops outside of the P-M cross-section envelope, the bulge defined by C-D-B is neglected and replaced with a straight line defined by C-B. Thus, the P-M interaction diagram of the beam-column from the plastic stress distribution method is defined by the points A_λ-E_λ-C_λ-D (discontinuous line for the beam-column strength in Figure 3-14), or simply by the bilinear A_λ-C_λ-D interaction diagram (called *P-M Simplified* in the AISC-05 Specifications). As shown in Figure 3-14 (continuous curve for the beam-column strength), the set of points between A and C obtained with the strain compatibility method should be reduced by the stability factor χ to A_λ and C_λ, respectively, and a straight line from D to C_λ (without the bulge) drawn to complete the diagram. The P-M interaction diagram for composite beam-columns is then defined by the shaded area shown on Figure 3-13 and Figure 3-14. Depending on whether LRFD or ASD is used, the P-M envelope circumscribed by A_λ-C_λ-D then is reduced by the corresponding strength reduction factors ($\phi_c = 0.75, \phi_b = 0.90$) or the safety factors ($\Omega_c = 2.00$, $\Omega_b = 1.67$) for design purposes. The P-M interaction diagram by the AISC Specifications for composite beam-columns was established based on calibration with previous experimental data (Leon, Kim and Hajjar, 2007).

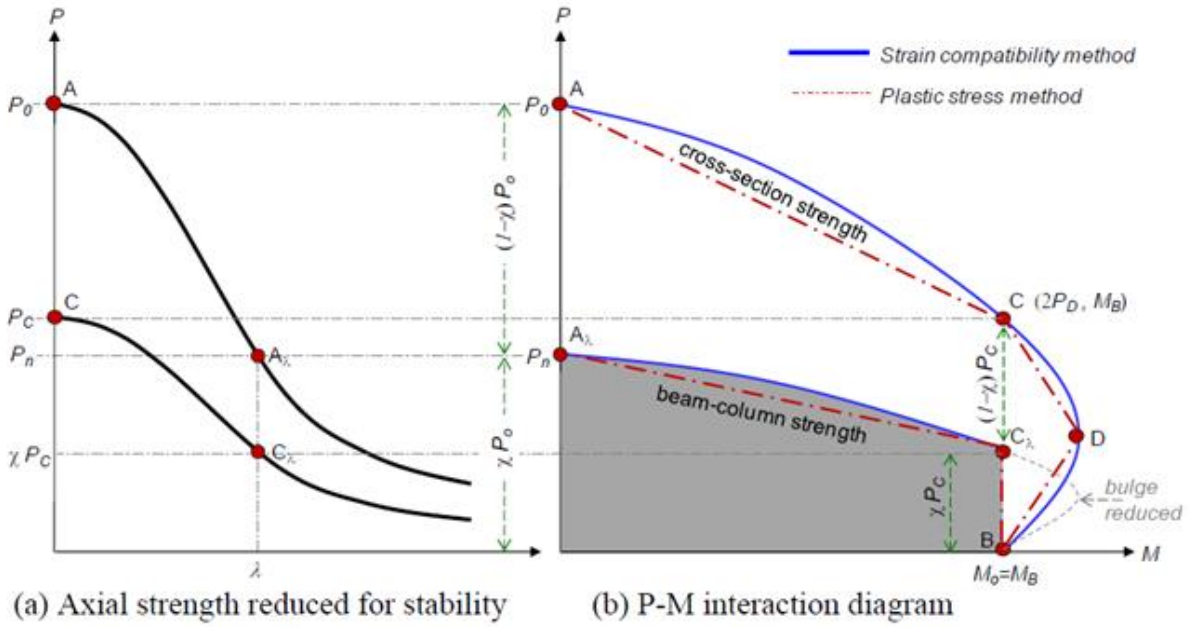

Figure 3-13: Reduction by the AISC (2005) Specifications on the P-M cross-section by the stability effects factor χ to get the P-M strength on composite beam-columns

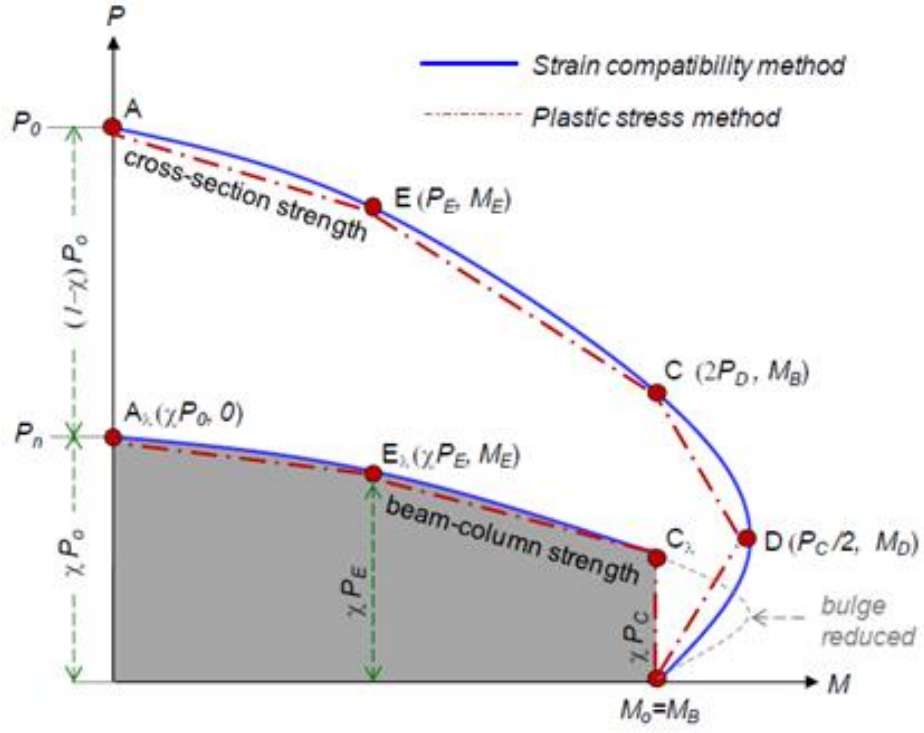

Figure 3-14: P-M interaction diagram for composite cross-sections (stocky columns) and beam-columns (reduced by stability effects) by the AISC (2005) Specifications

CHAPTER FOUR

NONLINEAR INELASTIC NUMERICAL ANALYSIS of CIRCULAR CFT COLUMNS and BEAM-COLUMNS

4.1 Introduction

The ordinary structural design process is based on the elastic behavior of the structural elements or the so-called first-order analysis. In this case, it is necessary to follow two types of verifications: the resistance capacity to guarantee the structural safety and the serviceability to ensure the proper function during the working life.

Since the real structural behavior is often complex, the designers usually employ simplified analysis methodologies to verify these two requirements. Basically, these methodologies are based on a simple material structural behavior; most of the times a linear and elastic behavior is used, and the assumption that the structural deformation due to the internal efforts is irrelevant and that it does not influence those efforts.

Although this is a normal procedure, there are some structures that require a more detailed analysis to guarantee a truthful result. For these structures, the linear first-order analysis must be replaced by a more reliable structural analysis methodology that can simulate the proper material behavior and the influence of the structural deformation during the loading procedure.

The real material behavior can be simplified to obtain the desired constitutive law according to the analysis methodology that was selected to study the structural behavior. For design purposes, elastic and plastic analyses are often chosen because they are based on simple stress-strain relationship. In the plastic analysis and design, the collapse load becomes the design criterion and this load is found from the material strength in the plastic range. This is a fast methodology that can provide a remarkable economy since the sections required by this method are smaller than those required by elastic analysis.

Although material nonlinearity is one of the most important sources of nonlinear structural behavior, it is important to realize that this nonlinearity is often associated with a nonlinear geometric behavior, namely in slender structures because those can have a significant nonlinear response before reaching the resistant capacity. If an elastic behavior is expected when a large loading is applied, then it is possible to exclude the material nonlinearity and in this case, only a nonlinear geometric analysis can be done. In this case, the source of the nonlinearity is related with initial imperfections in the structural members, global deformation of the structure (P-Δ effect) or local deformation of the structural members (P-δ effect).

In real life, the structural behavior is always nonlinear and the simplified analysis is only valid for small stress levels and for specific configurations where the linear equilibrium is possible. However, there are structures in which it is impossible to apply these simplifications and their analysis can only be performed with a nonlinear methodology.

Thus, a geometric nonlinear analysis is carried out when a structure undergoes large displacements and the change of its geometric shape causes a nonlinear displacement-strain relationship. In this case, the structure exhibits a significant change of its shape under applied loads such that the resulting large displacements change the coordinates of the structure or additional loads induced. So, the equilibrium relationships are written with respect to the deformed structural shape and the analysis is referred to as a second-order analysis. Unlike the first-order analysis, a second-order analysis requires an iterative procedure to obtain solutions since the deformed shape is not known during the equilibrium formulation.

4.2 Material constitutive models

The material constitutive relationship acts as the backbone for the nonlinear inelastic analyses. The modeling of steel and concrete including the confinement and local buckling effects is very essential for both strength and ductility of the concrete filled steel tube composite columns.

4.2.1 Stress-strain relation for confined concrete in CFT

The concrete confinement effect increases both the strength and ductility of concrete in CFT columns. For a slender structural member with significant second-order effects, the eccentricity of the axial force at the critical section becomes so large that the confinement effect on the concrete will be insignificant. In contrast, the descending branch of the concrete stress-strain relation is critical for the representation of the softening behavior of the post-peak of the slender CFT columns. Clearly, the softening response is very sensitive to the numerical solution scheme.

Most of the previous studies concentrated on short columns with normal strength materials and the study of the influence of high strength materials, confinment effect and steel tube local buckling for slender columns subjected to eccentric loading was not completely established. The model that was used by Liang (2009) was valid for both normal and high strength materials with accurate lateral confinement pressure model and was widely used by many researchers in recent time but it does not consider the degradation of confinement due to curvature effect for slender eccentrically loaded members.

In this paper, a model that captures the best features of the previous models were developed as described below and verified with experimental data showing more accurate results. The ascending branch skeleton is based on the model of Sakino et al (2004) whose skeleton best fits with experimental data and its stress-strain curve is represented using the equation 4-1 below

$$Y = \frac{AX + BX^2}{1 + CX + DX^2} \tag{4-1}$$

$$Y = \frac{\sigma}{f_{cc}} \quad ; \quad X = \frac{\varepsilon_c}{\varepsilon_{cc}} \quad ; \quad A = \frac{E_{cc} * \varepsilon_c}{f_{cc}} \tag{4-2}$$

$$B = 0.5 - 0.00171 * f_{cc} + 2.39 * \sqrt{f_{reff}} \tag{4-3}$$

$$C = A - 2 \quad ; \quad D = B + 1 \tag{4-4}$$

The ascending portion of the stress-strain curve is defined by the point of maximum concrete stress f_{cc} and the corresponding concrete strain ε_{cc}. As described in Liang's model (2009) these can be determined using the equations of Richart et al. (1928) modified with the strength reduction factor γ_c as follows:

$$f_{cc} = \begin{cases} \gamma_c f'_c + k_1 f_{r,eff} & \text{for circular cfst columns} \\ \gamma_c f'_c & \text{fo rectangular cfst columns} \end{cases} \quad (4\text{-}5)$$

$$\varepsilon'_{cc} = \begin{cases} \varepsilon'_c \left(1 + k_2 \frac{f_{r,eff}}{\gamma_c f'_c}\right) & \text{for circular cfst columns} \\ \varepsilon'_c & \text{for rectangular cfst columns} \end{cases} \quad (4\text{-}6)$$

Where $\boldsymbol{f_{r,eff}}$ is the effective lateral confining pressure on the concrete core and k_1 and k_2 are constants that was determined by experiments according to Richart et al. [1928], and are taken as 4.1 and 20.5 respectively.

$\boldsymbol{\gamma_c}$ is the strength reduction factor which accounts for effects of the column size, the quality of concrete and the loading rates on the concrete compressive strength. The strength reduction factor $\boldsymbol{\gamma_c}$ proposed by Liang [2009 part: 1] is expressed by

$$\gamma_c = 1.85 {D_c}^{-0.135} \qquad (0.85 \leq \gamma_c \leq 1.0) \quad (4\text{-}7)$$

Where D_c is the diameter of the concrete core for circular CFT columns and taken as the larger of (B−2t) and (D−2t) for a rectangular cross-section, B is the width of the cross-section, D is the depth of the cross-section, and t is the thickness of the steel tube wall.

The strain ε_c' is the strain at f_c' of unconfined concrete and can be taken as

$$\varepsilon'_c = \begin{cases} 0.002, & for\ \gamma_c f'_c \leq 28(MPa) \\ 0.002 + \frac{\gamma_c f'_c - 28}{54000}, & for\ 28 < \gamma_c f'_c \leq 82(MPa) \\ 0.003, & for\ \gamma_c f'_c > 82(MPa) \end{cases} \quad (4\text{-}8)$$

The accuracy of numerical techniques for circular CFT columns relies on the use of an accurate lateral confining pressure model for confined concrete. The lateral confining pressure depends on both the material properties and geometry of the column.

An accurate model for confining pressure was proposed by Liang and Fragomeni based on experimental results and numerical analyses was used in this study and described as follows from study [Qing Quan Liang and Sam Fragomeni (2009)]

$$f_{rp} = \begin{cases} 0.7(\nu_e - \nu_s)\frac{2t}{D-2t}\, f_{sy}, & for\ D/t \leq 47 \\ \left(0.006241 - 0.0000357\frac{D}{t}\right) f_{sy}, & for\ 47 < D/t \leq 150 \end{cases} \quad (4\text{-}9)$$

Where, $\boldsymbol{\nu_e}$ and $\boldsymbol{\nu_s}$ are the Poisson's ratios of a steel tube with and without in-fill concrete respectively. The Poisson's ratio $\boldsymbol{\nu_s}$ is taken as 0.5 at the maximum strength point and $\boldsymbol{\nu_e}$ according to Tang et al. [1996] is given by

$$\nu_e = 0.2312 + 0.3582\nu'_e - 0.1524\left(\frac{f'_c}{f_{sy}}\right) + 4.843\nu'_e\left(\frac{f'_c}{f_{sy}}\right) - 9.169\left(\frac{f'_c}{f_{sy}}\right)^2 \quad (4\text{-}10)$$

$$\nu'_e = 0.881\times10^{-6}(D/t)^3 - 2.58\times10^{-4}(D/t)^2 + 1.953\times10^{-2}(D/t) + 0.4011 \quad (4\text{-}11)$$

The proposed Eq. (4-9) is applicable to both normal and high strength materials.

When the curvature of the CFT section continues to build up, the concrete will keep losing effective confinement and the effective confining pressure will approach zero slowly. Therefore, the effective confining pressure can be related to a curvature-dependent reduction factor Φ (i.e. $\boldsymbol{f_{r,eff} = \Phi f_{rp}}$; $\boldsymbol{0 < \Phi \leq 1}$), and used to determine $\boldsymbol{f_{cc}}$ [Ouyang and Ho (2015)].

$$\Phi = e^{-15\phi} \quad (4\text{-}12)$$

The descending parts of the stress-strain curve for circular CFT columns are defined by Liang (2009a) as

$$\sigma_c = \begin{cases} \beta_c f'_{cc} + \left(\frac{\varepsilon_{cu}-\varepsilon_c}{\varepsilon_{cu}-\varepsilon'_{cc}}\right)\left(f'_{cc} - \beta_c f'_{cc}\right), & for\ \varepsilon'_{cc} < \varepsilon_c \leq \varepsilon_{cu} \\ \beta_c f'_{cc}, & for\ \varepsilon_c > \varepsilon_{cu} \end{cases} \quad (4\text{-}13)$$

And for rectangular CFT columns by Liang (2009a) as

$$\sigma_c = \begin{cases} f_{cc} & for\ \varepsilon_{cc} < \varepsilon_c < 0.005 \\ \beta_c f_{cc} + 100(0.015 - \varepsilon_c)\left(f'_{cc} - \beta_c f'_{cc}\right), & for\ 0.005 < \varepsilon_c \leq 0.015 \\ \beta_c f_{cc} & for\ \varepsilon_c > 0.015 \end{cases} \quad (4\text{-}14)$$

Where $\boldsymbol{\varepsilon_{cu}}$ is taken as 0.02 based on experimental results and $\boldsymbol{\beta_c}$ reflects the confinement effect provided by the steel tube on the post-peak strength and ductility of confined concrete.

For circular CFT column, an empirical equation for $\boldsymbol{\beta_c}$ used by Liang is adopted in this study and it was initially proposed by Hu et al. [2003], expressed by

$$\beta_c = \begin{cases} 1.0, & for\ D/t \leq 40 \\ 0.0000339(D/t)^2 - 0.010085(D/t) + 1.3491, & for\ 40 < D/t \leq 150 \end{cases} \quad (4\text{-}15)$$

And for rectangular CFT columns, it was proposed by Liang (2009a) based on experimental results presented by Tomii and Sakino (1979) and is given by

$$\beta_c = \begin{cases} 1.0 & for\ B_s/t \leq 24 \\ 1.5 - B_s/48t & for\ 24 < B_s/t \leq 48 \\ 0.5 & for\ B_s/t > 48 \end{cases} \quad (4\text{-}16)$$

Where $\boldsymbol{B_s}$ is taken as the larger of B and D for a rectangular cross-section.

4.2.2 The behavior of concrete in tension

Tension stiffening is an important phenomenon that should be included for an accurate analysis of sections under bending and axial load. Neglecting tension strength of concrete could lead to a loss in the smoothness of moment-curvature curves due to the sudden drop in stress from the cracking strength to zero at the onset cracking. In addition, tension stiffening results in a small change in peak strength, but this is usually negligible (Chiorean 2013).

Generally, the models that modify the constitutive equation of concrete, in which the descending branch of the tensile stress-strain curve of concrete is modified to take into account the tension-stiffening effect in an average way, are more widely used. The model to account for tension stiffening, developed by R.S.B. Stramandinoli and H.L. La Rovere (2008) is taken into account in the present study. Concrete is assumed to behave like a linear-elastic material until its tensile strength is reached so that a straight line defines initially the stress-strain curve. In the post-cracking range, an exponential decay curve is adopted until yielding of reinforcement takes place, and is defined by the following equation.

$$\sigma_{ct} = f_{ct} e^{-\alpha\left(\frac{\varepsilon_c}{\varepsilon_{cr}}\right)} \quad (4\text{-}17)$$

Where, f_{ct} is the concrete tensile strength and "ε_{cr} is the corresponding strain; α is an exponential decay parameter. An expression for the exponential decay parameter was described by the following equation:

$$\alpha = 0.017 + 0.255(n\rho) - 0.106(n\rho)^2 + 0.016(n\rho)^3 \quad (4\text{-}18)$$

In which ρ is the reinforcement ratio equal to ($\rho = \mathrm{A_s}/\mathrm{A_c}$) and n is the modular ratio of the steel-to-concrete ($n = \mathrm{E_s}/\mathrm{E_c}$).

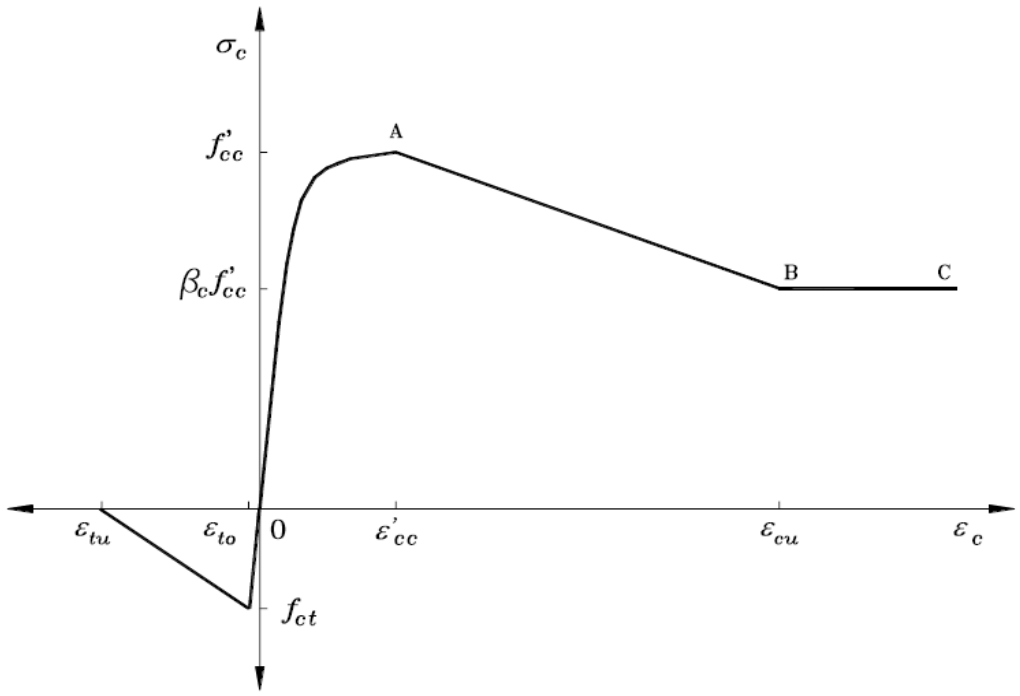

Figure 4-1: General stress-strain curve model for confined concrete in Circular CFT columns

4.2.3 Stress-strain relation for steel

The primary features of the behavior of steel components of composite members are plasticity, residual stress, and local buckling. This section describes a uniaxial steel constitutive relation that accounts for these features. The stress-strain backbone curves used by Tort and Hajjar (2007) for rectangular and Denavit and Hajjar (2010) for circular sections are adopted in this study. The models are based on the incremental bounding surface formulation proposed by Shen *et al*. (1995), with modifications for CFT members to better account for local buckling, residual strains and the hysteretic rules in the non-linear cyclic response.

According to Tort and Hajjar (2007) and Denavit and Hajjar (2010), the initiation of the local buckling starts at a strain given by:

$$\varepsilon_{lb} = \begin{cases} 0.214R^{-1.41}\left(F_y/E_s\right) & for\ CCFT \\ 3.14R^{-1.48}\left(F_y/E_s\right) & for\ RCFT \end{cases} \tag{4-19}$$

Where the factor R is given by:

$$R = \begin{cases} D/t\,.\left(F_y/E_s\right) & for\ CCFT \\ h/t\,\sqrt{F_y/E_s} & for\ RCFT \end{cases} \tag{4-20}$$

The previous equations can be rewritten in terms of the yielding strain (ε_y) and the wall-slenderness ratio (λ) of the steel tube as shown in Equation below.

$$\varepsilon_{lb} = \begin{cases} 0.214\lambda^{-1.41}{\varepsilon_y}^{-0.41} & for\ CCFT \\ 3.14\lambda^{-1.48}{\varepsilon_y}^{0.26} & for\ RCFT \end{cases} \quad (4\text{-}21)$$

Once the local buckling strain calculated with the previous equation has been exceeded, the stress-strain curve decays with a degradation slope calculated as:

$$K_s = \begin{cases} -E_s/30 & for\ CCFT \\ min[\,0, -3.22E_s(R-0.08)] & for\ RCFT \end{cases} \quad (4\text{-}22)$$

The previous descending branch becomes constant once the residual stress is achieved with a value defined as:

$$f_{rs} = \begin{cases} min[\,F_{lb}, 0.17\,F_{lb}/R] & for\ CCFT \\ min[\,F_{lb}, 0.16 - 0.73RF_{lb}] & for\ RCFT \end{cases} \quad (4\text{-}23)$$

In turn, the residual stresses are accounted in these formulations with an initial plastic strain, which is given by:

$${\varepsilon_0}^p = \begin{cases} 0.0006 & for\ CCFT \\ 0.0004 & for\ RCFT\ flat \\ 0.0006 & for\ RCFT\ corner \end{cases} \quad (4\text{-}24)$$

The steel tube in a CFT column is biaxially stressed due to the confinement effect and the presence of hoop tension in the steel tube reduces its yield stress in the longitudinal direction [P.K. Neogi, H.K. Sen, J.C. Chapman (1969)].

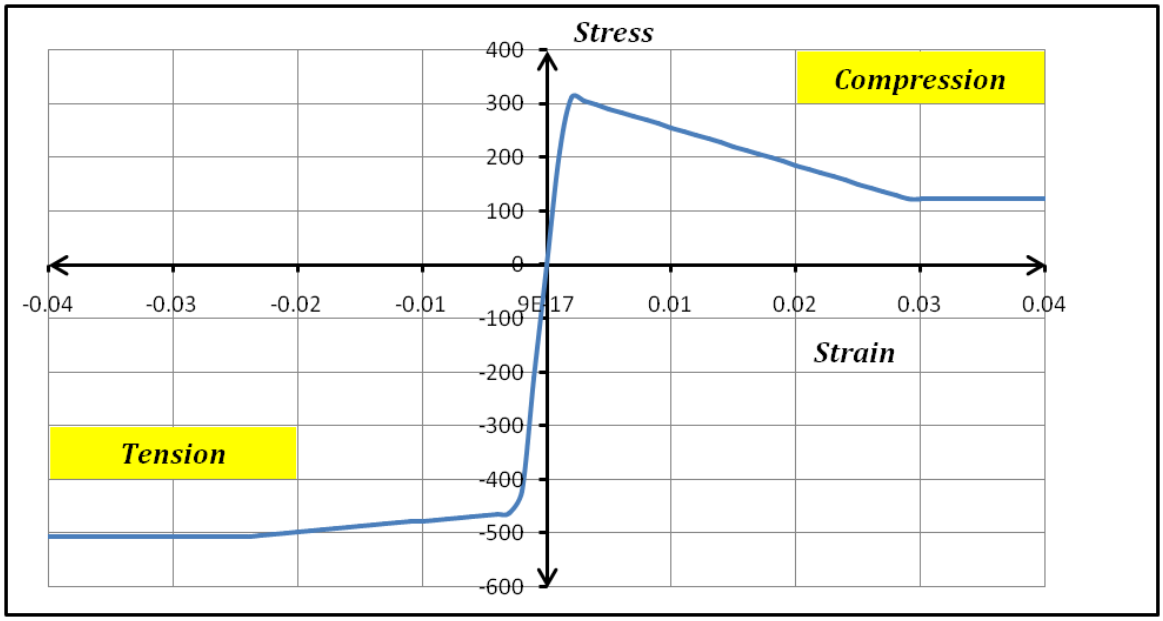

Figure 4-2: Typical stress-strain curve model for steel in CFT columns with local buckling and residual stress effects

4.3 Analysis of cross-sections

The nonlinear fiber element method has been found to be efficient for determining the ultimate strengths and inelastic moment–curvature responses of composite cross-sections under eccentric axial compression. For this analysis, it is assumed that there is no slippage between the steel tube and the concrete so that the cross-section remains plane after deformation, resulting in a linear strain distribution. Fiber stresses are calculated from fiber strains using material uniaxial stress-strain relationships incorporating confinement effects, tension-stiffening in concrete and local buckling of steel. The origin of the coordinate system is chosen at the centroid of the cross-section. Note that the fiber strain is a function of the curvature (φ) and the strain at the origin (ε_0) of the composite section subjected to axial load and bending.

4.3.1 Fiber - Section based analysis

Fiber element analysis is a numerical technique which models a structural element by dividing it into a number of two-end frame elements, and by linking each boundary to a discrete cross-section with a grid of fibers. The material stress-strain response in each fiber is integrated to get stress-resultant forces and rigidity terms, and from these, forces and rigidities over the length are obtained through finite element interpolation functions which must satisfy equilibrium and compatibility conditions.

There are several advantages which justify the use of fiber analysis. Some of these advantages include their ability to handle:

- *Complex cross-sections*: A fiber cross-section can have any general geometric configuration formed by sub-regions of simpler shapes; geometric properties of the more complex section are calculated through the numerical integration.
- *Tapered elements:* Since the length of the fiber is not considered, the cross-section defined at each of the two ends can be different, and therefore, the response of tapered members can be roughly estimated. Precision can be increased with more integration points.
- *Complex strength-strain behavior:* Since each fiber can have any stress-strain response, this technique allows modeling nonlinear behavior in steel members (steel σ-ε and residual stresses), reinforced concrete members (unconfined and confined concrete σ-ε, and steel reinforced σ-ε), and composite members.
- *Accuracy and efficiency*: Since each fiber is associated to a given uniaxial stress-strain (σ-ε) material response, higher accuracy, and more realistic behavior effects can be captured by a fiber-based model than in a frame-based model, and at less computing time than for a 3D finite-based model.

The concept behind the fiber section model is rather simple. The section is subdivided into *n* fibers (not necessarily of equal area) and the stresses are integrated over the cross-sectional area to obtain stress resultants such as force or moment.

Each fiber in the section can be assigned concrete or structural steel material properties. Making use of the ‘‘plane sections remain plane’’ assumption and from relevant constitutive models, fiber stresses are calculated from the fiber strains. There are different approaches to finding the fiber strains as the load history on the section progresses. The approach adopted in this study was that of Spacone et al. (1996a,b) which defines the section axial strain and curvatures with respect to a fixed reference system and do not need to trace the evolution of the position of the neutral axis. El-Tawil and Deierlein (2001a,b), on the other hand, follow the migration of the section neutral axis during the load history. A fiber section method is a powerful tool that can be used to estimate the cross-sectional strength for design purposes.

4.3.2 Strain and stress distributions

The strain and stress distributions for a cross-section under axial compression, uni-axial bending and combined axial compression and uni-axial bending are shown in Fig. 4-3 below for the case of a material with rounded stress-strain relationship.

For the pure axial load state (Fig. 4-3a), the strains are uniform throughout the cross-section at ϵ_A. When the uniform strain is less than the material yield strain, $\epsilon_A < \epsilon_y$, the cross-section stresses are below f_y, and when $\epsilon_A \geq \epsilon_y$ the cross-section is deforming inelastically according to the chosen material stress-strain curve, up to limiting ultimate values for the cross-section of ϵ_u and f_u.

For the case of simple bending (Fig. 4-3b), there is no uniform strain present, only linearly-varying flexural strains with a maximum value of ϵ_B. The strain and stress profiles are anti-symmetric about the zero strain neutral axis (which is located at mid-depth for symmetric sections), and the upper and lower outer-fibers reach $\pm\epsilon_u$ and $\pm f_u$.

The combination of an axial load and bending moment is illustrated in Fig. 4-3c, where the compressive outer-fiber strain is limited to ϵ_u. The interaction of axial strains and bending strains are taken as the summation of the uniform strains ϵ_A and the linearly varying strains with maximum magnitude ϵ_B. This combination leads to strain and stress profiles between the axial and flexural states. Although strains ϵ_A and ϵ_B are linearly superimposed, the stresses are based on the given material model. Therefore ϵ_A is not solely responsible for defining the axial force and neither is ϵ_B exclusive to bending; it is the combination of ϵ_A and ϵ_B that defines the axial and bending capacity.

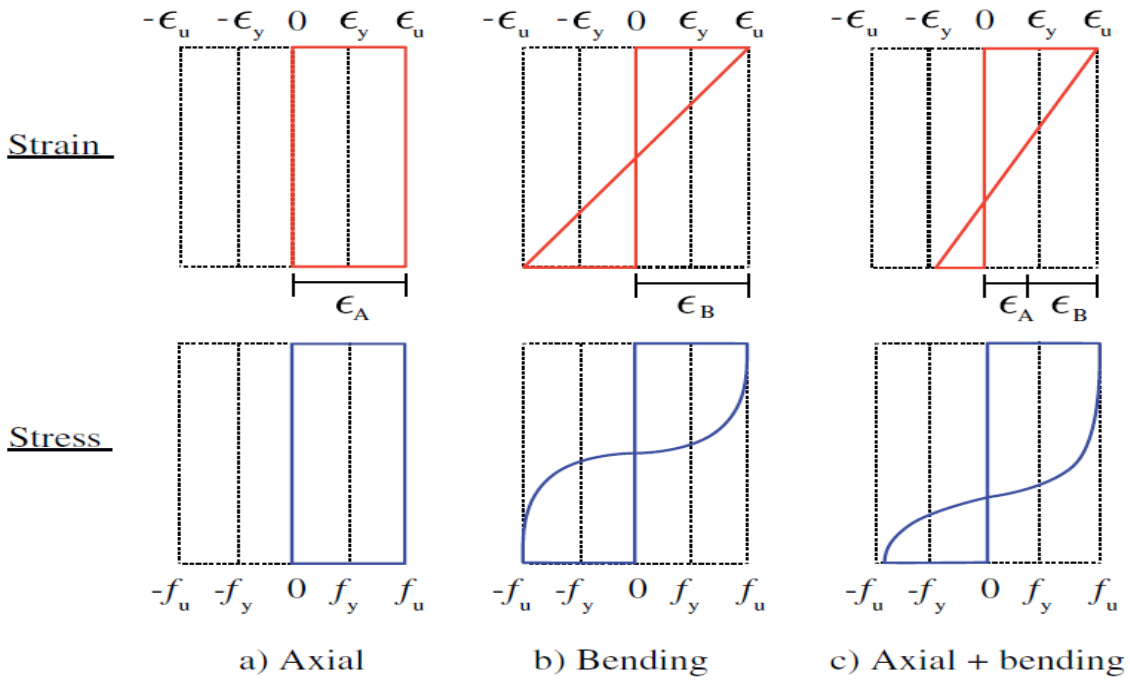

Figure 4-3: Cross-section strain and stress distributions under axial compression, uni-axial bending and combined axial compression and uni-axial bending (A. Liew et al. 2017)

4.3.3 Cross-section Discretisation

The cross-section to be investigated must first be divided into fiber layers, to convert the continuous cross-section into the discrete fiber sections; the greater the number of discrete layers, the closer the numerical approximation is to the exact solution. Once the cross-section has been discretized into small fibers and assigned coordinates ($\boldsymbol{y_i}$) and an area $\boldsymbol{A_i}$, the contribution for each can be summed to give the total cross-section response.

For rectangular hollow sections the definition of the elemental area $\boldsymbol{A_i}$ is straightforward, as the cross-section can be conveniently discretised into small rectangles. This can either be performed in strips that span the cross-section width or height, or by small elements that are organized across both directions of the cross-section. Here, the root radii r is also explicitly included in the discretisation, as their effect can be significant.

Circular and elliptical hollow sections need to be treated in a different manner, since dividing either shape into small rectangular elements is not as ideal, as an error will arise at the curved edges of the cross-section. For numerical analysis, the composite section was subdivided into a steel tube and concrete parts, and each of the steel tube and concrete sections was layered, as shown in Fig. below.

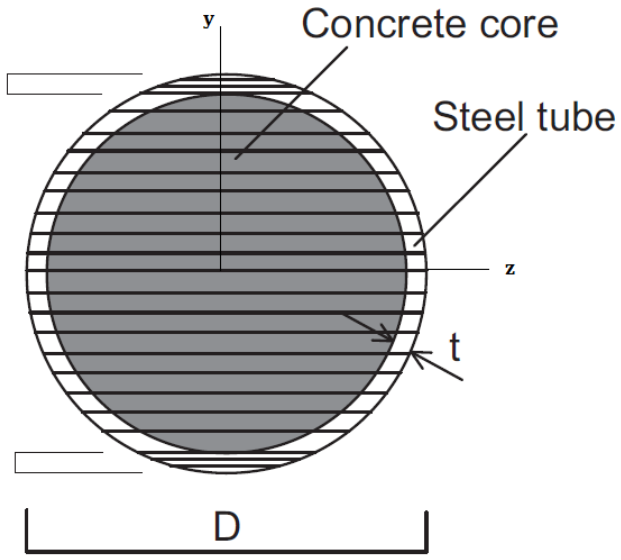

Figure 4-4: Cross-section Discretization

Once the cross-section is discretized, in using the Strain Compatibility Method (SCM) there are two relevant variables: the area of the layers ($\boldsymbol{A_i}$) and their respective positions ($\boldsymbol{y_i}$). Note that the total axial strain at the $\boldsymbol{i^{th}}$ slice,$\boldsymbol{\varepsilon_i}$, is given by a linear function. Therefore:

$$\varepsilon_i = \varepsilon_0 + \phi y_i \tag{4-25}$$

Where $\boldsymbol{y_i}$ is the distance between the centroid of the analyzed layer and the cross-section plastic centroids (PCs) taking PC of the cross-section as the origin of the local coordinate, $\boldsymbol{\varepsilon_0}$ is the membrane strain in the cross-section PC, and $\boldsymbol{\phi}$ its curvature.

4.3.4 Cross-section capacities

The axial forces and bending moments are obtained in the context of the Strain Compatibility Method (SCM). Compared to the simplified design codes procedures [EC, AISC], a more realistic approach is produced by the coupling of the deformed shape of section and the constitutive relationships of the materials comprising it. For the calculation of the axial load and bending moment acting on the cross-section, the following integration-to-discrete summed numerical approximations are used,

$$P = \sum_{i=1}^{ns} \sigma_{s,i} A_{s,i} + \sum_{j=1}^{nc} \sigma_{c,j} A_{c,j} \tag{4-26}$$

$$M = \sum_{i=1}^{ns} \sigma_{s,i} A_{s,i}\, y_i + \sum_{j=1}^{nc} \sigma_{c,j} A_{c,j} y_j \tag{4-27}$$

Where P is the axial force,$\sigma_{s,i}$ is the stress of steel fiber i, $A_{s,i}$ is the area of steel fiber i, $\sigma_{c,j}$ is the stress of concrete fiber j, $A_{c,j}$ is the area of concrete fiber j, y_i is the coordinate of steel element i's centroid, y_j is the coordinate of concrete element j's centroid, *ns* is the total number of steel fiber elements and *nc* is the total number of concrete fiber elements. It is important that a sufficient number of elements are used to represent the cross-section, such that the error in the

approximations for the axial load and bending moment capacities is small. These approximation errors arise from a coarse representation of the geometry affecting $\boldsymbol{y_i}$ and $\boldsymbol{A_i}$, particularly with regard to curved edges, leading to errors in $\boldsymbol{\epsilon_i}$ or by using too few elements that assuming a constant strain and stress for an element is unreasonable.

The ultimate axial load (P_o) of a composite cross section in the absence of bending can be obtained from the axial load–strain responses and the ultimate bending moment (M_o) from the axial load–moment–curvature responses.

4.3.5 Secant's method algorithms

4.3.5.1 Determining the neutral axis depth

Computational algorithms based on the Secant's method are developed to iterate the neutral axis depth in a CFT composite cross-section with material and geometrical non-linear effects. The neutral axis depth d_n of the composite cross-section is iteratively adjusted to maintain the force equilibrium. The Secant's method algorithm requires two initial values of the neutral axis depth $d_{n,1}$ and $d_{n,2}$ to start the iterative process. The neutral axis depth d_n is adjusted by using the following proposed equations:

$$d_{n,j+2} = d_{n,j+1} - \frac{(d_{n,j+1} - d_{n,j}) r_{pu,j+1}}{r_{pu,j+1} - r_{pu,j}} \tag{4-28}$$

Where the subscript **j** is the iteration number, and $\mathbf{r_{pu}}$ is the residual load (axial force or bending moment) that is given by

$$r_{pu} = external\ load - internal\ load \tag{4-29}$$

The equilibrium condition is satisfied when $|\boldsymbol{r_{pu}}| < \in_{\boldsymbol{k}}$, where $\in_{\boldsymbol{k}}$ is the prescribed convergence tolerance.

4.3.6 Cross-section's axial load–moment-curvature relationships

4.3.6.1 Theoretical formulation

For a given cross-section, such as an open or closed metal I-section or tubular section, moment–curvature ($M-\phi$) curves can be created. Such curves can be used to describe the behavior of each cross-section and subsequently the entire length of a structural member, subjected to a given applied load. Generating the $M-\phi$ curve is straightforward when there is no applied axial load since the strains throughout the cross-section are exclusive to flexure, which can be described as linearly varying with depth, with the highest strains at the outer fibers. This is based on the assumption that plane sections remain plane during bending, which has been shown to be valid for practical structural steel cross-sections in bending. This also stems from the fact that cross-section dimensions are generally considerably smaller than column lengths, permitting the

neglect of shear deformations. Combining this assumed strain profile with a particular material model, M– ϕ curves can be generated analytically.

The determination of M– ϕ curves in the presence of a given axial load is more challenging, due to the interaction between the axial and bending strains and material non-linearity. Finding accurate analytical curves for cross-section shapes typically used in structural applications and with more realistic material stress-strain curves are significantly more challenging as a continuous function is needed in the entire M– ϕ –N domain, which is initially straight in the elastic region and then transitions through to a curved shape in the inelastic regime.

In this study, iterative computational algorithms have been developed for determining the axial load–moment-curvature relationships for CFT column sections. For a given axial load increment, the corresponding ultimate moment capacity of the composite section is determined from the complete moment–curvature curve which is obtained by gradually increasing the curvature. For each curvature increment, the moment capacity is determined when the calculated axial force is equal to the applied axial load. The Secant method algorithms were developed and are used in the numerical model to iterate the neutral axis depth in a circular CFT columns section until equilibrium conditions are satisfied.

4.3.6.2 Computational procedure

For a given curvature, the corresponding internal axial force and bending moment are determined when the equilibrium of calculated internal axial force and applied external axial load is maintained. By repeating this process, a set of curvatures and corresponding bending moments is obtained and used to plot the axial load–moment–curvature curve. The computer flowchart for determining the axial load–moment–curvature response of circular CFT column sections is presented in Fig. below.

The main steps of the computational procedure are given as:

1) Input data.
2) Discretize the composite section into fiber elements.
3) Set initial curvature of the section $\phi = \Delta\phi$
4) Set starting neutral axis depths $d_{n,1} = 0,$ and $d_{n,2} = 20 * D$
5) Compute the axial strains at the centroid of the section ($\boldsymbol{\varepsilon_0}$) using $\boldsymbol{\phi}$ for both neutral axis depths $\mathbf{d_{n,1}}$ and $\mathbf{d_{n,2}}$;

$$\varepsilon_{0,i} = \phi(d_{n,i} - D/2)$$

6) Compute fiber stresses from fiber strains using material constitutive models.
7) Calculate the section axial forces **P**.
8) Compute $\mathbf{r_{pu,1}}$ and $\mathbf{r_{pu,2}}$ corresponding to $\mathbf{d_{n,1}}$ and $\mathbf{d_{n,2}}$, respectively

$$r_{pu} = P_{ext} - P$$

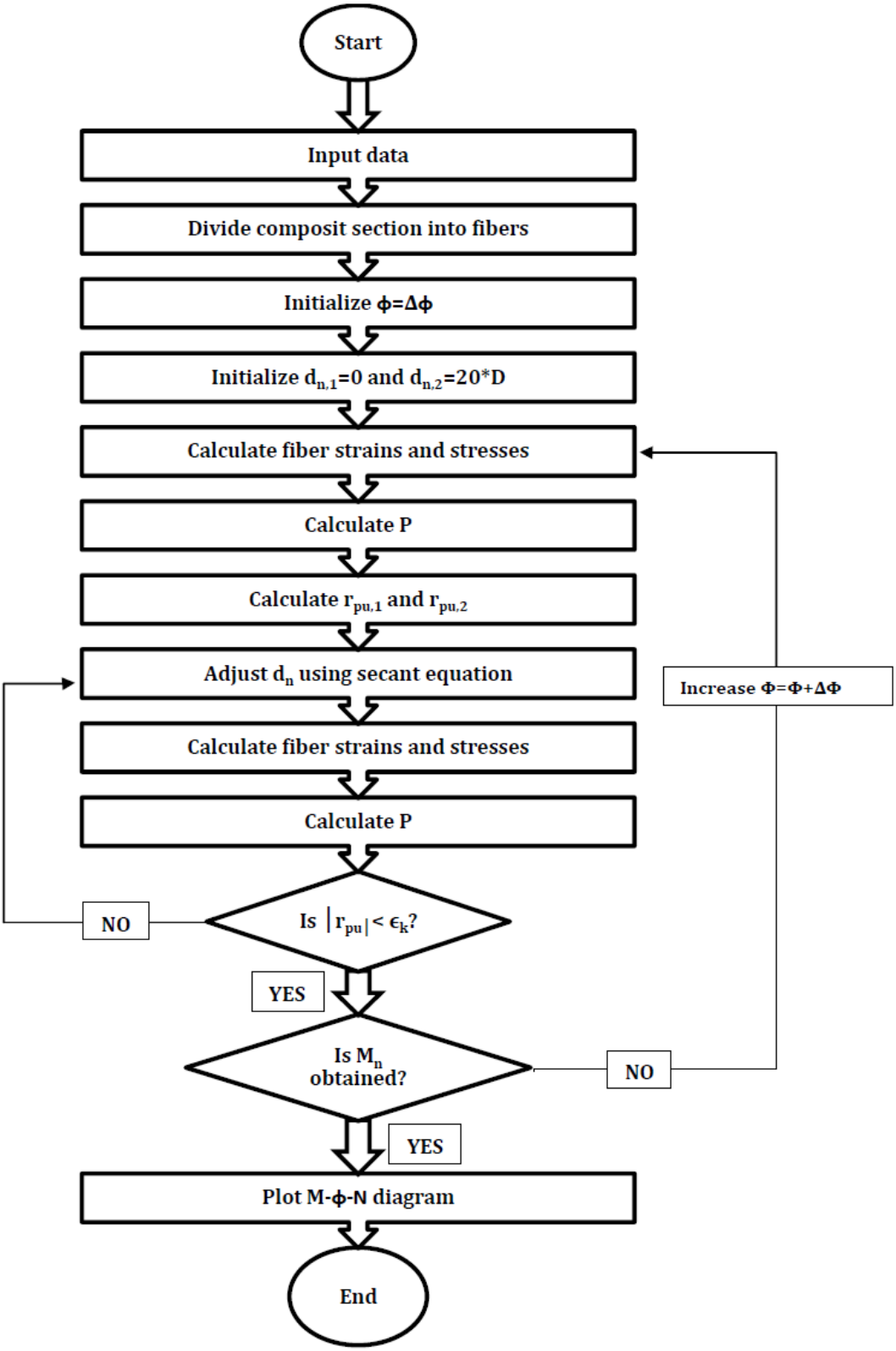

Figure 4-5: Flowchart for determining the Axial load-Moment-Curvature curve for circular CFT columns

9) Adjust the neutral axis depth $\mathbf{d_n}$ using Equation

$$d_{n,j+2} = d_{n,j+1} - \frac{(d_{n,j+1} - d_{n,j})r_{pu,j+1}}{r_{pu,j+1} - r_{pu,j}}$$

10) Update the axial strain at the centroid of the cross-section ($\boldsymbol{\varepsilon_0}$) of the section using $\boldsymbol{\phi}$ and the adjusted $\mathbf{d_n}$;

$$\varepsilon_0 = \phi(d_n - D/2)$$

11) Calculate fiber stresses from fiber strains using material constitutive models.
12) Compute the section axial force **P** and bending moment **M**.
13) Repeat steps **(9)–(13)** until $|\mathbf{r_{pu}}| < \epsilon_\mathbf{k}$
14) Increase the curvature of the section by $\phi = \phi + \Delta\phi$.
15) Repeat steps **(5)–(14)** until the ultimate bending moment $\mathbf{M_n}$ is obtained

The convergence tolerance $\epsilon_\mathbf{k}$ is set to $\mathbf{10^{-4}}$ in the analysis. The computational procedure proposed can predict the complete axial load–moment–curvature response of circular CFT columns section.

4.4 Structural system (Beam-Column member analysis)

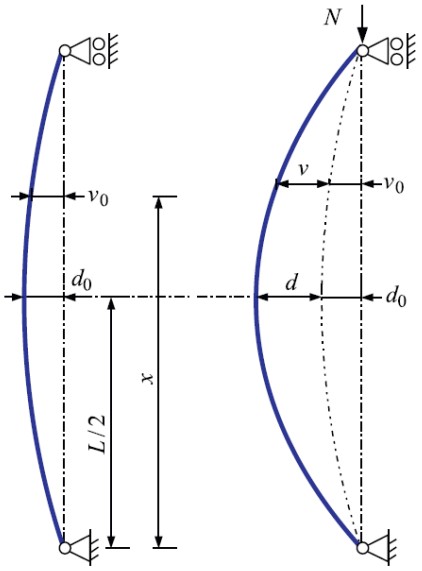

Figure 4-6: Pin-ended and concentrically loaded imperfect column

A pin-ended prismatic column of length L depicted in Fig which, in its unloaded state, has an imperfection $\boldsymbol{v_0}(x)$ with maximum mid-height magnitude $\boldsymbol{d_0}$. This function is an equivalent geometric imperfection distribution for the element, representing residual stresses and out-of-straightness. After the application of a concentric axial load N, a new total deflected shape $v_t =$

$v + v_0$ (initial $\boldsymbol{v_0}$ plus additional displacements $\boldsymbol{v}$), which is in equilibrium with the applied axial load, has a maximum displacement at $x = \mathrm{L}/2$ of $d_t = d + d_0$.

For a perfectly straight column, $d_0 = v_0 = 0$

4.4.1 Member Load–deflection analysis

4.4.1.1 Theoretical formulation

The load-deflection responses of circular CFT slender beam–columns under increased loading are influenced by the inelastic cross-sectional behavior, slenderness, eccentricity of loading and second order effects. The inelastic stability analysis of a slender beam–column must account for the geometric and material nonlinearities of the beam–column. A numerical model has been developed for the inelastic stability analysis of both normal and high strength circular CFT slender beam–columns, which incorporates the effects of both geometric and material nonlinearities.

The beam–column considered is pin-ended and subjected to single curvature bending. The pin-ended beam–column model is schematically depicted in Fig. below with eccentric loading. The deflected shape of the beam–column can be represented by various displacement functions. In this numerical model, the deflected shape of circular CFT beam-columns is assumed to be a part-sine and is expressed by

$$u = u_m \, sin\left(\frac{\pi z}{L}\right) \tag{4-30}$$

Where, u_m is the deflection at the mid-height of the beam–column and L is the effective length of the beam–column. The initial geometric imperfection of the beam–column may be described by the same form of the displacement function as

$$u_{oy} = u_o \, sin\left(\frac{\pi z}{L}\right) \tag{4-31}$$

Where, u_o is the initial geometric imperfection at the mid-height of the beam–column.

The curvature (ϕ) of the beam–column can be obtained from the above equation as

$$\phi = \frac{\partial^2 u}{\partial z^2} = \left(\frac{\pi}{L}\right)^2 u_m \, sin\left(\frac{\pi z}{L}\right) \tag{4-32}$$

The curvature at the mid-height of the beam–column is given by

$$\phi_m = \left(\frac{\pi}{L}\right)^2 u_m \tag{4-33}$$

The external bending moment at the mid-height of the beam–column with an initial geometric imperfection u_o and under eccentric loading can be calculated by

$$M_{me} = P(e + u_m + u_o) \tag{4-34}$$

Where P is the applied load and e is the eccentricity of the applied load as shown in Fig. below.

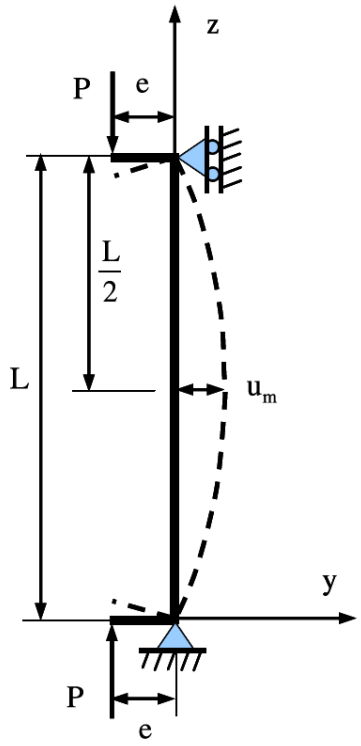

Figure 4-7: Pin-ended beam–column model

To predict the complete load-deflection responses of a slender beam–column, incremental and iterative computational algorithms have been developed. The mid-height deflection of the slender beam–column under axial load with an eccentricity is gradually increased. For a given mid-height deflection, the applied axial load **P** that causes this deflection is determined by solving for the internal force that satisfies the equilibrium condition in which the external moment $\mathbf{M_{me}}$ is equal to the internal moment $\mathbf{M_{mi}}$ at the mid-height of the beam–column. The neutral axis depth $\mathbf{d_n}$ of the composite section is adjusted iteratively in order to maintain the moment equilibrium at the mid-height of the beam–column. For this purpose, the **Secant method** is used and the neutral axis depth is adjusted by the following proposed equation:

$$d_{n,j+2} = d_{n,j+1} - \frac{(d_{n,j+1} - d_{n,j}) r_{pu,j+1}}{r_{pu,j+1} - r_{pu,j}} \tag{4-35}$$

Where the subscript **j** is the iteration number, and $\mathbf{r_{pu}}$ is the residual moment that is given by

$$r_{pu} = P(e + u_m + u_o) - M_{mi} \tag{4-36}$$

The equilibrium condition is satisfied at the mid-height of the beam–column when $|r_{pu}| < \in_k$, where $\in_k$ is the prescribed convergence tolerance. It should be noted that the secant algorithm requires two initial values of the neutral axis depth $\mathbf{d_{n,1}}$ and $\mathbf{d_{n,2}}$ to start the iterative process.

4.4.1.2 Computational procedure

For a given mid-height deflection, the corresponding internal axial force **P** and bending moment $\mathbf{M_{mi}}$ are determined when the equilibrium of internal and external moments is maintained at the mid-height of the beam–column. By repeating this process, a set of axial loads and mid-height deflections is obtained and used to plot the axial load–deflection curve. The computer flowchart for determining the axial load–deflection responses of circular CFT slender beam–columns is presented in Fig. below.

The main steps of the computational procedure are given as:

1) Input data.
2) Discretize the composite section into fiber elements.
3) Set initial deflection at the mid-height of the beam–column. $u_m = \Delta_{um}$
4) Calculate the curvature $\boldsymbol{\phi_m}$ at the mid-height of the beam–column using the equation

$$\phi_m = \left(\frac{\pi}{L}\right)^2 u_m$$

5) Set starting neutral axis depths $d_{n,1} = 0$, and $d_{n,2} = 20 * D$
6) Compute the axial strains at the centroid of the section ($\boldsymbol{\varepsilon_0}$) using $\boldsymbol{\phi_m}$ for both neutral axis depths $\mathbf{d_{n,1}}$ and $\mathbf{d_{n,2}}$;

$$\varepsilon_{0,i} = \phi_m(d_{n,i} - D/2)$$

7) Compute fiber stresses from fiber strains using material constitutive models.
8) Calculate the section axial forces **P** and moment $\mathbf{M_{mi}}$.
9) Compute $\mathbf{r_{pu,1}}$ and $\mathbf{r_{pu,2}}$ corresponding to $\mathbf{d_{n,1}}$ and $\mathbf{d_{n,2}}$, respectively
10) Adjust the neutral axis depth $\mathbf{d_n}$ using secant Equation
11) Update the axial strain at the centroid of the cross-section ($\boldsymbol{\varepsilon_0}$) of the section using $\boldsymbol{\phi_m}$ and the adjusted $\mathbf{d_n}$;

$$\varepsilon_0 = \phi_m(d_n - D/2)$$

12) Calculate fiber stresses from fiber strains using material constitutive models.
13) Compute the section axial force **P** and moment$\mathbf{M_{mi}}$.
14) Repeat steps **(10)–(13)** until $|r_{pu}| < \in_k$
15) Increase the deflection at mid-height of the beam–column by $u_m = u_m + \Delta_{um}$.
16) Repeat steps **(4)–(15)** until the ultimate axial load $\mathbf{P_n}$ is obtained or the deflection limit is reached.

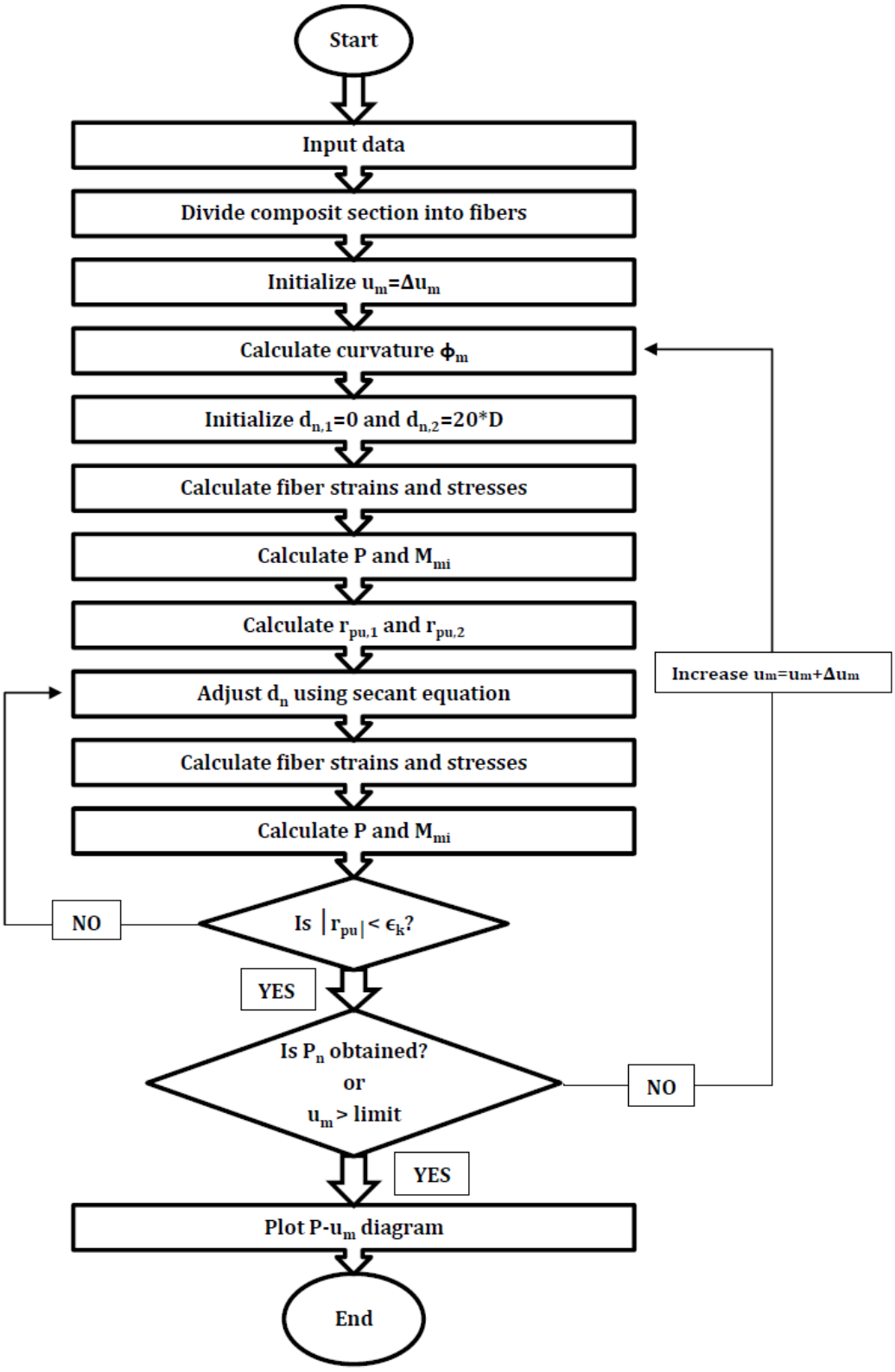

Figure 4-8: Flowchart for determining the Axial load-Deflection curve for circular CFT columns

The convergence tolerance $\in_{\mathbf{k}}$ is set to $\mathbf{10^{-4}}$ in the analysis. The computational procedure proposed can predict the complete load–deflection response of circular CFT slender beam–columns under axial and eccentric loads.

4.4.2 Axial load–moment interaction strength analysis

4.4.2.1 Theoretical formulation

The axial load–moment interaction strengths of both normal and high strength circular CFT slender beam–columns are influenced by many parameters including the steel ratio, column slenderness ratio, concrete compressive strengths, steel yield strengths, initial geometric imperfections, and concrete confinement. It is difficult to use an equation to accurately express the axial load–moment interaction curves. To accurately determine the axial load–moment interaction diagrams, nonlinear inelastic analysis techniques must be employed. The load-deflection analysis procedure described in the above Section can be used to develop the axial load–moment interaction diagram for a circular CFT slender beam-column by increasing the eccentricity from zero to indefinite. However, the load-deflection analysis procedure is found to be inefficient for developing a complete axial load–moment interaction diagram, particularly when the eccentricity ratio is large. As this study focuses on CFT columns and beam-columns under compression, half part of the complete axial load–moment interaction diagram (Compression part, $\boldsymbol{P \geq 0}$) was developed using the load–deflection analysis procedure by increasing the eccentricity starting from zero until sections internal axial compression load capacity becomes zero.

The ultimate pure axial load $\boldsymbol{P_{oa}}$ of a beam-column is calculated by specifying the eccentricity of the applied load to zero in the axial load–deflection analysis and assuming the column as perfectly straight i.e. $\boldsymbol{u_0 = 0}$. Similarly, the ultimate pure bending strength of a slender beam-column is obtained by specifying the applied external axial load to zero in the axial load–moment–curvature relationship analysis.

4.5 Developing the MS Excel spreadsheet analysis tool

An easy and user-friendly MS Excel spreadsheet analysis tool using visual basic programmed Macros was developed using the above numerical models to enhance the applicability of the study. The codes in VBA are organized in four modules as described below:

- **Module 1**: Contains sub procedure codes that use the user-defined functions from the rest three modules and gives the numerical output results.
- **Module 2**: Contains user-defined function procedure codes for integrating the axial load and bending moment of the cross section; and also contains function procedures for section and beam-column equilibrium secant methods. All functions under this module use user-defined functions from the rest two modules (module 3 and 4).
- **Module 3**: Contains user-defined function procedure codes for determining stress-strain relations of both concrete and structural steel materials.

- **Module 4**: Contains user-defined function procedure codes for determining the fiber layer area and centroids of both concrete and steel layers.

The detail program codes of the modules are described at appendix B.

The Excel spreadsheet consists of four sheets as described below:

- **Sheet 1**: Designed for input-output user-friendly interface and contains programmed macros for data inputs and graphical outputs that use the main codes in module 1. The data input macros use sheet 4 which contains material property specifications while the output macro buttons use the numerical output results in sheet 2 to plot them in graphs and display on sheet 1.
- **Sheet 2**: Contains numerical output results for axial load-strain, moment-curvature, and load-deflection analysis.
- **Sheet 3**: Contains numerical output results for axial load-moment interaction relations of both cross-sectional and member analysis.
- **Sheet 4**: Contains material property specifications for both concrete and structural steel used in input parameters described above. It also contains a short description note about the tool and the instructions on how to use it.

The figure below shows the input-output user-friendly interface designed on sheet one of the spreadsheet.

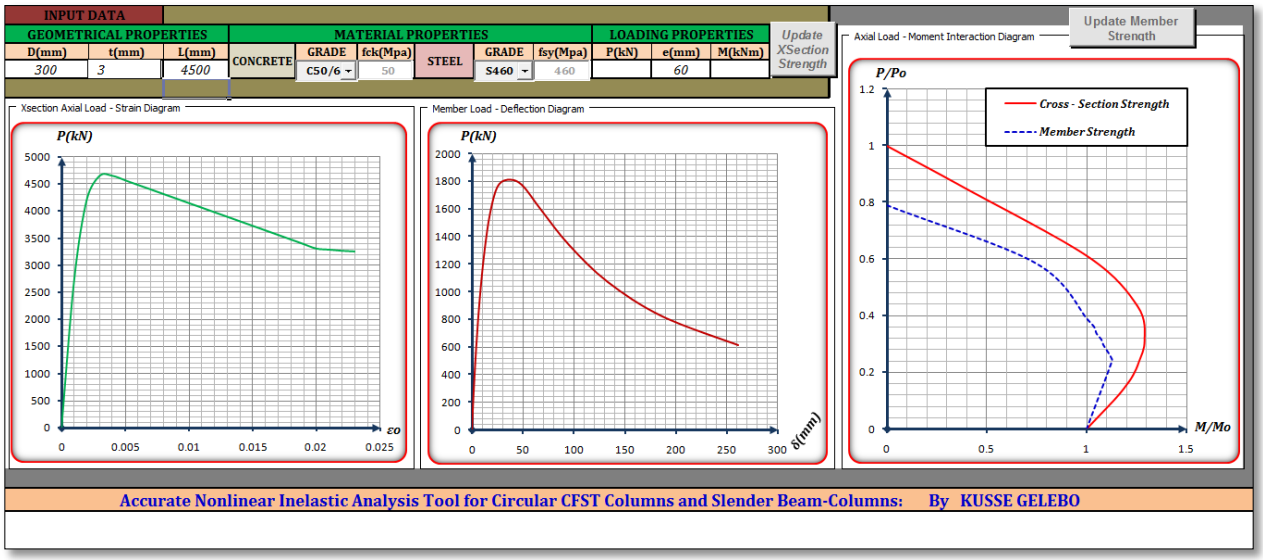

Figure 4-9: The input-output user-friendly interface of the developed tool

4.6 Verification of the numerical model

The experimental results used in the validation of CCFT members in this study were taken from a variety of sources, as shown in Tables in the appendix A.

4.6.1 Short Column ultimate strength capacity and axial load-strain curves

Axial load-strain curves for circular CFT columns provide useful information on the axial stiffness, ultimate strength, post-peak behavior and axial ductility of the columns. The fiber element analysis program was used to analyze various circular CFT columns under axial compression. The ultimate axial strengths and axial load-strain curves of CFT short columns predicted by the proposed numerical model program are compared with more than 120 experimental results reported by various researchers at different time. The geometric and material properties of tested specimens are provided in Table A-1 at appendix A.

The ultimate sectional strengths of circular CFT short columns predicted by the numerical analysis ($\boldsymbol{P_{num}}$) and experimental axial strengths ($\boldsymbol{P_{exp}}$) are listed in Table A-2 at the appendix A. It can be seen from the Table that there is a good agreement between computational solutions and experimental measurements. The mean ratio of the measured value of the tested specimens to the predicted cross-sectional strength is 1.014. The statistical analysis conducted shows that the standard deviation of the ratio Pexp / Pnum is 0.096 with a variance of 0.009, which is within the acceptable range of 10%.

The predicted axial load-strain curves for some sample Specimens are compared against experimental results provided by those researchers and described in Figures below. The figure shows that the computer program predicts well the experimentally observed axial load-strain behavior of CFT short columns. The lateral confining pressure model plays an important role in determining the stress-strain behavior of the sandwiched concrete in circular CFT columns.

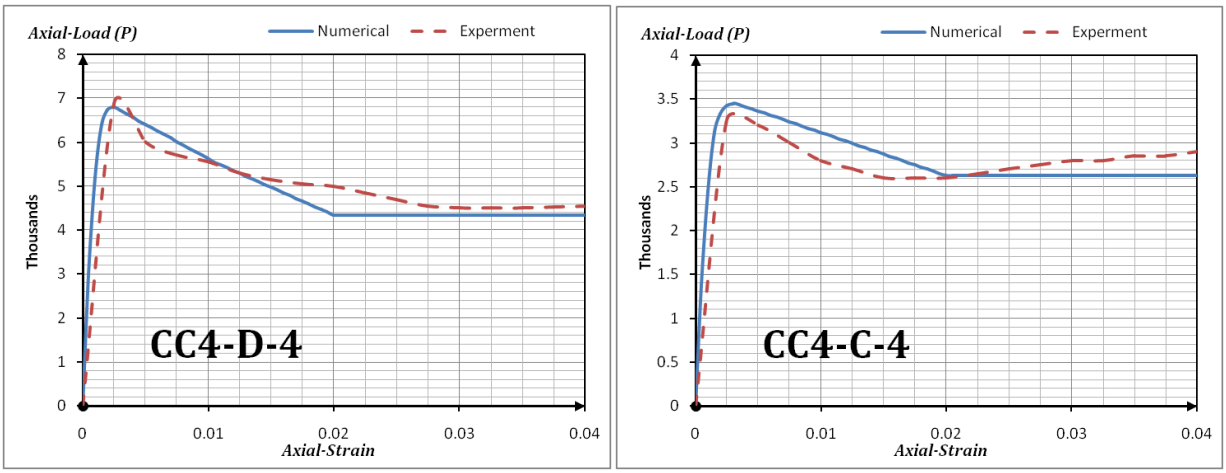

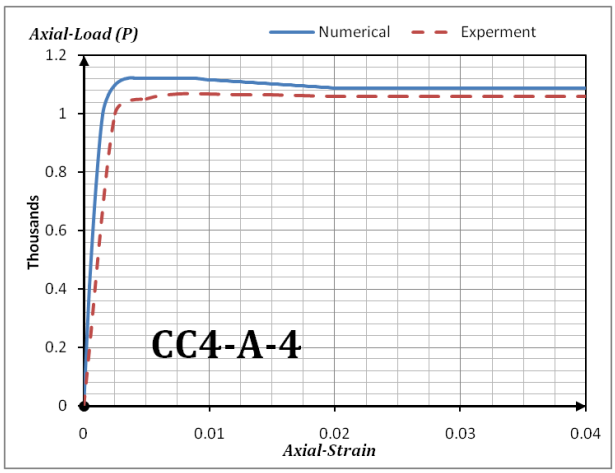
Axial-Load (P)
Numerical
Experment
Thousands
1.2
1
0.8
0.6
0.4
0.2
0
0
0.01
0.02
0.03
0.04
Axial-Strain
CC4-A-4

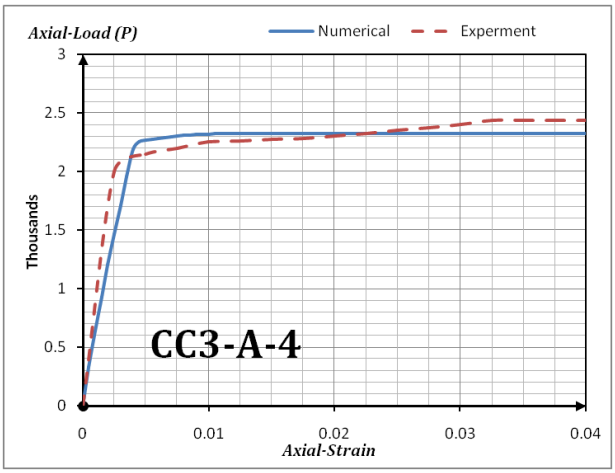
Axial-Load (P)
Numerical
Experment
Thousands
3
2.5
2
1.5
1
0.5
0
0
0.01
0.02
0.03
0.04
Axial-Strain
CC3-A-4

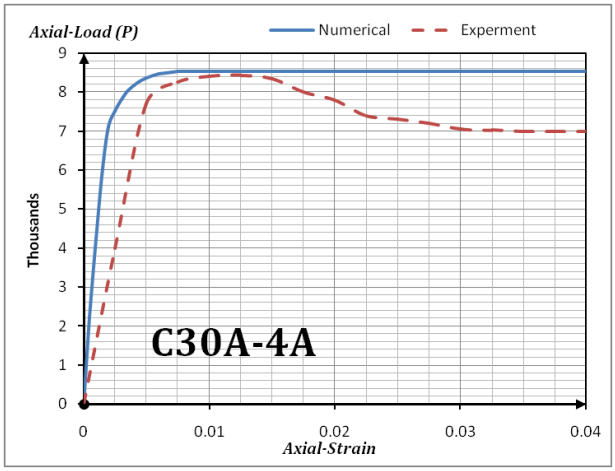
Axial-Load (P)
Numerical
Experment
Thousands
9
8
7
6
5
4
3
2
1
0
0
0.01
0.02
0.03
0.04
Axial-Strain
C30A-4A

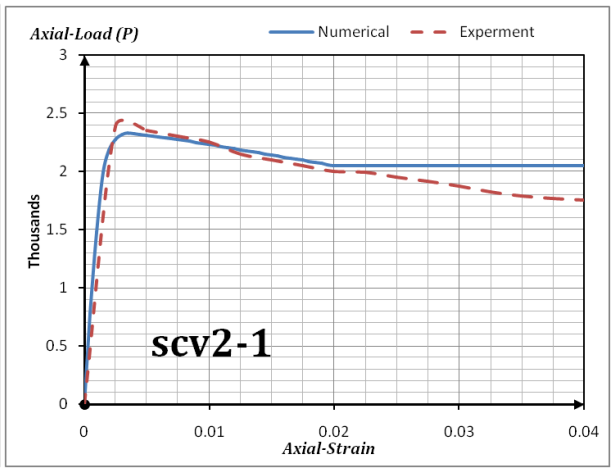
Axial-Load (P)
Numerical
Experment
Thousands
3
2.5
2
1.5
1
0.5
0
0
0.01
0.02
0.03
0.04
Axial-Strain
scv2-1

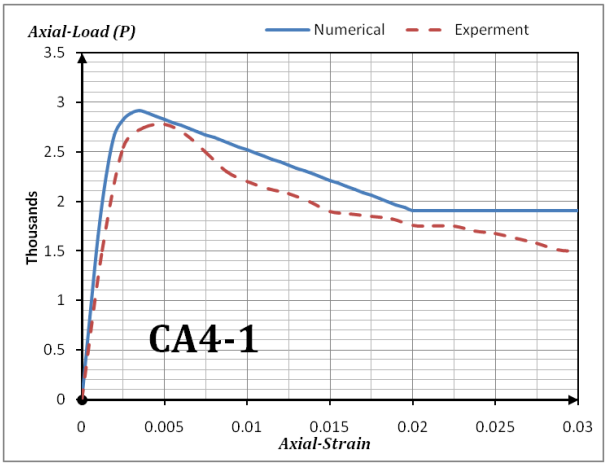
Axial-Load (P)
Numerical
Experment
Thousands
3.5
3
2.5
2
1.5
1
0.5
0
0
0.005
0.01
0.015
0.02
0.025
0.03
Axial-Strain
CA4-1

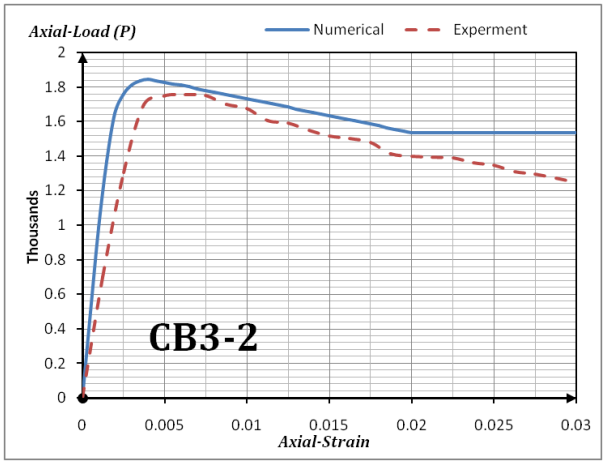
Axial-Load (P)
Numerical
Experment
Thousands
2
1.8
1.6
1.4
1.2
1
0.8
0.6
0.4
0.2
0
0
0.005
0.01
0.015
0.02
0.025
0.03
Axial-Strain
CB3-2

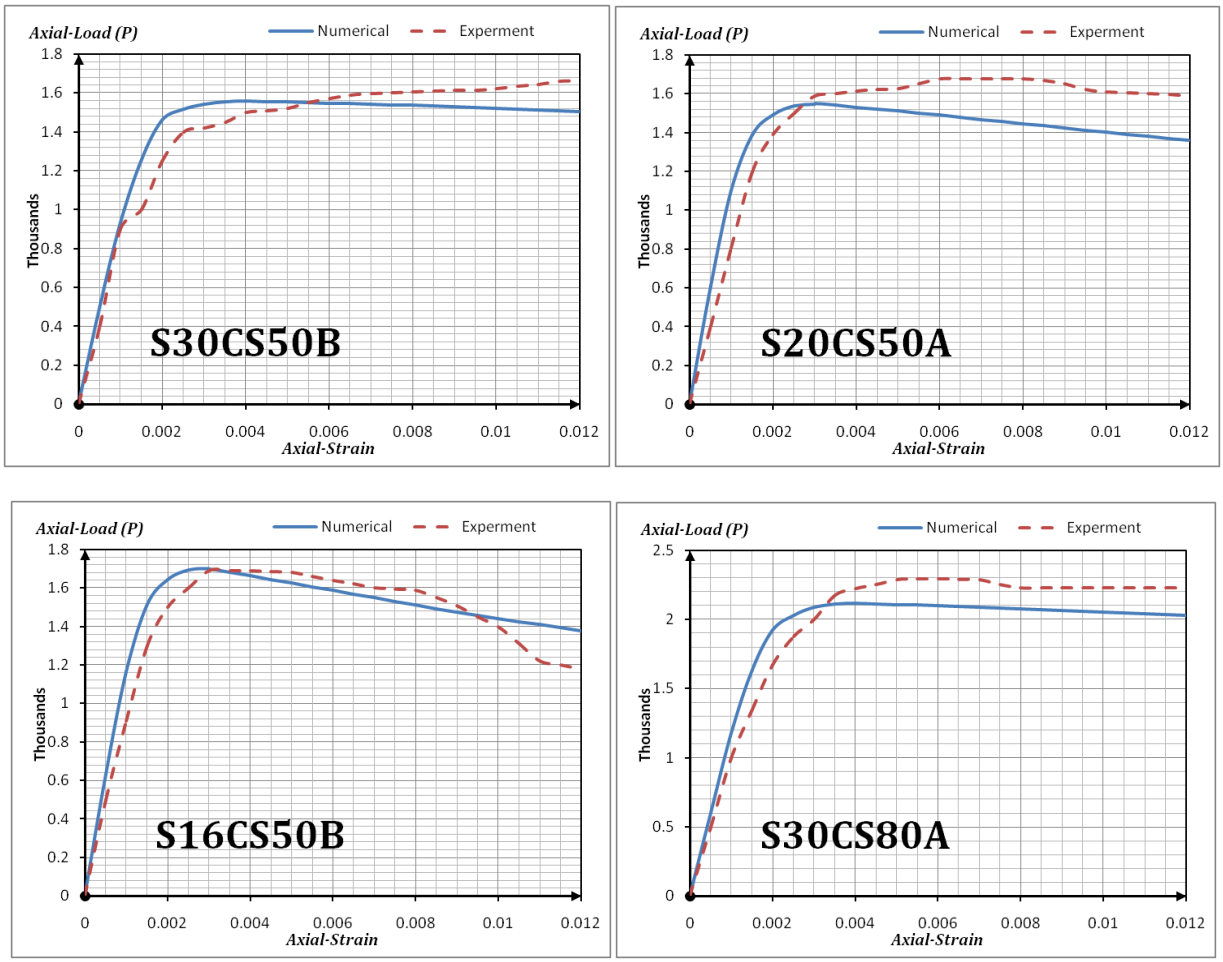

Figure 4-10: Comparison of predicted and experimental axial load-strain curves for some samples of circular CFT short columns

It appears that the predicted post-yield behavior of CFT columns is in excellent agreement with corresponding test data. It can be concluded that the numerical model can accurately capture the complete axial load-strain characteristics of circular CFT short columns.

4.6.2 Beam-column ultimate strength and Load- Deflection curves

The column specimens were pin-ended circular concrete-filled steel tube composite beam-columns under an eccentrically applied axial force. Table A-3 at the appendix A details the dimensions and material properties of all the composite column specimens involved. A total of 123 full-scale slender CCFT beam-column specimens are used for validating the proposed nonlinear numerical approach. Table A-4 at appendix A summarizes the maximum load carrying capacity calculated by the present scheme and the tests. This section illustrates comparisons of the responses and the corresponding maximum strength of the circular concrete-filled steel tube composite beam-columns obtained from the proposed numerical analysis approach and 123 available experimental results.

Clearly, good agreements between P_{num} and P_{exp} have been evidenced, in which the average value, the standard deviation (SD) and the variance of the P_{exp} / P_{num} ratio are 1.043, 0.127 and 0.016, respectively. More importantly, the proposed analysis approach is able to capture the complete axial load and deflection responses of the circular concrete filled steel tube composite beam-columns under the eccentrically applied compression force.

Not only can the pre-peak behavior be captured accurately, but also the sophisticated post-peak softening response is mapped out efficiently using the proposed nonlinear inelastic fiber element analysis procedure, which incorporates the initial geometric imperfection, second order p-delta effects, constitutive models of concrete confinement, inelastic buckling of structural steel and tension stiffening of concrete, simultaneously. Furthermore, the axial load and deflection relationship associated with some of the samples are displayed in Figures below.

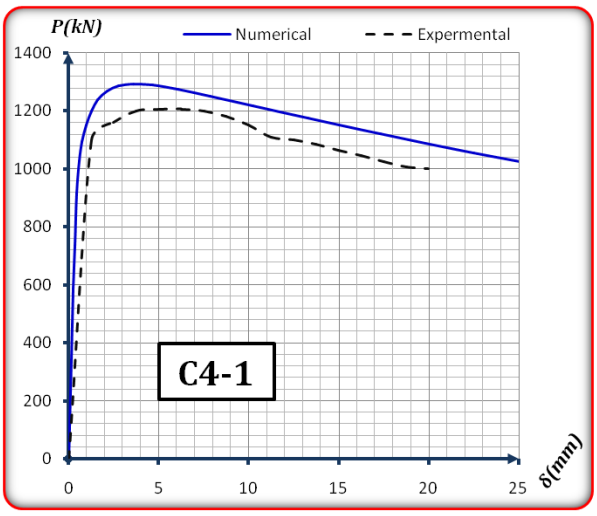

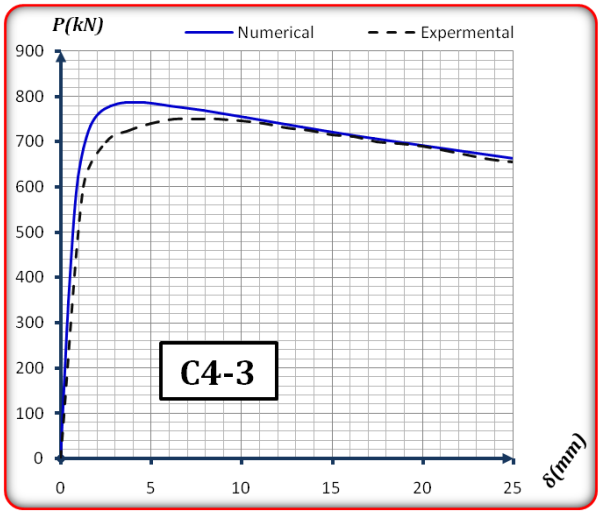

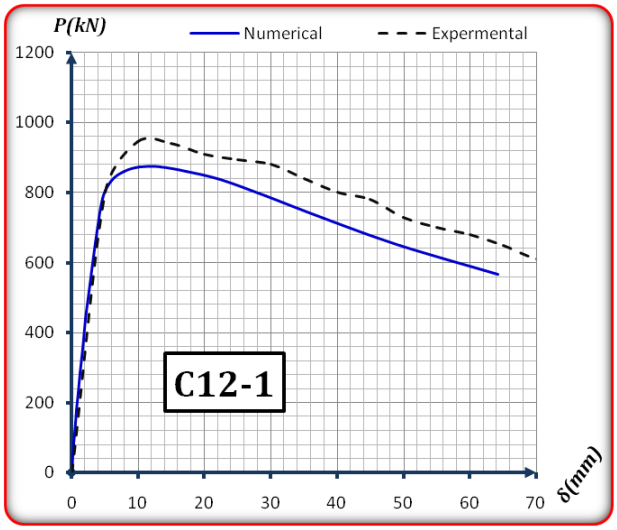

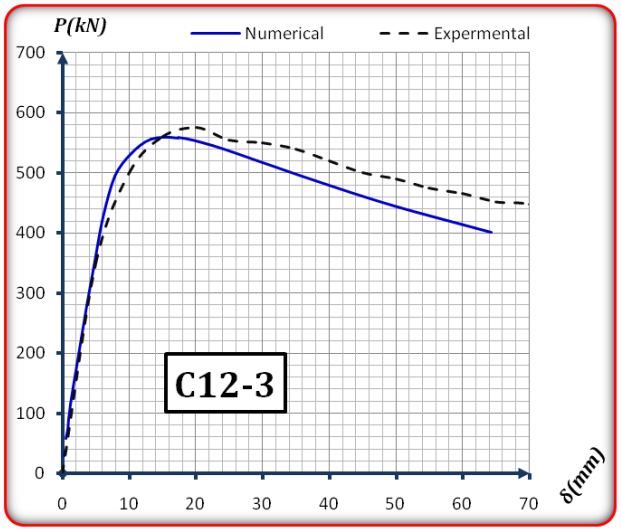

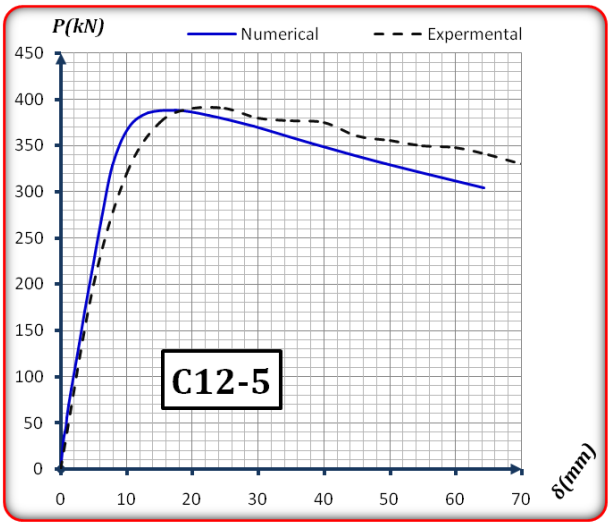
P(kN)
Numerical
Expermental
C12-5
δ(mm)

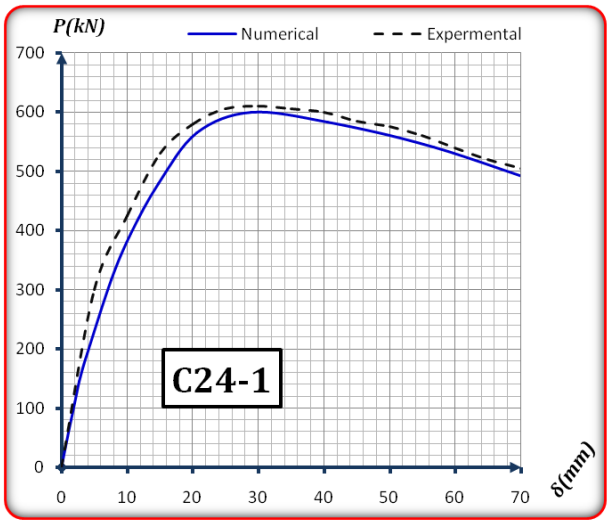
P(kN)
Numerical
Expermental
C24-1
δ(mm)

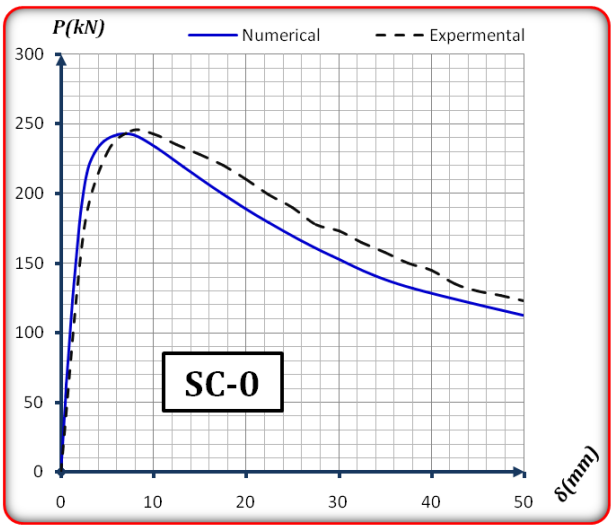
P(kN)
Numerical
Expermental
SC-0
δ(mm)

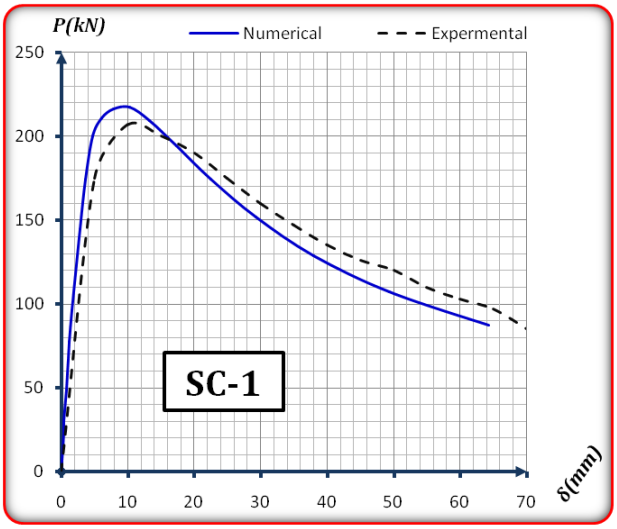
P(kN)
Numerical
Expermental
SC-1
δ(mm)

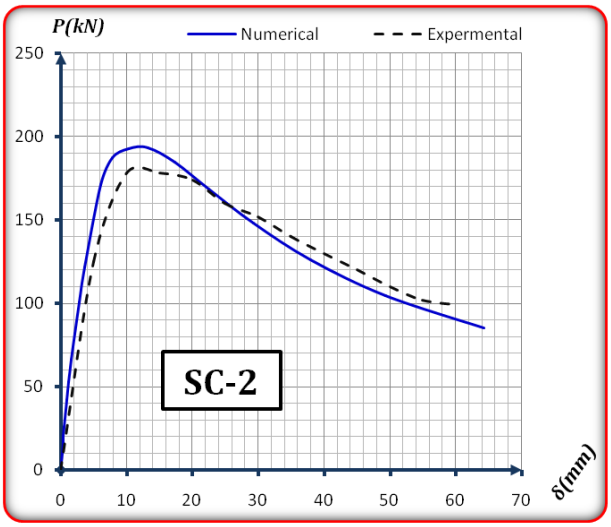
P(kN)
Numerical
Expermental
SC-2
δ(mm)

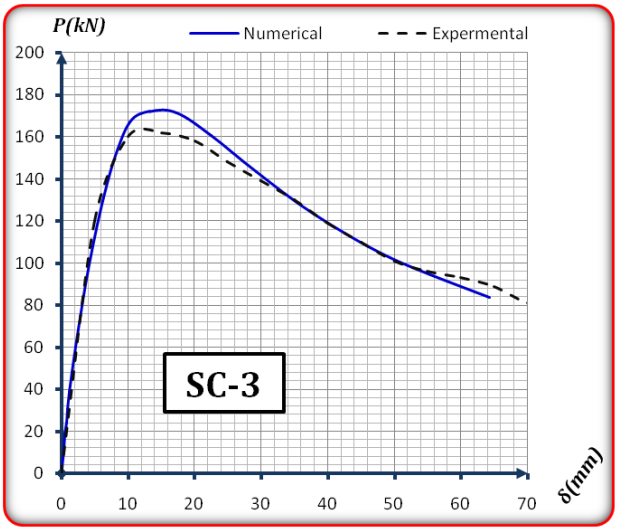
P(kN)
Numerical
Expermental
SC-3
δ(mm)

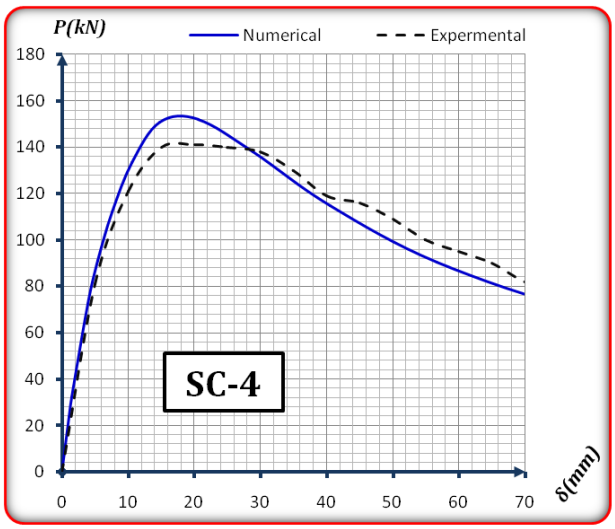
P(kN)
Numerical
Expermental
180
160
140
120
100
80
60
40
20
0
0
10
20
30
40
50
60
70
δ(mm)
SC-4

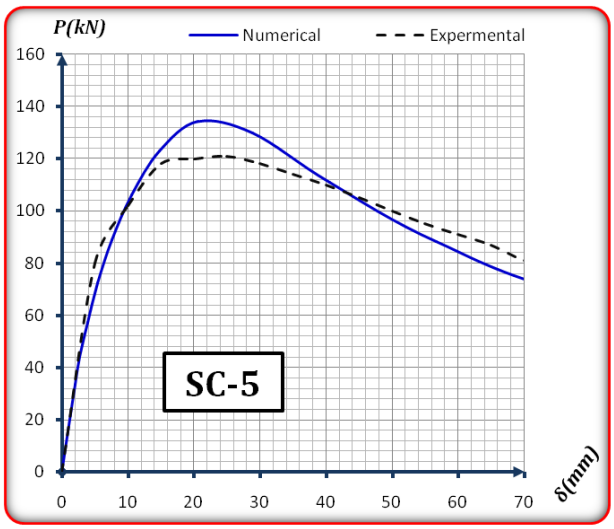
P(kN)
Numerical
Expermental
160
140
120
100
80
60
40
20
0
0
10
20
30
40
50
60
70
δ(mm)
SC-5

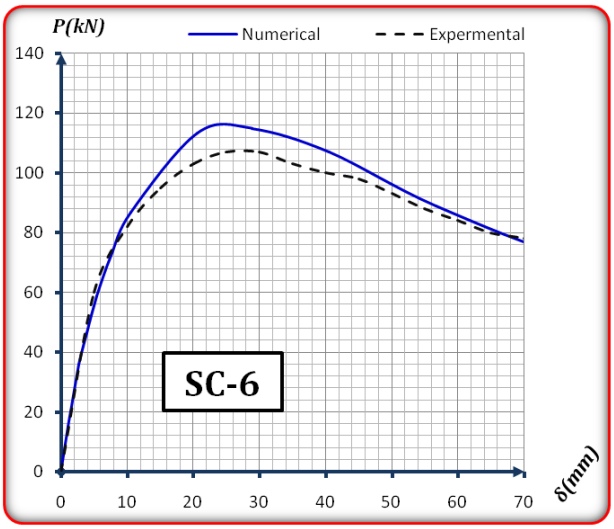
P(kN)
Numerical
Expermental
140
120
100
80
60
40
20
0
0
10
20
30
40
50
60
70
δ(mm)
SC-6

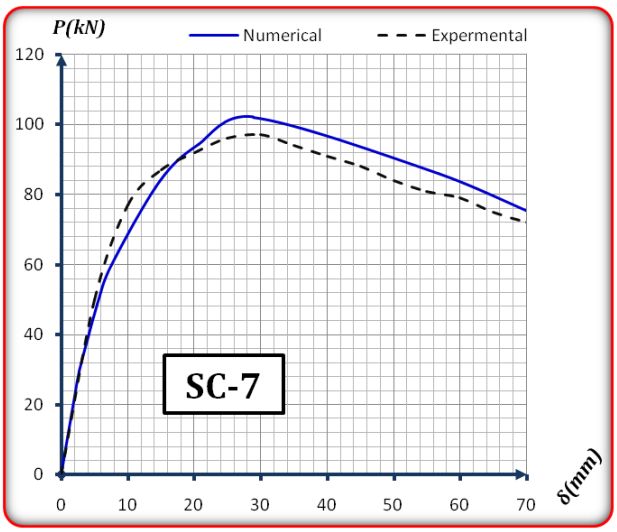
P(kN)
Numerical
Expermental
120
100
80
60
40
20
0
0
10
20
30
40
50
60
70
δ(mm)
SC-7

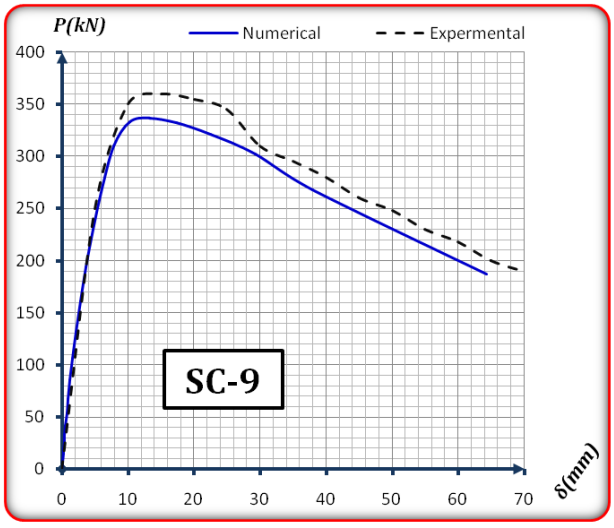
P(kN)
Numerical
Expermental
400
350
300
250
200
150
100
50
0
0
10
20
30
40
50
60
70
δ(mm)
SC-9

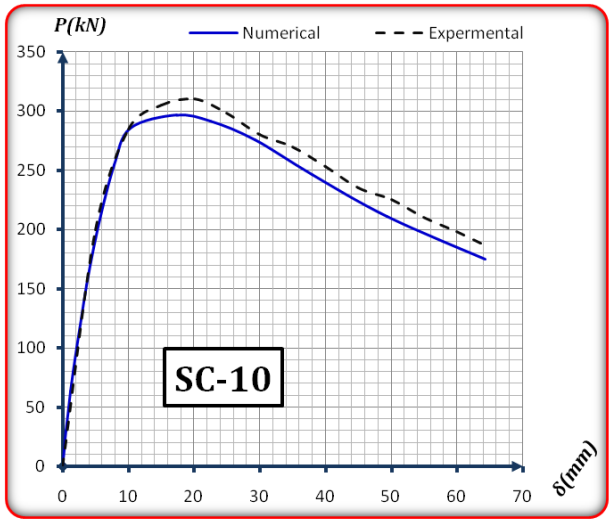
P(kN)
Numerical
Expermental
350
300
250
200
150
100
50
0
0
10
20
30
40
50
60
70
δ(mm)
SC-10

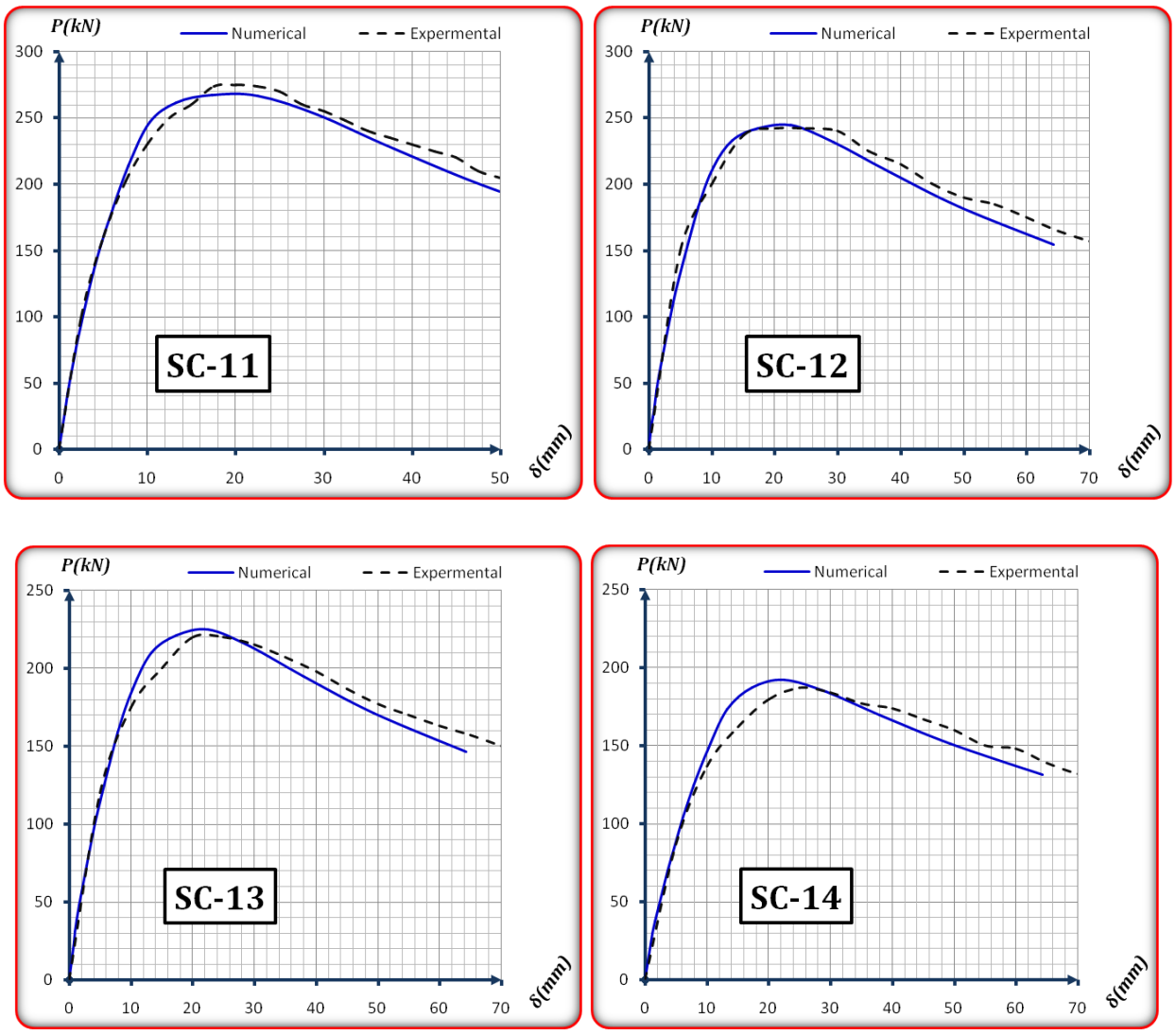

Figure 4-11: Comparison of predicted and experimental load-deflection curves for some samples of circular CFT columns and beam-columns

4.6.3 Evaluation of various numerical models

The accuracy and reliability of various numerical models proposed by various researchers and the author in this paper are evaluated. Numerical models proposed by Tang et al. [1996], Hu et al. [2003] and Q.Q. Liang & S. Fragomeni [2009] have been investigated in the present fiber element analysis program developed. Table A-5 and A-6 at the appendix A shows a properties and comparison matrix of ultimate axial strengths determined using these three numerical models and the fiber element analysis program for the 38 tested circular CFT columns. The predicted ultimate axial strengths are also compared with experimental results in the Table. The material properties of these specimens can be found in the Table. It can be seen from Table that the numerical models given by Tang et al. and Hu et al. generally overestimate the ultimate axial strengths of circular CFT columns while that of Q.Q. Liang & S. Fragomeni slightly

underestimates those values. The mean of the predicted to experimental ultimate strength by the model given by Tang et al. is 1.065 with a standard deviation of 0.072 and its variance is 0.005. The mean of the predicted to experimental ultimate strength by the model given by Hu et al. is 1.04 with a standard deviation of 0.085 and its variance is 0.007. The mean of the predicted to experimental ultimate strength by the model given by Q.Q. Liang & S. Fragomeni is 0.985 with a standard deviation of 0.046 and its variance is 0.002. The mean of the ultimate axial strength predicted by the proposed fiber element analysis technique to the experimental value is 1.015 with a standard deviation of 0.049 and its variance is 0.002. The evaluation demonstrates that the proposed material stress-strain relation models and the fiber element analysis program provide reliable results for both normal and high strength circular CFT columns under compression.

4.7 Parametric studies

The fiber element analysis tool developed and verified was employed to conduct parametric studies to examine the effects of the tube diameter-to-thickness ratio (D/t), length-to-diameter ratio (L/D), eccentricity-to-diameter ratio (e/D), concrete compressive strengths and steel yield strengths on the stiffness, strength, and ductility of circular CFT columns and beam-columns under eccentric compression.

4.7.1 Effects of D/t ratio

Local buckling of thin-walled steel tubes depends on its depth-to-thickness ratio (D/t). The effects of the diameter-to-thickness ratio of steel tubes on the stiffness, strength and ductility of circular CFT columns under axial loading and beam-columns under eccentric compression were studied using the fiber element analysis program developed. The outer diameter of the circular CFT column section was set at 300 mm. The typical D/t ratios of 40, 50, 75, 100 and 150 were considered by changing the thickness of the steel tube walls while maintaining the same cross section size. The yield strength of steel tubes was 460MPa. All columns were assumed to be cast with 50MPa concrete.

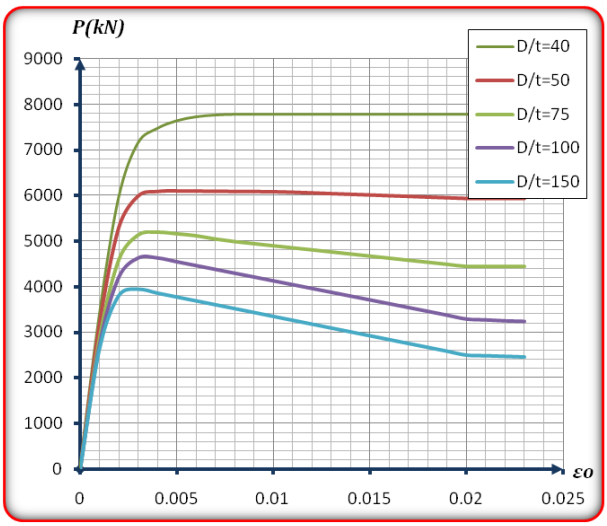

Figure 4-12: Effects of D/t ratio on the axial load-strain behavior of circular CFT columns

The axial load-strain curves for circular CFT columns with various D/t ratios presented in the Figure 4-12 above shows those circular CFT columns with D/t ratios ranging from around 60 and above exhibit strain softening behavior. In addition, the ultimate axial load of circular CFT columns decreases with increases in the D/t ratio. Note that increasing the D/t ratio reduces the steel area in the column section. It can be observed from the figure that increasing the D/t ratio reduces the axial ductility performance of circular CFT columns.

On Beam-Columns

The numerical model was utilized to examine the effects of D/t ratio on the load-deflection and axial load-moment interaction curves for circular CFT slender beam-columns. The column L/D ratio was 20. The loading eccentricity ratio (e/D) was taken as 0.15 in the analysis. The initial geometric imperfection of the beam-columns at mid-height was specified as L/1000. The influences of D/t ratio on the axial load-deflection curves for circular CFT slender beam-columns are illustrated in Figure below.

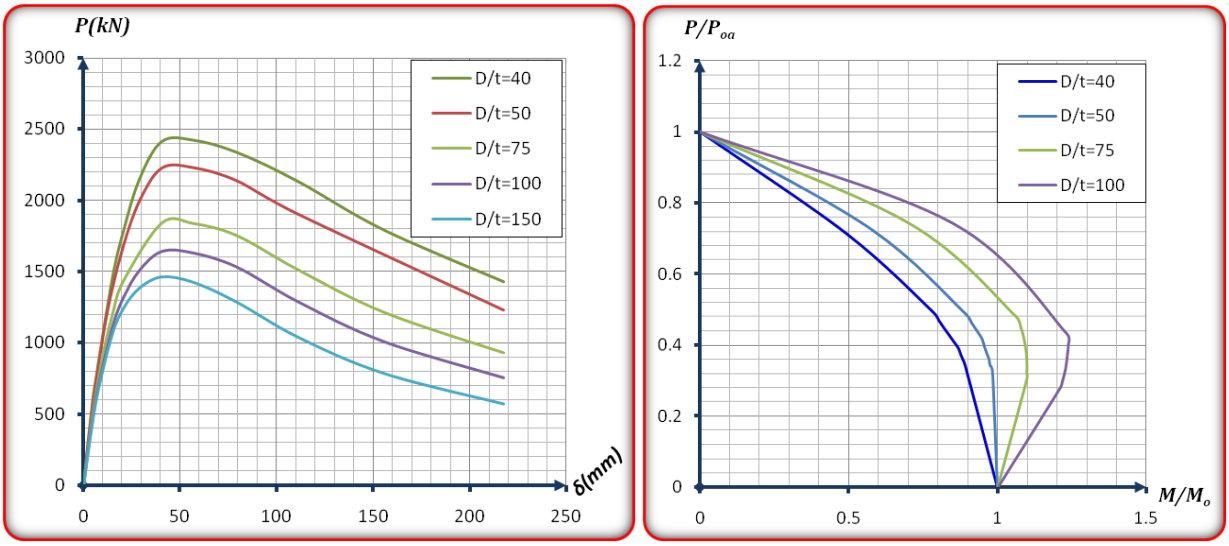

Figure 4-13: Effects of D/t ratio on the axial load-deflection and axial load-moment interaction curves for circular CFT beam-columns

The figure shows that increasing the D/t ratio of the slender beam-columns slightly reduces their initial stiffness. However, increasing the D/t ratio significantly reduces the ultimate axial strength of eccentrically loaded CFT slender beam-columns. This is attributed to the fact that a column section with a larger D/t ratio has a lesser steel area and it may undergone local buckling which reduces the ultimate strength of the column.

Fig. also demonstrates the influence of D/t ratio on the axial load-moment interaction diagrams for circular CFT slender beam-columns. In each interaction curve, the axial load (P_n) was divided by the ultimate axial strength (P_{oa}) of the axially loaded slender beam-column, while the moment (M_n) was divided by the ultimate pure bending moment (M_o) of the beam-column. It can be seen from Fig. that decreasing the D/t ratio of the slender beam-column narrows the

axial load-moment interaction diagram for the slender beam-column. In addition, the flexural strength at the maximum moment point is shown to increase remarkably with increasing the D/t ratio.

4.7.2 Effects of concrete compressive strengths

A circular CFT column with a diameter of 300 mm filled with normal and high strength concrete was analyzed using the fiber element analysis program to examine the effects of concrete compressive strengths on the behavior of columns under axial load. The compressive concrete strengths were 20, 35, 50, 70 and 90MPa. The thickness of the steel tube wall was 4mm so that its D/t ratio was 75. The steel yield strength of the steel tube was 460MPa.

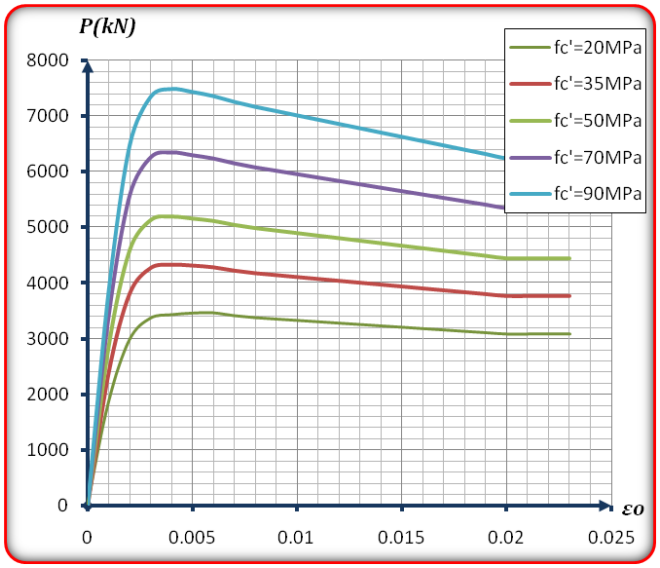

Figure 4-14: Effects of concrete compressive strength on the axial load-strain behavior of circular CFT columns

Fig. 4-14 shows the axial load-strain curves for the circular CFT column filled with different concrete strengths. This indicates that increasing the concrete compressive strength significantly increases the ultimate axial strength and stiffness of circular CFT columns. It is visible that the ultimate axial load of circular CFT columns increases linearly with increasing the concrete compressive strengths. It also seen that the axial ductility performance of the circular CFT column decreases considerably with an increase in the concrete compressive strength.

Beam-column

The inelastic stability analyses of a circular CFT slender beam–column with a diameter of 300 mm filled with different strength concrete were undertaken to examine the effects of concrete compressive strengths on the strength and behavior of circular CFT slender beam–columns. The column slenderness ratio L/D was 20 and the initial geometric imperfection at the mid-height was taken as L/1000. The eccentricity ratio e/D of 0.15 was considered.

The effects of concrete compressive strengths on the axial load-deflection curves for circular CFT slender beam–columns are demonstrated in Fig. below. It would appear from Fig. that the flexural stiffness and strength of circular CFT slender beam–columns increase with increasing the concrete compressive strength.

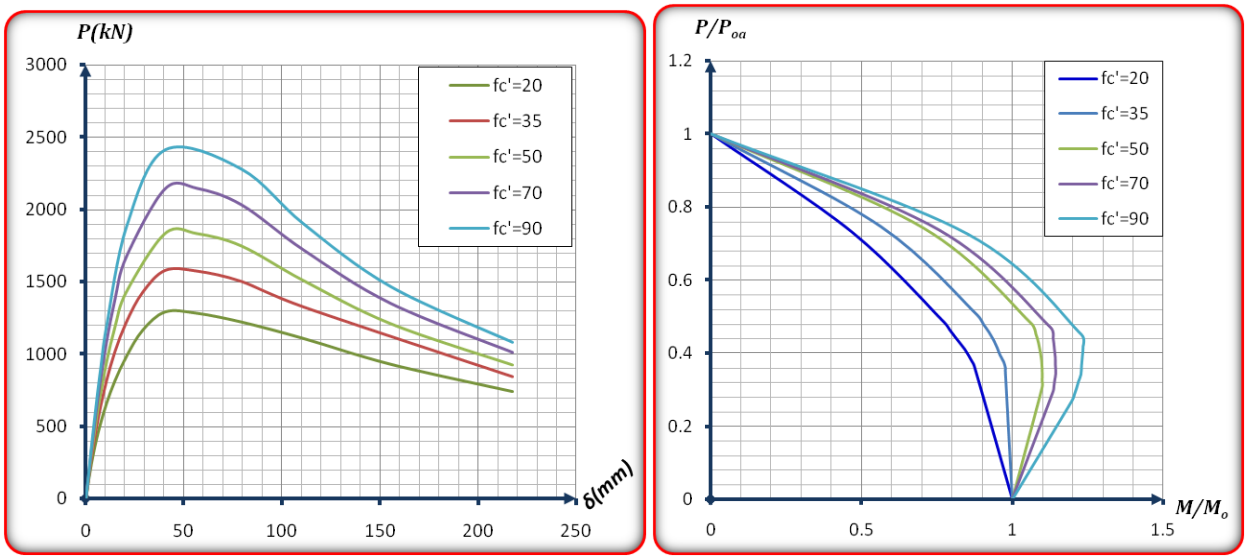

Figure 4-15: Effects of concrete compressive strength on the axial load-deflection and axial load-moment interaction curves for circular CFT beam-columns

Fig. also gives normalized axial load-moment interaction diagrams for circular slender steel tubes filled with different strength concrete. It can be seen from Fig. that increasing the concrete compressive strength enlarges the normalized axial load-moment interaction diagram for the slender beam-column. In addition, the flexural strength at the maximum moment point is shown to increase considerably with increasing the concrete compressive strength. Moreover, the ultimate pure bending strengths of circular CFT beam-columns increase with an increase in the concrete compressive strength.

4.7.3 Effects of steel yield strengths

The fiber element analysis program developed was utilized to investigate the effects of steel yield strengths on the behavior of circular CFT columns. The diameter of the columns was set at 300mm and the D/t ratio was 75. Steel tubes were made of steels with yield strengths of 235, 355, 460, 550 and 690MPa. The steel tubes were filled with 50MPa concrete.

The axial load-strain curves for the circular CFT columns made of different strength steel tubes are presented in Figure below. It can be observed from the figure that increasing the steel yield strength significantly increases the ultimate axial loads of circular CFT columns. These columns do not exhibit strain hardening characteristics because of the large D/t ratio of 75. From the figure, it is clear that the ultimate axial strength of circular CFT columns increases linearly with increasing the steel yield strength.

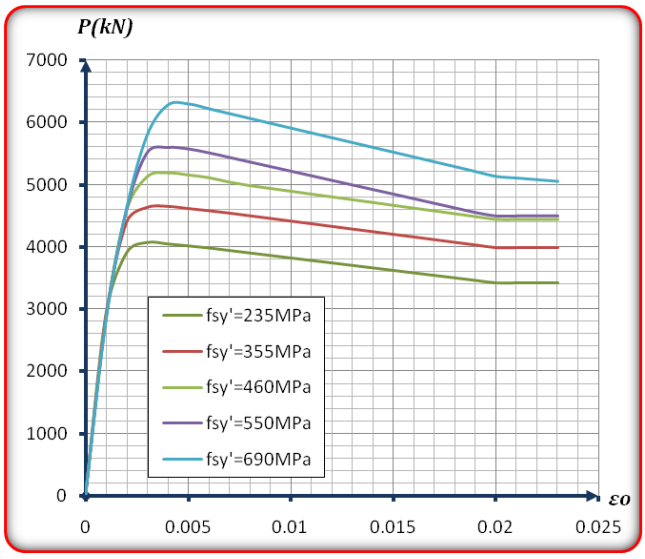

Figure 4-16: Effects of steel yield strength on the axial load-strain behavior of circular CFT columns

Beam-column

The computer program developed was employed to investigate the effects of steel yield strengths on the strength and behavior of circular CFT slender beam–columns. Circular CFT slender beam–columns made of different strength steel tubes were studied. The diameter of the beam-column sections was 300 mm and their thickness was 4 mm. The column slenderness ratio L/D was 20 while the eccentricity ratio e/D was taken as 0.15. An initial geometric imperfection of L/1000 at the mid-height was taken into account in the analysis.

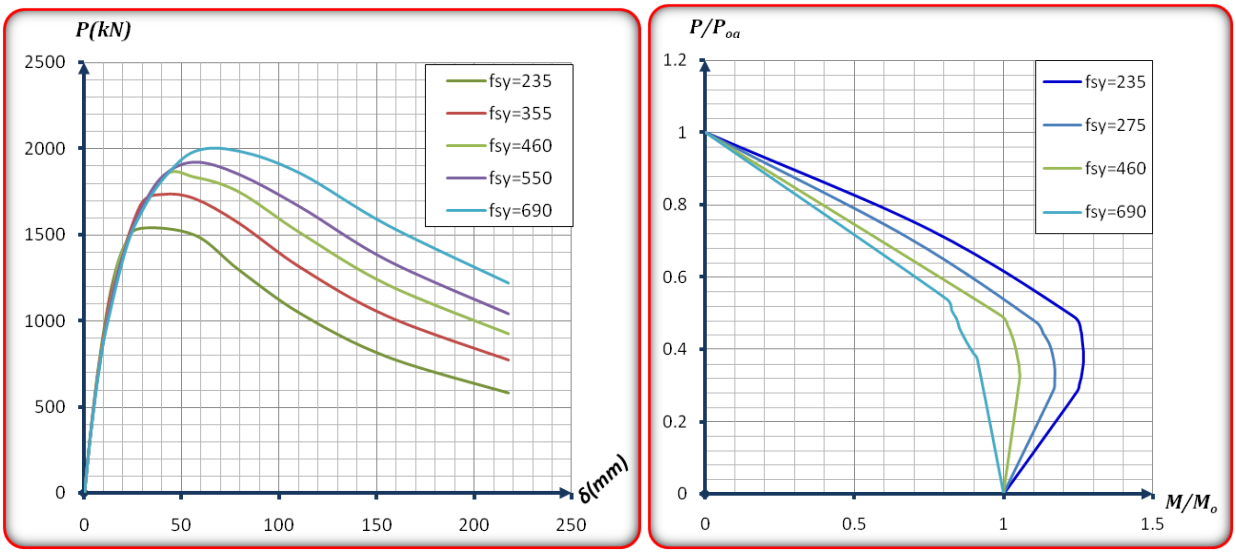

Figure 4-17: Effects of steel yield strength on the axial load-deflection and axial load-moment interaction curves for circular CFT beam-columns

The predicted axial load-deflection curves for circular CFT slender beam-columns with various steel yield strengths are shown in the Figure above. It can be observed from the figure that the steel yield strength does not have an effect on the initial flexural stiffness of slender beam-columns. However, the ultimate axial strength of slender beam-columns increases significantly with an increase in the steel yield strength.

Fig. 4-17 also presents normalized axial load-moment interaction diagrams for circular CFT beam-columns made of different strength grade steel tubes. The normalized axial load-moment interaction surface is shown to enlarge with decreasing the steel yield strength. In addition, the maximum bending strength is shown to increase significantly with an increase in the steel yield strength. Moreover, the ultimate pure bending strength of beam-columns increases significantly with increasing the steel yield strength.

4.7.4 Effects of L/D ratio

The numerical model developed was used to examine the effects of the column slenderness ratio (L/D) which is one of the important factors that influence the fundamental behavior of circular CFT slender beam–columns. The numerical model created was used to study the effects of the column slenderness ratio on the stiffness, strength, and ductility of eccentrically loaded circular CFT beam–columns. The diameter of the circular CFT beam–column section was 300 mm while the tube thickness was 4mm. Column slenderness ratios (L/D) of 7.5, 15, 20, 25 and 30 were considered in the parametric study while the dimension of the section was not changed. The loading eccentricity ratio (e/D) of 0.15 was considered in the analysis. The initial geometric imperfection at the mid-height of the beam–columns were taken as L/1000. The yield strength of steel tubes was 460MPa. All columns were filled with 50MPa concrete. The figure below demonstrates the effects of column slenderness ratio on the axial load-deflection curves for circular CFT beam–columns. The figure shows that increasing the column slenderness ratio significantly reduces the flexural stiffness and ultimate axial strength of eccentrically loaded circular CFT beam–columns. In addition, the deflections and displacement ductility of the beam–columns increase with an increase in the column slenderness ratio.

The axial load-moment strength interaction curves for circular CFT beam-columns with column slenderness ratios of 0, 7.5, 12, 20, 25 and 30 are also presented in Figure. In each interaction curve, the ultimate axial strength was normalized to the ultimate axial load (P_o) of the axially loaded beam-column section while the ultimate moment was normalized to the ultimate pure bending moment (M_o) of the beam-column. The curve for L/D = 0 represents the ultimate strength of the composite section which is not affected by the inelastic stability analysis. It appears from Fig. that reducing the L/D ratio of the beam-column enlarges the normalized axial load-moment interaction diagram for the beam-column. For beam-columns under the same axial load level, increasing the column slenderness ratio reduces the ultimate bending strengths. However, the ultimate pure bending strength of a beam-column is not affected by its slenderness ratio.

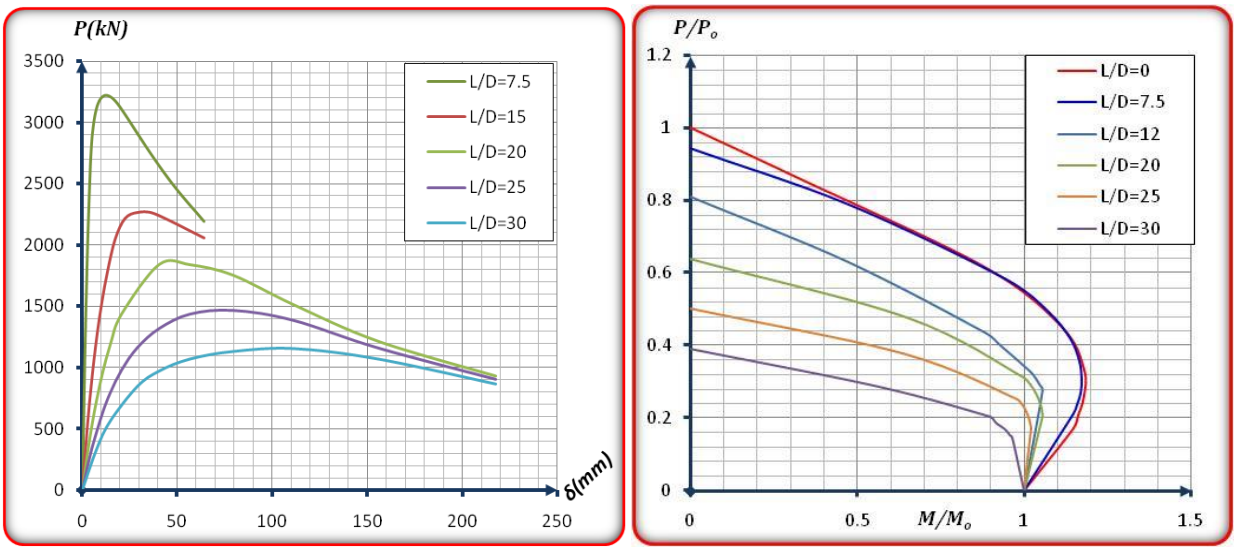

Figure 4-18: Effects of L/D ratio on the axial load-deflection and axial load-moment interaction curves for circular CFT beam-columns

4.7.5 Effects of eccentricity ratio

The end eccentricity ratio (e/D) of the applied load has a significant effect on the fundamental behavior of circular CFT slender beam–columns. The effects of eccentricity ratio on the performance of circular CFT slender beam–columns were investigated using the computational algorithms developed. The diameter of the circular CFT beam–column section was 300 mm while its thickness was 4 mm. The column slenderness ratio (L/D) was 20. The eccentricity ratios (e/D) of 0.05, 0.15, 0.25, 0.4 and 0.6 were considered in the analysis. The initial geometric imperfection at the mid-height of the beam–columns was taken as L/1000. The yield strength of steel tubes was 460MPa. The Young's modulus of steel tubes was taken as 210 GPa. The beam-column was filled with 50 MPa concrete.

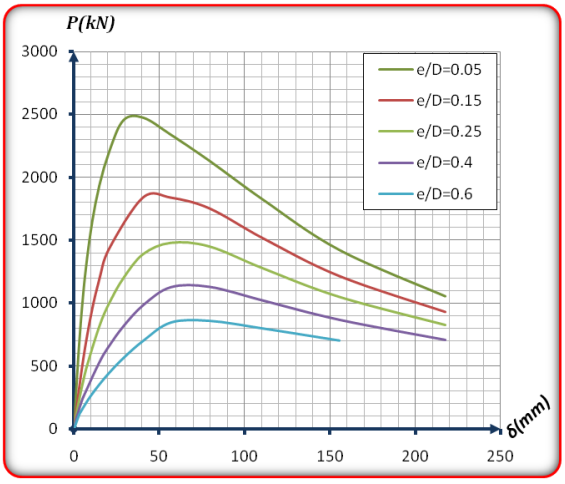

Figure 4-19: Effects of eccentricity ratio on the axial load-deflection curves for circular CFT beam-columns

Fig. 4-19 above illustrates the effects of eccentricity ratios on the axial load-deflection curves for circular CFT slender beam-columns. It can be seen from Figs. that when increasing the e/D ratio in any beam-column, the effect of axial load reduces and the beam-column becomes a more flexural one. Furthermore, increasing the e/D ratio might influence the deflection ductility of a slender beam-column.

4.8 Concluding Remarks

The ultimate strength capacity and the full response of the short and slender circular concrete-filled steel tube composite columns and beam-columns subjected to eccentric compressive load have been investigated using the sophisticated nonlinear inelastic numerical approach. The numerical scheme has carefully taken into account of the nonlinearity of material behaviors such as the strain hardening and softening, geometric nonlinearity, geometric imperfection, local buckling of the structural steel, the confinement effects from the structural steel, and the tension stiffening of concrete. The initial geometric imperfection and P-delta effects are cooperated directly into the numerical analysis. The numerical approach for pin-ended circular CFT composite columns and beam-columns is developed based on the fiber element formulation using mid-height deflection control. With the numerical model a fast, easy and user-friendly MS Excel spreadsheet analysis tool using visual basic programmed Macros that generates axial load-strain, axial load-deflection, axial load-moment-curvature, and P-M interaction diagrams was developed to enhance the applicability of the study. Good agreements between the numerical results with experiments have proved that the proposed numerical scheme is very efficient for predicting both the ultimate strength and the axial load and deflection response of the stub and slender circular concrete-filled steel tube composite columns and beam-columns.

The validated numerical approach and the analysis tool is used in the parametric studies to extend the investigation of the circular concrete-filled steel tube composite columns and beam-columns behaviors due to the changes in the column depth to thickness ratios, effective length ratios, eccentricity ratios, concrete strength, and structural steel yield stress. It is concluded that slender beam-columns (i.e. having large effective length-to-depth ratio) are more ductile than stocky ones (i.e. having small effective length-to-depth ratio). Similarly, the columns subjected to large eccentricity ratios are more ductile than those with small eccentricity ratios. Increasing the concrete strength enhances the ultimate axial strength, but with lower ductility. Furthermore, increasing the steel strength improves mainly the stocky column ultimate strength but not the initial stiffness and ductility.

CHAPTER FIVE

CONCLUSIONS AND RECOMMENDATIONS

5.1 Summary

An efficient fiber element based numerical approach has been developed to simulate the nonlinear inelastic behaviors of circular concrete-filled steel tube (CCFT) composite columns and beam-columns. Not only stub columns, where slenderness and geometric imperfection are negligible, but also slender circular CFT columns were investigated. The present analysis approach realistically accommodates various important influences, such as materials nonlinearity, geometric nonlinearity, geometric imperfection, concrete confinement, local buckling of structural steel tubes and tension stiffening of the concrete. The definition of concrete confinement model for circular concrete-filled steel tube section has been proposed and validated with experimental tests. Secant numerical method has been developed to ensure the convergence solution. A total of more than 200 experimental tests of circular concrete-filled steel tube columns and beam-columns have been used to validate the developed numerical approach by comparing the ultimate load capacity, load-axial strain/shortening, and load- deflection response curves. The proposed simplified numerical model covers a wide range of parameters. The verified analysis tool was used to extend the study of critical influences on the performance of circular CFT columns and beam-columns such as the column effective length ratio, depth thickness ratio, load eccentricity ratio, structural steel yield stress, and concrete compressive strength. The proposed numerical approach is capable of tracing the complete circular CFT columns performance including the challenging post-peak inelastic softening response. Nonlinear inelastic load-deflection curve, load-axial strain/shortening response, axial force-bending moment interaction diagram, and axial force-moment-curvature curve can be effectively generated using the developed tool. Despite rich features of the proposed numerical scheme, the computational time is highly efficient and suitable for practical design and analysis of circular concrete-filled steel tube columns and beam-columns using the tool. The numerical models developed can provide structural designers with advanced analysis and design tools that can be used to design safe and economical composite buildings.

5.2 Concluding Remarks

Some relevant concluding remarks from this study are as follows:

- Good agreements between the numerical results with experiments have proved that the proposed numerical scheme is very efficient for predicting both the ultimate strength and the axial load and deflection response of the stub and slender circular concrete-filled steel tube composite columns and beam-columns.
- The numerical model analysis has successfully captured the axial load-strain and axial load-deflection response along with important features such as the development of

triaxial state of stress in the concrete core, the decrease in the yield strength of steel tube due to biaxial effect and local buckling of steel tube.

- The proposed numerical model can significantly improve the accuracy and efficiency in simulating circular concrete-filled steel tube columns. Meanwhile, the developed tool can be directly utilized to analyze the load-deformation curves of circular CFT stub columns and slender beam-columns using simple spreadsheet software tool. This can help design engineers to conduct a preliminary design of circular CFT columns.

- Concrete confinement needs to be taken into account in the numerical analysis of circular CFT columns and beam-columns since it affects mainly the maximum load-carrying capacity. However, these concrete confinements have less effect on the slender columns.

- Local buckling of structural steel plays very important roles in predicting the realistic response of circular CFT structures. It influences both the ultimate capacity and post-peak softening response.

- Increasing the concrete compressive strength enhances the overall load capacity but it also deteriorates the ductility which makes the columns become more brittle. And when e/D becomes larger, increasing the concrete strength does not significantly increase the axial capacity of the beam-columns.

- Higher structural steel yield stress enhances only the maximum strength capacity of the composite stocky columns more significantly than the slender ones and does not affect the overall ductility.

- Slender circular CFT beam-columns are found to be more ductile than stocky ones. Similarly, columns with large eccentricity are more ductile than those with small eccentricity. The effective length mainly affects the flexural capacity of the beam-columns at the early increasing of *e/D* but its effect become less when *e/D* is large.

- The numerical models proposed overcomes the limitations of traditional plastic analysis methods which are applicable to compact steel sections only, and the analysis tool can compensate for the drawbacks of experiments. The proposed numerical models allow the designer to analyze and design circular CFT beam-columns made of the compact, non-compact or slender steel sections with any strength grades and high strength concrete.

5.3 Recommendations for Future Research

The numerical models developed have been shown to be accurate computer simulation tools which can be used to investigate the fundamental behavior of CFT slender beam-columns. Further research is still needed to extend the numerical models developed to composite columns under other loading conditions. The recommendations for possible future research are described as follows:

- The numerical model and the analysis tool presented in the thesis have been developed for circular concrete-filled steel tube composite columns/beam-columns. Similarly, the same approach can be implemented for other types of composite sections, e.g. CFT with other cross-section shapes such as rectangular, elliptical, polygonal, double-tube columns, double-skin columns, fully encased, partially encased steel sections, composite shear wall, and so on.

- The present study focuses on circular CFT columns with normal and high strength and normal weight concrete. It would be interesting to investigate the behavior of such composite columns for other materials, i.e. lightweight concrete, fiber-reinforced concrete, as well as CFT columns utilizing different material such as stainless steel and geo-polymer concrete, etc.

- The effects of temperature dependent properties have not been incorporated in the present study yet. Therefore, the research on the circular CFT structural behavior under elevated temperature is of importance.

- This study considers the structural response under static loading. Hence, further numerical models can be developed to investigate the circular CFT structure under cyclic loading or preload effects.

- The numerical models developed can be implemented in the advanced analysis programs for the nonlinear analysis of composite frames with short-term loading. The behavior of CFT beam-columns may change with time. The limitation of the proposed model is that it did not account for the effects of long-term loading on the behavior of CFT beam-columns. Therefore, the numerical models need to be extended for the nonlinear time-dependent analysis of slender steel-concrete composite beam-columns.

- Other areas other research may also include:

  - ✓ Interaction between steel and concrete.
  - ✓ Effect of combined axial loading and bi-axial bending conditions
  - ✓ The use of stiffeners in circular CFT columns

REFERENCES

1) AIJ. (2008). *Recommendations for Design and Construction of Concrete Filled Steel Tubular Structures*. Architectural Institute of Japan, Tokyo, Japan.

2) AISC 360-05. (2005). *Specification for Structural Steel Buildings*. American Institute of Steel Construction, Chicago, Illinois, USA.

3) AISC 360-10. (2010). *Specification for structural steel buildings*. Chicago. Chicago, Illinois: American Institute of Steel Construction.

4) AISC-LRFD (2005). *Load and resistance factor specification for structural steel buildings*. AISC, Chicago, IL.

5) Andrew Liew, Leroy Gardner and Philippe Block. Moment-Curvature-Thrust Relationships for Beam-Columns. *Structures 11 (2017) 146–154*

6) BC4 (2015). *Design Guide for Concrete Filled Tubular Members with High Strength Materials - An Extension of Eurocode 4 Method to C90/105 Concrete and S550 Steel*. Building and Construction Authority, Singapore.

7) CHIOREAN, C.G. A computer method for nonlinear inelastic analysis of 3D composite steel-concrete frame structures. Engineering Structures, v.57, 2013; p.125-152.

8) Choi, K. K., and Xiao, Y. (2010). "Analytical studies of concrete-filled circular steel tubes under axial compression." *Journal of Structural Engineering*, ASCE, **136**(5), 565-573.

9) Denavit, M. D. (2012). "Characterization of Behavior of Steel-Concrete Composite Members and Frames with Applications for Design [Dissertation]." The University of Illinois at Urbana-Champaign.

10) El-Heweity, M. M. (2012). "On the performance of circular concrete-filled high strength steel columns under axial loading." *Alexandria Engineering Journal*, **51**(2), 109-119.

11) Ellobody, E. (2013). "Numerical modelling of fiber reinforced concrete-filled stainless steel tubular columns." *Thin-Walled Structures*, **63**, 1-12.

12) Ellobody, E., Young, B. and Lam, D. (2006). "Behaviour of normal and high strength concrete-filled compact steel tube circular stub columns." *Journal of Constructional Steel Research*, **62**(7), 706-715.

13) El-Tawil, S., Sanz-Picon, C. F., and Deierlein, G. G. (1995). ''Evaluation of ACI-318 and AISC (LRFD) strength provisions for composite columns.'' *J. Constr. Steel Res.*, 34~1!, 103–126.

14) EN 1994-1-1 (2004). Eurocode 4: Design of composite steel and concrete structures – Part 1-1: General rules and rules for buildings.

15) Fujimoto, T., Mukai, A., Nishiyama, I., and Sakino, K. (2004). "Behavior of eccentrically loaded concrete-filled steel tubular columns." *Journal of Structural Engineering*, ASCE, **130**(2), 203-212.

16) Furlong, R. W. (1967). "Strength of Steel-Encased Concrete Beam-Columns." *Journal of the Structural Division, ASCE,* 93(ST5), 113–124.

17) Giakoumelis, G., and Lam, D. (2004). "Axial Capacity of Circular Concrete-Filled Tube Columns." *Journal of Constructional Steel Research*, 60(7), 1049–1068.

18) Gourley, B. C., Tort, C., Denavit, M. D., Schiller, P. H., and Hajjar, J. F. (2008). *A Synopsis of Studies of the Monotonic and Cyclic Behavior of Concrete-Filled Steel Tube Members, Connections, and Frames*. Newmark Structural Laboratory Report NSEL-008, Department of Civil and Environmental Engineering, the University of Illinois at Urbana-Champaign, Urbana, Illinois, USA.

19) Gunthar Pangaribuan, 2016. An Introduction to EXCEL for Civil Engineers: From engineering theory to Excel practice. Jakarta.

20) Han, L. H., Yao, G. H., and Tao, Z. (2007b). "Behaviors of concrete-filled steel tubular members subjected to combined loading." *Thin-Walled Structures*, 45(6), 600-619.

21) Han, L.-H., and Yan, S. (2000). "Experimental Studies on The Strength with High Slenderness Ratio Concrete-Filled Steel Tubular Columns." *Proceedings of the Sixth ASCCS International Conference on Steel-Concrete Composite Structures*, Y. Xiao and S. Mahin, eds., Association for International Cooperation and Research in Steel-Concrete Composite Structures, Los Angeles, 419–426.

22) Han, L.-H., Zheng, L.-Q., He, S.-H., and Tao, Z. (2011). "Tests on curved concrete filled steel tubular members subjected to axial compression," Journal of Constructional Steel Research, 67 (6), pp. 965-976.

23) Han, L.-H.; Li, W. & Bjorhovde, R. 2014b. Developments and advanced applications of concrete-filled steel tubular (CFST) structures: Members. *Journal of Constructional Steel Research*, 100: 211-228.

24) Hatzigeorgiou, G. D. (2008). "Numerical Model for the Behavior and Capacity of Circular CFT Columns, Part I: Theory." *Engineering Structures*, 30(6), 1573–1578.

25) Hu, H. T., Huang, C. S., Wu, M. H. and Wu, Y. M. (2003). "Nonlinear analysis of axially loaded concrete-filled tube columns with confinement effect." *Journal of Structural Engineering*, ASCE, **129**(10), 1322-1329.

26) J. Y. Richard Liew and Mingxiang Xiong. 2015. Design Guide for Concrete Filled Tubular Members with High Strength Materials to Eurocode 4. Book, School of Civil and Environmental Engineering, National University of Singapore.

27) Johansson, M., and Gylltoft, K. (2002). "Mechanical Behavior of Circular Steel-Concrete Composite Stub Columns." *Journal of Structural Engineering*, ASCE, 128(8), 1073–1081.

28) Johansson, M., Claeson, C., Gylltoft, K. and Akesson, M. (2000). "Structural Behavior of Circular Composite Columns Under Various Means of Load Application," Proceedings of 6th ASCCS Conference Los Angeles, USA, March 22-24, 427-433.

29) Kim, D. K. (2005). "A Database for Composite Columns." M.S. Thesis, School of Civil and Environmental Engineering, Georgia Institute of Technology, Atlanta, Georgia.

30) Lai, Z. (2014). "Analytical Database on Noncompact and Slender CFT Members." Purdue University Research Repository. doi: 10.4231/R7QC01DR

31) Lee, S. H., Uy, B., Kim, S. H., Choi, Y. H. and Choi, S. M. (2011). "Behavior of high strength circular concrete-filled steel tubular (CFST) column under eccentric loading." *Journal of Constructional Steel Research*, **67**(1), 1-13.

32) Liang, Q. Q. (2011a). "High strength circular concrete-filled steel tubular slender beam-columns, Part I: Numerical analysis." *Journal of Constructional Steel Research*, **67**(2), 164-171.

33) Liang, Q. Q. (2011b). "High strength circular concrete-filled steel tubular slender beam-columns, Part II: Fundamental behavior." *Journal of Constructional Steel Research*, **67**(2), 172-180.

34) Liang, Q. Q. and Fragomeni, S. (2009). "Nonlinear analysis of circular concrete-filled steel tubular short columns under axial loading." *Journal of Constructional Steel Research*, **65**(12), 2186-2196.

35) Liang, Q. Q. and Fragomeni, S. (2010). "Nonlinear analysis of circular concrete-filled steel tubular short columns under eccentric loading." *Journal of Constructional Steel Research*, **66**(2), 159-169.

36) Lu, H., Han, L.-H., and Zhao, X.-L. (2009). "Analytical Behavior of Circular Concrete-Filled Thin-Walled Steel Tubes Subjected to Bending." *Thin-Walled Structures*, 47(3), 346–358.

37) Mander, J. B., and Priestley, M. J. N. and Park, R. (1988). "Theoretical stress-strain model for confined concrete." *Journal of Structural Engineering*, ASCE, **114**(8), 1804-1826.

38) Matsui, C., Tsuda, K., and Ishibashi, Y. (1995). "Slender Concrete-Filled Steel Tubular Columns under Combined Compression and Bending," Structural Steel, PSSC '95, Proceedings of the Fourth Pacific Structural Steel Conference, Shanmugam, N. E. and Choo, Y. S. (eds.), Singapore, October 25-27, 1995, Pergamon, Elsevier Science, Vol. 3, pp. 29-36.

39) Moon, J., Roeder, C. W., Lehman, D. E., and Lee, H.-E. (2012). "Analytical Modeling of Bending of Circular Concrete-Filled Steel Tubes." *Engineering Structures*, Elsevier Ltd, 42, 349–361.

40) Neogi, P. K., Sen, H. K. and Chapman, J. C. (1969). "Concrete-filled tubular steel columns under eccentric loading." *The Structural Engineer*, **47**(5), 187-195.

41) Nishiyama, I., Morino, S., Sakino, K., Nakahara, H., Fujimoto, T., Mukai, A., Inai, E., Kai, M., Tokinoya, H., Fukumoto, T., Mori, K., Yoshioka, K., Mori, O., Yonezawa, K., Uchikoshi, M., and Hayashi, Y. (2002). *Summary of Research on Concrete-Filled Structural Steel Tube Columns System Carried Out Under The US-Japan Cooperative Research Program on Composite and Hybrid Structures*. BRI Research Paper, Building Research Institute, Japan.

42) O'Shea, M. D., and Bridge, R. (1997a). *Tests on Circular Thin-Walled Steel Tubes Filled with Very High Strength Concrete*. Research Report No. R754, Department of Civil Engineering, The University of Sydney, Sydney, Australia.

43) O'Shea, M. D., and Bridge, R. (1997b). *Tests on Circular Thin-Walled Steel Tubes Filled with Medium and High Strength Concrete*. Research Report No. R755, Department of Civil Engineering, The University of Sydney, Sydney, Australia.

44) O'Shea, M. D., and Bridge, R. Q. (2000). "Design of Circular Thin-walled Concrete-filled Steel Tubes," Journal of Structural Engineering, ASCE, 126(11), 1295-1303.

45) Perea, T. (2010). "Analytical and Experimental Study on Slender Concrete-Filled Steel Tube Columns and Beam-Columns." Ph.D. Dissertation, School of Civil and Environmental Engineering, Georgia Institute of Technology, Atlanta, Georgia.

46) Perea, T., Leon, R. T., Hajjar, J. F., and Denavit, M. D. (2012). "Full-Scale Tests of Slender Concrete-Filled Tubes: Axial Behavior." *Journal of Structural Engineering*, ASCE.

47) Popovics, S. (1973). "A numerical approach to the complete stress-strain curve of concrete." *Cement and Concrete Research*, 3(5), 583–599.

48) Portolés, J. M., Romero, M. L., Bonet, J. L. and Filippou, F. C. (2011). "Experimental study of high strength concrete-filled circular tubular columns under eccentric loading." *Journal of Constructional Steel Research*, **67**(4), 623-633.

49) Portolés, J. M., Romero, M. L., Filippou, F. C. and Bonet, J. L. (2011). "Simulation and design recommendations of eccentrically loaded slender concrete-filled tubular columns." *Engineering Structures*, **33**(5), 1576-1593.

50) Sakino, K., and Nakahara, H. (2000). "Practical Analysis for High-Strength CFT Columns under Eccentric Compression." *Proceedings of the Sixth ASCCS International Conference on Steel-Concrete Composite Structures*, Y. Xiao and S. Mahin, eds., Los Angeles, California, 473–480.

51) Shanmugam, N. E., and Lakshmi, B. (2001). "State of the art report on steel-concrete composite columns." Journal of Constructional Steel Research, 57(10), 1041-1080.

52) Spacone, E. and El-Tawil, S. (2004). "Nonlinear analysis of steel-concrete composite structures: state of the art." *Journal of Structural Engineering*, ASCE, **130**(2), 159-168.

53) Spacone, E., Filippou, F. C., and Taucer, F. F. (1996a). ''Fiber beam-column model for nonlinear analysis of R/C frames. Part I: Formulation.'' *Earthquake Eng. Struct. Dyn.*, 25(7), 711–742.

54) Spacone, E., Filippou, F. C., and Taucer, F. F. (1996b). ''Fiber beam-column model for nonlinear analysis of R/C frames. Part II: Application.'' *Earthquake Eng. Struct. Dyn.*, 25(7), 728-742.

55) Susantha, K. A. S., Ge, H. and Usami, T. (2001). "Uniaxial stress-strain relationship of concrete confined by various shaped steel tubes." *Engineering Structures*, **23**(10), 1331-1347.

56) Tang, J., Hino, S., Kuroda, I. and Ohta, T. (1996). "Modeling of stress-strain relationships for steel and concrete in concrete filled circular steel tubular columns." *Steel Construction Engineering*, JSSC, **3**(11), 35-46.

57) Tao, Z., Han, L.-H., and Wang, D.-Y. (2008). "Strength and ductility of stiffened thin-walled hollow steel structural stub columns filled with concrete." Thin-Walled Structures, 46(10), 1113-1128.

58) Yoshioka, K., Inai, E., Hukumoto, N., Kai, M., Murata, Y., Noguchi, T., Tanaka, Y., Tokinoya, H., and Mukai, A. (1995). "Compressive Tests on CFT Short Columns. Part 1: Circular CFT Columns." *Proceedings of the Second Joint Technical Coordinating Committee (JTCC) on Composite and Hybrid Structures, Phase 5: Composite and Hybrid Structures*, National Science Foundation, Honolulu, Hawaii.

59) Zhichao Lai. (2014). "Experimental database, analysis, and design of noncompact and slender concrete-filled steel tube (CFST) members." PhD. Thesis, Purdue University Graduate School, West Lafayette, Indiana.

60) Zubydan, A. H. and ElSabbagh, A. I. (2011). "Monotonic and cyclic behavior of concrete-filled steel-tube beam-columns considering local buckling effect." *Thin-Walled Structure*, **49**(4), 465-481.

APPENDICES

APPENDIX A: VERIFICATION RESULTS

Table A-1: Material and Geometric Properties – CCFT Validation Set – Short Column

Col. No.	*Spec.*	*D (mm)*	*t (mm)*	*kl (mm)*	*f'c (Mpa)*	*Fy (Mpa)*	*L/D*	*D/t*	*Pexp (kN)*
Gardner and Jacobson, 1967									
1	22	76.454	1.676	152.4	40.887	363.367	1.993	45.606	434.570
2	23	76.454	1.702	152.4	25.925	363.367	1.993	44.925	372.298
3	19	76.454	1.702	152.4	24.960	363.367	1.993	44.925	355.840
4	3	101.6	3.073	203.2	34.130	605.381	2.000	33.058	1112.000
5	4	101.6	3.073	203.2	31.165	605.381	2.000	33.058	1067.520
6	8	120.904	4.064	241.3	34.406	451.623	1.996	29.750	1200.960
7	9	120.904	4.089	241.3	29.580	451.623	1.996	29.565	1200.960
8	10	120.904	4.089	241.3	25.925	451.623	1.996	29.565	1112.000
9	13	152.654	3.175	304.8	20.892	415.079	1.997	48.080	1200.960
10	14	152.654	3.150	304.8	23.098	415.079	1.997	48.468	1200.960
11	15	152.654	4.928	304.8	41.991	633.651	1.997	30.979	2908.992
12	16	152.654	4.902	304.8	43.439	633.651	1.997	31.140	2913.440
Gardner, 1968									
13	2a	168.656	2.642	304.8	34.130	297.864	1.807	63.846	1218.752
14	2b	169.164	2.616	304.8	36.544	317.170	1.802	64.660	1307.712
15	6a	168.148	3.607	304.8	32.751	221.330	1.813	46.620	1432.256
16	7a	168.656	5.004	304.8	32.889	260.631	1.807	33.706	1966.016
Chapman and Neogi, 1966									
17	A5	355.6	4.724	1879.6	20.961	276.490	5.286	75.269	3517.034
18	A6	355.6	8.026	2082.8	23.443	355.093	5.857	44.304	7432.608
19	B1	127.254	1.626	711.2	66.192	370.951	5.589	78.281	1285.472
20	B2X	127	2.946	711.2	66.192	328.892	5.600	43.103	1305.488
21	SC2	168.402	4.521	812.8	43.163	297.864	4.827	37.247	2232.896
22	SC3	168.148	4.521	812.8	43.163	297.864	4.834	37.191	2112.800
23	SC4	168.402	4.470	812.8	23.029	297.864	4.827	37.670	1743.616
Sakino and Hayashi, 1991									
24	H-20-2	178.054	8.992	251.46	45.438	283.385	1.412	19.802	3177.206
25	L-32-2	179.07	5.512	251.46	23.926	248.220	1.404	32.488	1814.339
26	H-32-1	179.07	5.512	251.46	43.645	248.220	1.404	32.488	2039.853
27	H-58-1	173.99	2.997	251.46	45.714	266.147	1.445	58.051	1608.397
Luksha and Nesterovich, 1991									
28	SB-1	159.004	5.080	477.52	33.165	391.636	3.003	31.300	2229.782
Furlong,1967									

Col. No.	*Spec.*	*D (mm)*	*t (mm)*	*kl (mm)*	*f'c (Mpa)*	*Fy (Mpa)*	*L/D*	*D/t*	*Pexp (kN)*
29		114.3	3.175	914.4	28.959	413.700	8.000	36.000	756.160
30		127	2.413	914.4	35.165	289.590	7.200	52.632	658.304
31		152.4	1.549	914.4	21.030	330.960	6.000	98.361	682.323
32		152.4	1.549	914.4	25.856	330.960	6.000	98.361	733.030
Gardner and Jacobson, 1967									
33	5	120.65	4.089	1049.02	34.406	451.623	8.695	29.503	1156.480
34	6	120.904	4.089	1049.02	29.580	451.623	8.676	29.565	1092.429
35	7	120.904	4.089	1049.02	25.925	451.623	8.676	29.565	949.648
36	20	76.454	1.702	609.6	40.887	363.367	7.973	44.925	411.440
37	21	76.454	1.702	609.6	25.925	363.367	7.973	44.925	330.486
Knolwes and Park, 1969									
38	5	88.9	5.842	508	40.887	399.910	5.714	15.217	991.904
39	9	82.55	1.397	812.8	40.887	482.650	9.846	59.091	400.320
Masuo, Adachi, Kawabata, Kobayashi, and Konishi, 1991									
40	1G2	190.754	5.994	1150.62	48.334	504.714	6.032	31.822	3147.850
41	2G2	267.462	7.010	1600.2	48.334	460.586	5.983	38.152	5187.258
Janss and Guiaux, 1970									
42	4	218.186	6.502	942.34	29.580	301.312	4.319	33.555	2754.646
43	5	218.44	6.375	942.34	31.372	301.312	4.314	34.263	2744.861
44	6	219.202	6.045	942.34	31.372	301.312	4.299	36.261	2803.574
45	13.3	95.504	3.734	505.46	33.648	280.627	5.293	25.578	666.755
Janss,1974									
46	2	405.892	5.004	1620.52	38.198	355.782	3.992	81.117	7548.701
47	4	405.892	5.004	1209.04	35.992	355.782	2.979	81.117	7450.400
48	8	356.108	8.204	1498.6	27.649	321.307	4.208	43.406	6813.446
49	9	356.108	7.747	1496.06	27.649	321.307	4.201	45.967	7185.744
50	13	275.082	8.992	1440.18	27.649	626.066	5.235	30.593	8038.870
Yoshoika et al., 1995									
51	CC4-A-2	149.098	2.972	447.04	25.374	283.385	2.998	50.171	941.197
52	CC4-A-4-1	148.844	2.972	447.04	40.405	283.385	3.003	50.085	1063.517
53	CC4-A-4-2	149.098	2.972	447.04	40.405	283.385	2.998	50.171	1079.530
54	CC4-A-8	149.352	2.972	447.04	76.810	283.385	2.993	50.256	1780.090
55	CC4-C-2	300.482	2.972	901.7	25.374	283.385	3.001	101.111	2381.459
56	CC4-C-4-1	300.228	2.972	901.7	41.025	283.385	3.003	101.026	3276.397
57	CC4-C-8	300.482	2.972	901.7	76.810	283.385	3.001	101.111	5537.760
58	CC4-D-2	450.088	2.972	1348.74	25.374	283.385	2.997	151.453	4413.306
59	CC4-D-4-1	449.834	2.972	1348.74	41.025	283.385	2.998	151.368	6867.267
60	CC4-D-8	449.834	2.972	1348.74	84.946	283.385	2.998	151.368	11661.322
61	CC6-A-2	121.92	4.547	365.76	25.374	578.491	3.000	26.816	1508.762

Col. No.	*Spec.*	*D (mm)*	*t (mm)*	*kl (mm)*	*f'c (Mpa)*	*Fy (Mpa)*	*L/D*	*D/t*	*Pexp (kN)*
62	CC6-A-4-2	121.92	4.547	365.76	40.405	578.491	3.000	26.816	1662.662
63	CC6-A-8	121.412	4.547	365.76	76.810	578.491	3.013	26.704	2099.011
64	CC6-C-2	238.506	4.547	716.28	25.374	578.491	3.003	52.458	3033.981
65	CC6-C-4-2	237.998	4.547	713.74	40.405	578.491	2.999	52.346	3646.026
66	CC6-C-8	237.744	4.547	713.74	76.810	578.491	3.002	52.291	5576.013
67	CC6-D-2	360.68	4.547	1082.04	25.374	578.491	3.000	79.330	5631.168
68	CC6-D-4-1	360.68	4.547	1082.04	41.025	578.491	3.000	79.330	7257.357
69	CC6-D-8	360.426	4.547	1082.04	84.946	578.491	3.002	79.274	11501.194
70	CC8-A-2	107.95	6.477	325.12	25.374	834.295	3.012	16.667	2274.262
71	CC8-A-4-2	108.204	6.477	325.12	40.405	834.295	3.005	16.706	2401.030
72	CC8-A-8	108.204	6.477	325.12	76.810	834.295	3.005	16.706	2711.501
73	CC8-C-2	221.996	6.477	665.48	25.374	834.295	2.998	34.275	4962.634
74	CC8-C-4-2	221.996	6.477	665.48	40.405	834.295	2.998	34.275	5712.566
75	CC8-C-8	222.504	6.477	668.02	76.810	834.295	3.002	34.353	7301.392
76	CC8-D-2	336.804	6.477	1010.92	25.374	834.295	3.002	52.000	8472.106
77	CC8-D-4-2	336.804	6.477	1010.92	41.025	834.295	3.002	52.000	9831.859
78	CC8-D-8	336.55	6.477	1010.92	84.946	834.295	3.004	51.961	13771.898
Lin, 1988									
79	D6	150.114	2.108	800.1	20.685	248.220	5.330	71.205	787.296
Kenny, Bruce, and Bjorhovde, 1994									
80		139.7	9.220	914.4	38.405	681.916	6.545	15.152	3046.880
81		177.8	12.751	914.4	38.405	593.660	5.143	13.944	5253.088
O'Shea and Bridge, 1997									
82	S30CS	165.1254	2.997	579.12	113.492	364.056	3.507	55.093	2675.027
83	S20CS	190.1444	2.007	660.4	113.492	271.663	3.473	94.759	3362.688
84	S16CS	190.1444	1.549	662.94	113.492	315.102	3.487	122.721	3262.608
85	S12CS	190.1444	1.143	660.4	113.492	184.786	3.473	166.356	3060.669
Matsui etal., 1997									
86	C4-0	165.354	4.089	660.4	31.855	353.024	3.994	40.435	1563.472
Giakoumelis and Lam, 2003									
87	C3	114.554	3.988	299.72	31.372	342.682	2.616	28.726	947.424
88	C4	114.554	3.988	299.72	93.565	342.682	2.616	28.726	1307.267
89	C5a	114.554	3.810	299.72	34.682	342.682	2.616	30.067	928.742
90	C6a	114.3	3.937	299.72	97.151	342.682	2.622	29.032	1358.419
91	C8	115.062	4.928	299.72	104.873	364.746	2.605	23.351	1786.317
92	C9	115.062	5.029	299.72	57.573	364.746	2.605	22.879	1412.240
93	C11	114.3	3.759	299.72	57.573	342.682	2.622	30.405	1066.630
94	C13	114.046	3.861	299.72	31.924	342.682	2.628	29.539	947.424
95	C14	114.554	3.835	299.72	98.874	342.682	2.616	29.868	1358.419

Col. No.	*Spec.*	*D (mm)*	*t (mm)*	*kl (mm)*	*f'c (Mpa)*	*Fy (Mpa)*	*L/D*	*D/t*	*Pexp (kN)*
Scheneider,1998									
96	C1	140.716	2.997	609.6	28.201	284.764	4.332	46.949	880.704
Han and Yao, 2003									
97	S-1	119.888	2.642	360.68	20.064	339.924	3.008	45.385	639.622
98	S-3	119.888	2.642	360.68	35.992	339.924	3.008	45.385	815.763
O'Shea and Bridge, 2000									
99	S30CL50B	165.1	2.819	561.34	48.265	363.367	3.400	58.559	1758.294
100	S30CL50C	165.1	2.819	571.5	38.198	363.367	3.462	58.559	1648.429
101	S16CL50B	189.992	1.524	657.86	48.265	306.138	3.463	124.667	1840.138
102	S12CL50C	189.992	1.118	657.86	38.198	185.476	3.463	170.000	1307.267
103	S30CL80C	165.1	2.819	581.66	56.401	363.367	3.523	58.559	2038.963
104	S12CL10A	189.992	1.118	660.4	107.976	185.476	3.476	170.000	3218.573
105	S30CS50B	165.1	2.819	581.66	48.265	363.367	3.523	58.559	1661.328
106	S20CS50A	189.992	1.930	662.94	41.025	256.494	3.489	98.421	1677.341
107	S16CS50B	189.992	1.524	665.48	48.265	306.138	3.503	124.667	1694.243
108	S12CS50A	189.992	1.118	665.48	41.025	185.476	3.503	170.000	1376.211
109	S30CS80A	165.1	2.819	581.66	80.189	363.367	3.523	58.559	2293.834
110	S20CS80B	189.992	1.930	662.94	74.673	256.494	3.489	98.421	2590.960
111	S16CS80A	189.992	1.524	662.94	80.189	306.138	3.489	124.667	2600.746
112	S12CS80A	189.992	1.118	662.94	80.189	185.476	3.489	170.000	2293.834
113	S30CS10A	165.1	2.819	576.58	107.976	363.367	3.492	58.559	2671.914
114	S20CS10A	189.992	1.930	660.4	107.976	256.494	3.476	98.421	3358.685
115	S16CS10A	189.992	1.524	660.4	107.976	306.138	3.476	124.667	3258.605
116	S12CS10A	189.992	1.118	660.4	107.976	185.476	3.476	170.000	3056.666
Kang, Lim, and Kim, 2002									
117	KLM2002	101.6	3.607	304.8	54.195	342.682	3.000	28.169	946.090
118	KLM2002	76.2	2.311	228.6	54.195	279.937	3.000	32.967	438.573
119	KLM2002	89.154	2.388	266.7	54.195	277.179	2.991	37.340	618.717
120	KLM2002	114.3	2.286	342.9	54.195	364.746	3.000	50.000	918.957
121	KLM2002	114.3	2.286	342.9	46.679	364.746	3.000	50.000	669.424

Table A-2: Comparison – CCFT Validation Set – Short Column

Col. No.	*Spec.*	*Pnum (kN)*	*Pexp (kN)*	*Pexp/Ppred by*				
				Numerical	*AISC 1999*	*AISC 2005*	*Eurocode*	*Plastic*
Gardner and Jacobson, 1967								
1	22	404.188	434.570	1.075	1.510	1.420	1.090	1.380
2	23	322.911	372.298	1.153	1.570	1.500	1.100	1.460

Col. No.	*Spec.*	*Pnum (kN)*	*Pexp (kN)*	*Pexp/Ppred by*				
				Numerical	*AISC 1999*	*AISC 2005*	*Eurocode*	*Plastic*
3	19	317.477	355.840	1.121	1.530	1.460	1.060	1.430
4	3	1012.319	1112.000	1.098	1.420	1.380	0.990	1.350
5	4	980.451	1067.520	1.089	1.400	1.360	0.970	1.340
6	8	1302.604	1200.960	0.922	1.250	1.210	0.870	1.180
7	9	1232.386	1200.960	0.975	1.300	1.260	0.900	1.240
8	10	1177.920	1112.000	0.944	1.250	1.210	0.850	1.190
9	13	1141.682	1200.960	1.052	1.320	1.270	0.900	1.240
10	14	1161.291	1200.960	1.034	1.280	1.230	0.880	1.200
11	15	2611.831	2908.992	1.114	1.450	1.400	1.020	1.370
12	16	2625.251	2913.440	1.110	1.440	1.390	1.010	1.360
Gardner, 1968								
13	2a	1209.827	1218.752	1.007	1.200	1.120	0.880	1.080
14	2b	1297.954	1307.712	1.008	1.200	1.120	0.880	1.080
15	6a	1323.117	1432.256	1.082	1.470	1.370	1.070	1.330
16	7a	1672.992	1966.016	1.175	1.610	1.530	1.130	1.490
Chapman and Neogi, 1966								
17	A5	3646.942	3517.034	0.964	0.940	1.080	0.940	1.040
18	A6	6351.840	7432.608	1.170	1.550	1.490	1.300	1.440
19	B1	1092.014	1285.472	1.177	1.450	1.340	1.220	1.260
20	B2X	1392.068	1305.488	0.938	1.310	1.220	1.100	1.160
21	SC2	1942.665	2232.896	1.149	1.590	1.500	1.290	1.440
22	SC3	1938.263	2112.800	1.090	1.510	1.430	1.220	1.370
23	SC4	1452.574	1743.616	1.200	1.640	1.580	1.300	1.520
Sakino and Hayashi, 1991								
24	H-20-2	2833.657	3177.206	1.121	1.490	1.430	1.030	1.400
25	L-32-2	1618.195	1814.339	1.121	1.520	1.450	1.020	1.420
26	H-32-1	2122.040	2039.853	0.961	1.300	1.230	0.920	1.190
27	H-58-1	1504.654	1608.397	1.069	1.250	1.160	0.930	1.120
Luksha and Nesterovich, 1991								
28	SB-1	1955.463	2229.782	1.140	1.550	1.490	1.140	1.450
Furlong,1967								
29		928.545	756.160	0.814	1.160	1.120	1.070	1.090
30		758.942	658.304	0.867	1.090	1.030	0.950	0.980
31		679.836	682.323	1.004	1.260	1.180	1.060	1.130
32		756.533	733.030	0.969	1.200	1.120	1.010	1.070
Gardner and Jacobson, 1967								
33	5	1298.791	1156.480	0.890	1.280	1.240	1.200	1.200
34	6	1232.386	1092.429	0.886	1.250	1.220	1.190	1.180
35	7	1177.920	949.648	0.806	1.130	1.100	1.070	1.070

Col. No.	*Spec.*	*Pnum (kN)*	*Pexp (kN)*	*Pexp/Ppred by*				
				Numerical	*AISC 1999*	*AISC 2005*	*Eurocode*	*Plastic*
36	20	404.188	411.440	1.018	1.480	1.400	1.330	1.340
37	21	322.911	330.486	1.023	1.440	1.380	1.310	1.340
Knolwes and Park, 1969								
38	5	1001.887	991.904	0.990	1.320	1.290	1.130	1.250
39	9	425.511	400.320	0.941	1.270	1.210	1.150	1.140
Masuo, Adachi, Kawabata, Kobayashi, and Konishi, 1991								
40	1G2	3672.532	3147.850	0.857	1.170	1.120	1.020	1.080
41	2G2	6144.652	5187.258	0.844	1.180	1.080	0.980	1.040
Janss and Guiaux, 1970								
42	4	2868.020	2754.646	0.960	1.310	1.250	1.020	1.210
43	5	2916.808	2744.861	0.941	1.280	1.220	1.000	1.180
44	6	2855.502	2803.574	0.982	1.340	1.280	1.050	1.230
45	13.3	660.008	666.755	1.010	1.430	1.370	1.160	1.320
Janss,1974								
46	2	7024.077	7548.701	1.075	1.230	1.140	0.980	1.090
47	4	6796.466	7450.400	1.096	1.250	1.160	0.970	1.120
48	8	6538.775	6813.446	1.042	1.380	1.310	1.070	1.270
49	9	6335.986	7185.744	1.134	1.490	1.420	1.170	1.370
50	13	7273.175	8038.870	1.105	1.400	1.360	1.210	1.330
Yoshoika et al., 1995								
51	CC4-A-2	897.442	941.197	1.049	1.290	1.220	0.890	1.190
52	CC4-A-4-1	1118.628	1063.517	0.951	1.140	1.060	0.820	1.030
53	CC4-A-4-2	1121.536	1079.530	0.963	1.150	1.080	0.830	1.040
54	CC4-A-8	1681.002	1780.090	1.059	1.240	1.140	0.950	1.090
55	CC4-C-2	2559.333	2381.459	0.930	1.060	0.990	0.820	0.950
56	CC4-C-4-1	3474.840	3276.397	0.943	1.050	0.960	0.830	0.920
57	CC4-C-8	5561.145	5537.760	0.996	1.070	0.970	0.870	0.920
58	CC4-D-2	4695.342	4413.306	0.940	0.980	0.910	0.780	0.860
59	CC4-D-4-1	6762.261	6867.267	1.016	1.050	0.960	0.850	0.910
60	CC4-D-8	12599.522	11661.322	0.926	0.950	0.860	0.790	0.810
61	CC6-A-2	1467.769	1508.762	1.028	1.280	1.250	0.840	1.240
62	CC6-A-4-2	1700.658	1662.662	0.978	1.270	1.230	0.860	1.210
63	CC6-A-8	2182.035	2099.011	0.962	1.300	1.250	0.920	1.220
64	CC6-C-2	3429.613	3033.981	0.885	1.080	1.040	0.720	1.020
65	CC6-C-4-2	3970.146	3646.026	0.918	1.090	1.040	0.760	1.020
66	CC6-C-8	5290.410	5576.013	1.054	1.210	1.140	0.890	1.100
67	CC6-D-2	6032.749	5631.168	0.933	1.130	1.080	0.850	1.040
68	CC6-D-4-1	7321.700	7257.357	0.991	1.160	1.090	0.890	1.050
69	CC6-D-8	10933.695	11501.194	1.052	1.170	1.080	0.930	1.030

Col. No.	*Spec.*	*Pnum (kN)*	*Pexp (kN)*	*Pexp/Ppred by*				
				Numerical	*AISC 1999*	*AISC 2005*	*Eurocode*	*Plastic*
70	CC8-A-2	2130.688	2274.262	1.067	1.220	1.210	0.830	1.200
71	CC8-A-4-2	2341.322	2401.030	1.026	1.220	1.210	0.840	1.190
72	CC8-A-8	2778.466	2711.501	0.976	1.240	1.210	0.870	1.190
73	CC8-C-2	5323.376	4962.634	0.932	1.130	1.110	0.750	1.100
74	CC8-C-4-2	6064.687	5712.566	0.942	1.190	1.150	0.800	1.130
75	CC8-C-8	7759.207	7301.392	0.941	1.240	1.190	0.870	1.160
76	CC8-D-2	9003.311	8472.106	0.941	1.160	1.130	0.870	1.100
77	CC8-D-4-2	10109.841	9831.859	0.973	1.170	1.130	0.890	1.100
78	CC8-D-8	13165.825	13771.898	1.046	1.210	1.140	0.940	1.090
Lin, 1988								
79	D6	659.430	787.296	1.194	1.490	1.410	1.210	1.340
Kenny, Bruce, and Bjorhovde, 1994								
80		3505.346	3046.880	0.869	1.090	1.070	1.040	1.050
81		5351.608	5253.088	0.982	1.410	1.570	1.270	1.320
O'Shea and Bridge, 1997								
82	S30CS	2834.887	2675.027	0.944	1.290	1.340	1.260	1.330
83	S20CS	3244.381	3362.688	1.036	1.360	1.400	1.390	1.430
84	S16CS	3220.922	3262.608	1.013	1.330	1.370	1.360	1.390
85	S12CS	3006.351	3060.669	1.018	1.310	1.340	1.370	1.380
Matsui etal., 1997								
86	C4-0	1691.377	1563.472	0.924	1.480	1.600	1.290	1.450
Giakoumelis and Lam, 2003								
87	C3	975.571	947.424	0.971	1.580	1.720	1.270	1.540
88	C4	1549.852	1307.267	0.843	1.310	1.380	1.180	1.320
89	C5a	991.433	928.742	0.937	1.530	1.660	1.240	1.500
90	C6a	1559.606	1358.419	0.871	1.340	1.420	1.210	1.360
91	C8	1683.051	1786.317	1.061	1.520	1.610	1.350	1.520
92	C9	1392.456	1412.240	1.014	1.580	1.710	1.320	1.560
93	C11	1230.150	1066.630	0.867	1.430	1.530	1.230	1.420
94	C13	959.878	947.424	0.987	1.600	1.750	1.300	1.570
95	C14	1564.788	1358.419	0.868	1.330	1.400	1.210	1.350
Scheneider,1998								
96	C1	967.915	880.704	0.910	1.470	1.580	1.310	1.460
Han and Yao, 2003								
97	S-1	675.629	639.622	0.947	1.490	1.620	1.210	1.450
98	S-3	887.604	815.763	0.919	1.270	1.200	0.950	1.160
O'Shea and Bridge, 2000								
99	S30CL50B	1587.465	1758.294	1.108	1.320	1.240	1.040	1.180
100	S30CL50C	1400.536	1648.429	1.177	1.420	1.340	1.110	1.280

Col. No.	*Spec.*	*Pnum (kN)*	*Pexp (kN)*	*Pexp/Ppred by*				
				Numerical	*AISC 1999*	*AISC 2005*	*Eurocode*	*Plastic*
101	S16CL50B	1560.561	1840.138	1.179	1.330	1.210	1.080	1.150
102	S12CL50C	1095.984	1307.267	1.193	1.290	1.170	1.060	1.110
103	S30CL80C	1738.985	2038.963	1.173	1.400	1.300	1.110	1.240
104	S12CL10A	2863.048	3218.573	1.124	1.230	1.110	1.020	1.030
105	S30CS50B	1587.465	1661.328	1.047	1.250	1.170	0.990	1.120
106	S20CS50A	1420.212	1677.341	1.181	1.360	1.250	1.100	1.190
107	S16CS50B	1560.561	1694.243	1.086	1.220	1.120	0.990	1.060
108	S12CS50A	1165.770	1376.211	1.181	1.280	1.160	1.050	1.090
109	S30CS80A	2183.388	2293.834	1.051	1.240	1.140	0.990	1.080
110	S20CS80B	2251.974	2590.960	1.151	1.300	1.180	1.060	1.110
111	S16CS80A	2361.744	2600.746	1.101	1.230	1.120	1.010	1.050
112	S12CS80A	2154.713	2293.834	1.065	1.160	1.050	0.960	0.980
113	S30CS10A	2700.153	2671.914	0.990	1.150	1.060	0.930	1.000
114	S20CS10A	3070.799	3358.685	1.094	1.220	1.110	1.010	1.040
115	S16CS10A	3053.630	3258.605	1.067	1.180	1.080	0.980	1.010
116	S12CS10A	2863.048	3056.666	1.068	1.170	1.050	0.970	0.980
Kang, Lim, and Kim, 2002								
117	KLM2002	983.719	946.090	0.962	1.360	1.290	1.030	1.250
118	KLM2002	467.139	438.573	0.939	1.320	1.240	1.010	1.190
119	KLM2002	608.300	618.717	1.017	1.420	1.330	1.100	1.280
120	KLM2002	885.933	918.957	1.037	1.270	1.190	0.980	1.140
121	KLM2002	816.222	669.424	0.820	1.010	0.940	0.770	0.910
Mean				***1.014***	1.301	1.256	1.035	1.205
Standard Deviation(SD)				***0.096***	0.154	0.184	0.162	0.169
Variance				***0.009***	0.024	0.034	0.026	0.029

Table A-3: Material and Geometric Properties – CCFT Validation Set – Beam-Column

Col. No.	*Spec.*	*D (mm)*	*t (mm)*	*kl (mm)*	*f'c (Mpa)*	*Fy (Mpa)*	*D/t*	*L/D*	*e(exp) (mm)*	*e/D*
Furlong, 1967										
1		114.3	3.175	914.4	28.959	413.700	36.000	8.000	25.400	0.222
2		114.3	3.175	914.4	28.959	413.700	36.000	8.000	29.972	0.262
3		114.3	3.175	914.4	28.959	413.700	36.000	8.000	44.450	0.389
4		114.3	3.175	914.4	28.959	413.700	36.000	8.000	146.304	1.280
5		152.4	1.549	1016	25.856	330.960	98.361	6.667	17.526	0.115
6		152.4	1.549	1016	25.856	330.960	98.361	6.667	60.198	0.395
7		152.4	1.549	1016	21.030	330.960	98.361	6.667	119.126	0.782

Col. No.	*Spec.*	*D (mm)*	*t (mm)*	*kl (mm)*	*f'c (Mpa)*	*Fy (Mpa)*	*D/t*	*L/D*	*e(exp) (mm)*	*e/D*
8		152.4	1.549	1016	21.030	330.960	98.361	6.667	111.252	0.730
9		127	2.413	1066.8	35.165	289.590	52.632	8.400	40.894	0.322
Neogi, Sen, and Chapman, 1969										
10	M1	169.418	5.105	3327.4	44.473	303.380	33.184	19.640	47.752	0.282
11	M2	169.164	5.258	3327.4	43.232	303.380	32.174	19.670	38.100	0.225
12	M3	168.91	5.664	3327.4	33.992	289.590	29.821	19.699	47.752	0.283
13	M4	168.402	6.553	3327.4	30.407	293.038	25.698	19.759	47.752	0.284
14	M5	169.164	7.188	3327.4	25.580	306.138	23.534	19.670	47.752	0.282
15	M6	169.164	7.290	3327.4	26.546	306.138	23.206	19.670	38.100	0.225
16	M7	168.91	8.814	3302	26.408	317.170	19.164	19.549	47.752	0.283
17	M8	140.208	9.601	3327.4	33.234	268.216	14.603	23.732	31.750	0.226
18	M9	140.208	9.754	3327.4	21.650	268.216	14.375	23.732	31.750	0.226
19	M10	140.97	5.004	3327.4	34.061	288.211	28.173	23.604	31.750	0.225
20	C6	127	2.845	1409.7	66.744	265.458	44.643	11.100	6.350	0.050
21	C7	127	1.727	1714.5	60.055	189.613	73.529	13.500	6.350	0.050
22	C8	127	3.023	1714.5	60.055	265.458	42.017	13.500	6.350	0.050
23	C9	127.254	1.778	2032	40.129	189.613	71.571	15.968	16.002	0.126
24	C10	127	3.251	2032	40.129	265.458	39.063	16.000	16.002	0.126
25	C12	127	3.251	2032	42.611	265.458	39.063	16.000	22.352	0.176
Knowles and Park, 1969										
26	1	88.9	5.842	812.8	41.370	399.910	15.217	9.143	7.620	0.086
27	2	88.9	5.842	1422.4	41.370	399.910	15.217	16.000	7.620	0.086
28	5	82.55	1.397	812.8	41.370	482.650	59.091	9.846	7.620	0.092
Rangan and Joyce, 1992										
29		101.6	1.600	807.72	67.364	217.882	63.492	7.950	9.906	0.098
30		101.6	1.600	807.72	67.364	217.882	63.492	7.950	29.972	0.295
31		101.6	1.600	1313.18	67.364	217.882	63.492	12.925	9.906	0.098
32		101.6	1.600	1313.18	67.364	217.882	63.492	12.925	29.972	0.295
33		101.6	1.600	1564.64	67.364	217.882	63.492	15.400	9.906	0.098
34		101.6	1.600	1818.64	67.364	217.882	63.492	17.900	9.906	0.098
35		101.6	1.600	1818.64	67.364	217.882	63.492	17.900	29.972	0.295
36		101.6	1.600	2321.56	67.364	217.882	63.492	22.850	9.906	0.098
37		101.6	1.600	2321.56	67.364	217.882	63.492	22.850	29.972	0.295
Cai, 1991										
38	PB1-1	166.116	5.004	665.48	41.094	313.723	33.198	4.006	20.066	0.121
39	PB3-2	166.116	5.004	1988.82	41.094	277.179	33.198	11.972	20.066	0.121
40	PB3-3	166.116	5.004	1988.82	41.094	277.179	33.198	11.972	39.878	0.240
41	PB3-4	166.116	5.004	1988.82	41.094	297.864	33.198	11.972	39.878	0.240
42	PB3-5	166.116	5.004	1988.82	41.094	297.864	33.198	11.972	100.076	0.602

Col. No.	*Spec.*	*D (mm)*	*t (mm)*	*kl (mm)*	*f'c (Mpa)*	*Fy (Mpa)*	*D/t*	*L/D*	*e(exp) (mm)*	*e/D*
Kloppel and Goder, 1957										
43	7	94.996	12.497	1419.86	20.271	274.421	7.602	14.947	1.270	0.013
44	8	94.996	12.751	1419.86	20.271	272.353	7.450	14.947	2.286	0.024
45	9	94.996	12.395	1419.86	20.271	272.353	7.664	14.947	1.778	0.019
46	10	94.996	12.598	861.06	20.271	274.421	7.540	9.064	2.032	0.021
47	11	94.996	12.700	861.06	20.271	272.353	7.480	9.064	1.524	0.016
48	12	94.996	12.700	861.06	20.271	272.353	7.480	9.064	2.286	0.024
49	42	94.996	3.683	861.06	24.960	386.120	25.793	9.064	0.508	0.005
50	44	94.996	3.861	1419.86	24.960	326.823	24.605	14.947	0.508	0.005
51	45	94.996	3.912	1419.86	24.960	386.120	24.286	14.947	2.286	0.024
52	69	215.9	6.045	2219.96	22.891	389.568	35.714	10.282	2.794	0.013
53	70	215.9	5.969	2219.96	22.891	393.015	36.170	10.282	5.334	0.025
54	72	215.9	6.299	2219.96	29.786	404.737	34.274	10.282	1.778	0.008
55	73	94.996	3.861	1981.2	24.064	332.339	24.605	20.856	1.524	0.016
56	75	94.996	3.581	1981.2	24.064	355.093	26.525	20.856	0.254	0.003
57	76	94.996	3.734	1981.2	24.064	326.823	25.442	20.856	3.048	0.032
58	83	120.904	3.658	1049.02	21.099	295.106	33.056	8.676	2.286	0.019
59	84	120.904	3.734	1049.02	21.099	327.513	32.381	8.676	5.334	0.044
60	85	120.904	3.759	1049.02	24.201	308.207	32.162	8.676	4.064	0.034
61	86	120.904	3.988	1049.02	24.201	326.823	30.318	8.676	4.572	0.038
62	89	120.904	5.613	1049.02	21.099	344.061	21.538	8.676	4.572	0.038
63	90	120.904	5.410	1049.02	21.099	343.371	22.347	8.676	1.524	0.013
64	95	120.904	3.708	2311.4	21.099	295.106	32.603	19.118	0.508	0.004
65	96	120.904	3.759	2311.4	21.099	327.513	32.162	19.118	2.540	0.021
66	97	120.904	3.708	2311.4	24.201	308.207	32.603	19.118	1.524	0.013
67	101	120.904	5.690	2311.4	21.099	344.061	21.250	19.118	3.556	0.029
68	102	120.904	5.486	2311.4	21.099	343.371	22.037	19.118	1.016	0.008
69	103	120.904	5.639	2311.4	24.201	330.271	21.441	19.118	1.016	0.008
70	104	120.904	5.436	2311.4	24.201	321.997	22.243	19.118	1.524	0.013
Kvedaras and Tomaszewicz, 1994										
71	S1	250.19	2.007	2202.18	72.604	239.946	124.684	8.802	23.012	0.092
72	S3	250.19	2.007	2202.18	69.915	239.946	124.684	8.802	18.009	0.072
73	S5	250.19	2.007	2202.18	35.716	239.946	124.684	8.802	30.023	0.120
Johansson, Claeson, Gylltoft, and Akesson, 2000										
74	LFE	159.004	4.496	2697.48	64.468	433.006	35.367	16.965	10.008	0.063
Kilpatrick and Rangan, 1997										
75	SC-16	101.6	2.413	2176.78	95.978	410.253	42.105	21.425	50.038	0.493
76	SC-33	101.6	2.413	2176.78	95.978	410.253	42.105	21.425	20.015	0.197
Matsui et al.,1997										

Col. No.	*Spec.*	*D (mm)*	*t (mm)*	*kl (mm)*	*f'c (Mpa)*	*Fy (Mpa)*	*D/t*	*L/D*	*e(exp) (mm)*	*e/D*
77	C4-1	165.354	4.089	660.4	31.855	353.024	40.435	3.994	20.726	0.125
78	C4-3	165.354	4.089	660.4	31.855	353.024	40.435	3.994	62.052	0.375
79	C8-1	165.354	4.089	1323.34	31.855	353.024	40.435	8.003	20.726	0.125
80	C8-3	165.354	4.089	1323.34	31.855	353.024	40.435	8.003	62.052	0.375
81	C8-5	165.354	4.089	1323.34	31.855	353.024	40.435	8.003	103.276	0.625
82	C12-1	165.354	4.089	1983.74	31.855	353.024	40.435	11.997	20.726	0.125
83	C12-3	165.354	4.089	1983.74	31.855	353.024	40.435	11.997	62.052	0.375
84	C12-5	165.354	4.089	1983.74	31.855	353.024	40.435	11.997	103.276	0.625
85	C18-1	165.354	4.089	2976.88	31.855	353.024	40.435	18.003	20.726	0.125
86	C18-3	165.354	4.089	2976.88	31.855	353.024	40.435	18.003	62.052	0.375
87	C18-5	165.354	4.089	2976.88	31.855	353.024	40.435	18.003	103.276	0.625
88	C24-1	165.354	4.089	3967.48	31.855	353.024	40.435	23.994	20.726	0.125
89	C24-3	165.354	4.089	3967.48	31.855	353.024	40.435	23.994	62.052	0.375
90	C24-5	165.354	4.089	3967.48	31.855	353.024	40.435	23.994	103.276	0.625
91	C30-1	165.354	4.089	4968.24	31.855	353.024	40.435	30.046	20.726	0.125
92	C30-3	165.354	4.089	4968.24	31.855	353.024	40.435	30.046	62.052	0.375
93	C30-5	165.354	4.089	4968.24	31.855	353.024	40.435	30.046	103.276	0.625
Han and Yao, 2003										
94	S-2	119.888	2.642	360.68	20.064	339.924	45.385	3.008	13.970	0.117
95	S-4	119.888	2.642	360.68	35.992	339.924	45.385	3.008	13.970	0.117
O'Shea and Bridge, 2000										
96	S30E250B	165.1	2.819	581.66	48.265	363.367	58.559	3.523	7.112	0.043
97	S30E150B	165.1	2.819	579.12	48.265	363.367	58.559	3.508	17.272	0.105
98	S20E150A	189.992	1.930	662.94	41.025	256.494	98.421	3.489	16.256	0.086
99	S16E150B	189.992	1.524	662.94	48.265	306.138	124.667	3.489	15.494	0.082
100	S30E280A	165.1	2.819	579.12	80.189	363.367	58.559	3.508	9.398	0.057
101	S20E280B	189.992	1.930	662.94	74.673	256.494	98.421	3.489	9.906	0.052
102	S30E180A	165.1	2.819	579.12	80.189	363.367	58.559	3.508	17.780	0.108
103	S20E180B	189.992	1.930	662.94	74.673	256.494	98.421	3.489	20.828	0.110
104	S16E180A	189.992	1.524	662.94	80.189	306.138	124.667	3.489	14.224	0.075
105	S30E210B	165.1	2.819	579.12	112.664	363.367	58.559	3.508	6.858	0.042
106	S30E110B	165.1	2.819	579.12	112.664	363.367	58.559	3.508	15.494	0.094
107	S20E110B	189.992	1.930	665.48	112.664	256.494	98.421	3.503	17.018	0.090
108	S16E110B	189.992	1.524	660.4	112.664	306.138	124.667	3.476	12.954	0.068
Kilpatrick & Rangan, 1999										
109	SC-0	76	2.200	802	58.000	435.000	34.545	10.553	15.000	0.197
110	SC-1	76	2.200	1032	58.000	435.000	34.545	13.579	15.000	0.197
111	SC-2	76	2.200	1262	58.000	435.000	34.545	16.605	15.000	0.197
112	SC-3	76	2.200	1487	58.000	435.000	34.545	19.566	15.000	0.197

Col. No.	*Spec.*	*D (mm)*	*t (mm)*	*kl (mm)*	*f'c (Mpa)*	*Fy (Mpa)*	*D/t*	*L/D*	*e(exp) (mm)*	*e/D*
113	SC-4	76	2.200	1717	58.000	435.000	34.545	22.592	15.000	0.197
114	SC-5	76	2.200	1947	58.000	435.000	34.545	25.618	15.000	0.197
115	SC-6	76	2.200	2172	58.000	435.000	34.545	28.579	15.000	0.197
116	SC-7	76	2.200	2402	58.000	435.000	34.545	31.605	15.000	0.197
117	SC-9	102	2.400	1947	58.000	410.000	42.500	19.088	10.000	0.098
118	SC-10	102	2.400	1947	58.000	410.000	42.500	19.088	15.000	0.147
119	SC-11	102	2.400	1947	58.000	410.000	42.500	19.088	20.000	0.196
120	SC-12	102	2.400	1947	58.000	410.000	42.500	19.088	25.000	0.245
121	SC-13	102	2.400	1947	58.000	410.000	42.500	19.088	30.000	0.294
122	SC-14	102	2.400	1947	58.000	410.000	42.500	19.088	40.000	0.392
123	SC-15	102	2.400	1947	58.000	410.000	42.500	19.088	50.000	0.490

Table A-4: Comparison – CCFT Validation Set –Beam-Column

Col. No.	*Spec.*	*Pnum (kN)*	*Pexp (kN)*	*Pexp/Ppred*				
				Numerical	*AISC 1999*	*AISC 2005*	*Eurocode*	*Plastic*
Furlong, 1967								
1		495.768	444.800	0.897	1.340	1.100	1.090	0.940
2		459.733	400.320	0.871	1.310	1.060	1.070	0.900
3		365.530	333.600	0.913	1.360	1.070	1.130	0.940
4		128.451	111.200	0.866	1.080	0.800	1.080	0.850
5		528.710	567.565	1.073	1.710	1.190	1.140	1.030
6		285.621	286.006	1.001	1.800	1.000	1.200	0.980
7		139.111	136.109	0.978	1.500	0.830	1.260	0.970
8		149.382	135.219	0.905	1.410	0.780	1.160	0.890
9		327.303	349.168	1.067	1.820	1.080	1.270	1.010
Neogi, Sen, and Chapman, 1969								
10	M1	561.660	610.710	1.087	1.290	0.830	1.100	0.630
11	M2	619.217	688.995	1.113	1.290	0.860	1.090	0.650
12	M3	539.364	588.915	1.092	1.250	0.880	1.090	0.680
13	M4	574.806	613.379	1.067	1.180	0.880	1.040	0.670
14	M5	613.869	640.957	1.044	1.130	0.890	1.040	0.670
15	M6	682.158	725.024	1.063	1.140	0.900	1.040	0.690
16	M7	727.232	743.706	1.023	1.090	0.880	1.020	0.670
17	M8	545.543	538.208	0.987	1.030	0.820	0.990	0.590
18	M9	529.841	538.208	1.016	1.060	0.880	1.020	0.640
19	M10	380.472	409.216	1.076	1.190	0.840	1.100	0.580

Col. No.	*Spec.*	*Pnum (kN)*	*Pexp (kN)*	*Pexp/Ppred*				
				Numerical	*AISC 1999*	*AISC 2005*	*Eurocode*	*Plastic*
20	C6	725.558	1026.598	1.415	1.780	1.280	1.230	1.060
21	C7	557.275	835.779	1.500	2.410	1.390	1.460	1.090
22	C8	632.560	789.520	1.248	1.470	1.080	1.060	0.870
23	C9	314.787	347.389	1.104	1.830	0.940	1.150	0.750
24	C10	403.931	516.858	1.280	1.520	1.070	1.140	0.840
25	C12	373.994	494.173	1.321	1.670	1.090	1.260	0.860
Knowles and Park, 1969								
26	1	665.416	554.221	0.833	1.030	0.950	0.930	0.820
27	2	479.423	469.264	0.979	1.020	0.890	0.920	0.710
28	5	288.235	301.574	1.046	1.470	1.130	1.100	0.960
Rangan and Joyce, 1992								
29		450.988	430.122	0.954	2.000	0.990	1.050	0.870
30		250.641	234.854	0.937	2.310	0.780	1.220	0.840
31		366.106	350.058	0.956	1.770	0.870	1.000	0.700
32		205.131	189.930	0.926	1.960	0.670	1.210	0.680
33		333.031	314.918	0.946	1.680	0.830	0.990	0.630
34		300.358	279.779	0.931	1.590	0.790	0.960	0.560
35		169.282	140.112	0.828	1.550	0.540	1.100	0.500
36		243.191	220.176	0.905	1.450	0.740	0.980	0.440
37		140.664	125.878	0.895	1.530	0.550	1.220	0.450
Cai, 1991								
38	PB1-1	1450.966	1470.064	1.013	1.670	1.330	1.260	1.190
39	PB3-2	864.083	1156.035	1.338	1.580	1.190	1.230	0.990
40	PB3-3	687.670	915.843	1.332	1.730	1.180	1.390	1.000
41	PB3-4	714.930	895.827	1.253	1.610	1.120	1.310	0.940
42	PB3-5	404.614	476.826	1.178	1.530	0.960	1.490	0.960
Kloppel and Goder, 1957								
43	7	857.835	946.979	1.104	1.200	1.180	1.150	1.010
44	8	836.568	937.638	1.121	1.220	1.190	1.180	1.020
45	9	833.342	906.947	1.088	1.190	1.160	1.140	1.000
46	10	896.824	1017.702	1.135	1.200	1.180	1.160	0.990
47	11	905.500	1007.917	1.113	1.160	1.150	1.130	0.960
48	12	883.807	1033.715	1.170	1.230	1.210	1.190	1.020
49	42	579.522	686.326	1.184	1.400	1.350	1.320	1.090
50	44	506.048	566.675	1.120	1.380	1.330	1.280	1.130
51	45	523.999	605.818	1.156	1.420	1.330	1.320	1.100
52	69	2310.322	2461.523	1.065	1.280	1.220	1.210	0.990
53	70	2236.347	2421.046	1.083	1.320	1.240	1.230	1.020

Col. No.	*Spec.*	*Pnum (kN)*	*Pexp (kN)*	*Pexp/Ppred*				
				Numerical	*AISC 1999*	*AISC 2005*	*Eurocode*	*Plastic*
54	72	2761.959	2932.122	1.062	1.320	1.260	1.230	1.010
55	73	413.989	498.176	1.203	1.470	1.370	1.390	1.010
56	75	424.046	472.822	1.115	1.320	1.280	1.270	0.930
57	76	381.688	412.774	1.081	1.350	1.220	1.260	0.900
58	83	626.570	695.222	1.110	1.360	1.280	1.230	1.050
59	84	675.233	746.374	1.105	1.470	1.360	1.320	1.130
60	85	701.780	836.669	1.192	1.590	1.470	1.420	1.220
61	86	719.221	866.915	1.205	1.550	1.430	1.390	1.190
62	89	856.474	998.131	1.165	1.380	1.310	1.280	1.080
63	90	915.540	1017.702	1.112	1.330	1.290	1.240	1.040
64	95	580.851	640.512	1.103	1.380	1.330	1.290	1.050
65	96	569.063	629.392	1.106	1.380	1.280	1.280	0.990
66	97	591.121	695.222	1.176	1.480	1.390	1.370	1.080
67	101	696.281	786.406	1.129	1.300	1.200	1.220	0.930
68	102	769.028	815.763	1.061	1.260	1.220	1.200	0.940
69	103	770.519	873.587	1.134	1.330	1.270	1.250	0.990
70	104	741.196	865.136	1.167	1.400	1.320	1.310	1.030
Kvedaras and Tomaszewicz, 1994								
71	S1	2265.248	2602.080	1.149	2.750	0.990	1.110	0.890
72	S3	2388.895	2401.920	1.005	2.200	0.900	0.970	0.780
73	S5	1273.425	1301.040	1.022	1.990	0.940	1.050	0.840
Johansson, Claeson, Gylltoft, and Akesson, 2000								
74	LFE	1325.060	1231.206	0.929	1.210	0.940	0.980	0.670
Kilpatrick and Rangan, 1997								
75	SC-16	175.789	157.014	0.893	1.300	0.650	1.040	0.470
76	SC-33	325.263	282.448	0.868	1.400	0.880	1.000	0.440
Matsui et al.,1997								
77	C4-1	1147.770	1213.859	1.058	2.210	1.350	1.400	1.120
78	C4-3	627.086	754.826	1.204	2.190	1.290	1.440	1.120
79	C8-1	1069.075	1040.832	0.974	1.880	1.040	1.390	1.050
80	C8-3	587.348	658.749	1.122	1.640	0.830	1.400	1.100
81	C8-5	387.552	434.570	1.121	1.770	1.530	1.130	1.080
82	C12-1	953.460	947.869	0.994	1.920	1.630	1.280	1.060
83	C12-3	555.228	571.568	1.029	1.930	1.430	1.290	0.980
84	C12-5	357.867	386.531	1.080	2.120	1.570	1.580	1.280
85	C18-1	771.831	741.482	0.961	2.410	1.530	1.720	1.330
86	C18-3	472.061	460.368	0.975	2.060	1.200	1.150	0.750
87	C18-5	320.569	330.486	1.031	1.730	1.370	1.140	0.840
88	C24-1	614.113	609.376	0.992	1.190	1.220	0.930	0.840

Col. No.	*Spec.*	*Pnum (kN)*	*Pexp (kN)*	*Pexp/Ppred*				
				Numerical	*AISC 1999*	*AISC 2005*	*Eurocode*	*Plastic*
89	C24-3	389.492	350.502	0.900	1.160	1.160	0.920	0.710
90	C24-5	276.003	277.110	1.004	1.680	1.460	1.100	0.960
91	C30-1	477.668	479.494	1.004	2.550	1.240	1.290	0.850
92	C30-3	318.388	309.136	0.971	1.880	1.370	1.260	0.860
93	C30-5	234.910	238.413	1.015	1.440	1.080	1.090	0.650
Han and Yao, 2003								
94	S-2	449.579	532.870	1.185	1.590	1.380	1.320	1.260
95	S-4	565.857	599.590	1.060	1.540	1.200	1.130	1.080
O'Shea and Bridge, 2000								
96	S30E250B	1415.870	1524.330	1.077	1.510	1.230	1.110	1.080
97	S30E150B	1212.433	1122.675	0.926	1.490	1.040	0.990	0.930
98	S20E150A	1105.399	1283.248	1.161	2.110	1.220	1.140	1.090
99	S16E150B	1218.533	1259.229	1.033	1.970	1.060	1.000	0.930
100	S30E280A	1850.442	1939.328	1.048	1.660	1.150	1.060	1.020
101	S20E280B	1888.816	2202.205	1.166	2.230	1.190	1.090	1.050
102	S30E180A	1573.776	1652.432	1.050	1.880	1.090	1.040	0.980
103	S20E180B	1498.451	1729.382	1.154	2.700	1.050	1.110	1.010
104	S16E180A	1819.903	1924.205	1.057	2.410	1.050	1.010	0.940
105	S30E210B	2443.614	2244.906	0.919	1.450	0.980	0.900	0.870
106	S30E110B	2047.240	1879.280	0.918	2.010	1.190	0.900	0.830
107	S20E110B	2225.676	2385.018	1.072	3.280	1.240	1.030	0.930
108	S16E110B	2457.930	2418.822	0.984	2.880	1.250	0.940	0.870
Kilpatrick & Rangan, 1999								
109	SC-0	263.483	245.300	0.931				
110	SC-1	233.952	208.000	0.889				
111	SC-2	206.277	182.100	0.883				
112	SC-3	180.602	162.100	0.898				
113	SC-4	157.152	141.600	0.901				
114	SC-5	136.719	122.000	0.892				
115	SC-6	119.287	106.600	0.894				
116	SC-7	103.760	95.600	0.921				
117	SC-9	400.700	360.700	0.900				
118	SC-10	350.453	309.700	0.884				
119	SC-11	313.357	274.600	0.876				
120	SC-12	281.691	241.400	0.857				
121	SC-13	254.045	220.600	0.868				
122	SC-14	209.742	189.100	0.902				
123	SC-15	174.344	158.500	0.909				
Mean				***1.043***	1.612	1.117	1.169	0.909

Col. No.	*Spec.*	*Pnum (kN)*	*Pexp (kN)*	*Pexp/Ppred*				
				Numerical	*AISC 1999*	*AISC 2005*	*Eurocode*	*Plastic*
Standard Deviation (SD)				***0.127***	0.434	0.227	0.155	0.191
Variance				***0.016***	0.188	0.051	0.024	0.036

Table A-5: Material and Geometric Properties – for various CCFT models Evaluation

Specimen	**D(mm)**	**t(mm)**	**D/t**	**f_{sy}(MPa)**	**f_c'(MPa)**	**$P_{u,exp}$(kN)**
CC4-A-2	149	2.96	50.4	308	25.4	941
CC4-A-4-1	149	2.96	50.4	308	40.5	1064
CC4-A-4-2	149	2.96	50.4	308	40.5	1080
CC4-A-8	149	2.96	50.4	308	77	1781
CC4-C-2	301	2.96	101.7	279	25.4	2382
CC4-C-4-1	300	2.96	101.4	279	41.1	3277
CC4-C-4-2	300	2.96	101.4	279	41.1	3152
CC4-C-8	301	2.96	101.7	279	80.3	5540
CC6-A-2	122	4.54	26.9	576	25.4	1509
CC6-A-4-1	122	4.54	26.9	576	40.5	1657
CC6-A-4-2	122	4.54	26.9	576	40.5	1663
CC6-A-8	122	4.54	26.9	576	77	2100
CC6-C-2	239	4.54	52.6	507	25.4	3035
CC6-C-4-1	238	4.54	52.4	507	40.5	3583
CC6-C-4-2	238	4.54	52.4	507	40.5	3647
CC6-D-2	361	4.54	79.5	525	25.4	5633
CC6-D-4-1	361	4.54	79.5	525	41.1	7260
CC6-D-4-2	360	4.54	79.3	525	41.1	7045
CC6-D-8	360	4.54	79.3	525	85.1	11505
CC8-A-2	108	6.47	16.7	853	25.4	2275
CC8-A-4-1	109	6.47	16.8	853	40.5	2446
CC8-A-4-2	108	6.47	16.7	853	40.5	2402
CC8-A-8	108	6.47	16.7	853	77	2713
CC8-C-2	222	6.47	34.3	843	25.4	4964
CC8-C-4-1	222	6.47	34.3	843	40.5	5638
CC8-C-4-2	222	6.47	34.3	843	40.5	5714
CC8-C-8	222	6.47	34.3	843	77	7304
CC8-D-2	337	6.47	52.1	823	25.4	8475
CC8-D-4-1	337	6.47	52.1	823	41.1	9668
CC8-D-4-2	337	6.47	52.1	823	41.1	9835
CC8-D-8	337	6.47	52.1	823	85.1	13776

Specimen	D(mm)	t(mm)	D/t	f_{sy}(MPa)	f_c'(MPa)	$P_{u,exp}$(kN)
CU-040	200	5	40	265.8	27.15	2016.9
CU-070	280	4	70	272.6	31.15	3025.2
C3	114.43	3.98	29.4	343	26.69	948
C8	115.04	4.92	23.4	365	89.16	1787
C9	115.02	5.02	22.9	365	48.96	1413
C11	114.29	3.75	30.5	343	48.96	1067
C14	114.54	3.84	29.8	343	84.1	1359

Table A-6: Comparison between the proposed model and various CCFT numerical models

Specimen	$P_{u,exp}$(kN)	Proposed Model		Tang et al. model [1996]	Hu et al. model [2003]	Liang & Fragomeni [2009]
		$P_{u,num}$(kN)	$P_{u,num}/P_{u,exp}$	$P_{u,num}/P_{u,exp}$	$P_{u,num}/P_{u,exp}$	$P_{u,num}/P_{u,exp}$
CC4-A-2	941	933.102	0.992	1.112	0.950	0.950
CC4-A-4-1	1064	1158.56	1.089	1.274	1.054	1.054
CC4-A-4-2	1080	1158.56	1.073	1.256	1.038	1.038
CC4-A-8	1781	1714.72	0.963	1.106	0.942	0.942
CC4-C-2	2382	2535.29	1.064	1.038	1.032	1.032
CC4-C-4-1	3277	3442.59	1.051	1.056	1.025	1.025
CC4-C-4-2	3152	3442.59	1.092	1.098	1.066	1.066
CC4-C-8	5540	5749	1.038	1.028	1.025	1.025
CC6-A-2	1509	1461.6	0.969	0.990	1.152	0.938
CC6-A-4-1	1657	1695.53	1.023	1.064	1.138	0.995
CC6-A-4-2	1663	1695.53	1.020	1.060	1.133	0.992
CC6-A-8	2100	2191.57	1.044	1.104	1.068	1.021
CC6-C-2	3035	3125.6	1.030	1.083	0.992	0.992
CC6-C-4-1	3583	3658.59	1.021	1.138	0.988	0.988
CC6-C-4-2	3647	3658.59	1.003	1.118	0.971	0.971
CC6-D-2	5633	5672.77	1.007	0.978	0.973	0.973
CC6-D-4-1	7260	6968.8	0.960	0.986	0.928	0.928
CC6-D-4-2	7045	6938.92	0.985	1.012	0.953	0.953
CC6-D-8	11505	10557.4	0.918	0.991	0.895	0.895
CC8-A-2	2275	2164.62	0.951	0.931	1.136	0.909
CC8-A-4-1	2446	2398.58	0.981	0.979	1.116	0.940
CC8-A-4-2	2402	2369.55	0.986	0.985	1.121	0.946
CC8-A-8	2713	2808.77	1.035	1.062	1.088	0.999
CC8-C-2	4964	5348.43	1.077	1.075	1.268	1.025
CC8-C-4-1	5638	6093.1	1.081	1.094	1.199	1.031
CC8-C-4-2	5714	6093.1	1.066	1.080	1.183	1.017

Specimen	$P_{u,exp}$(kN)	Proposed Model		Tang et al. model [1996]	Hu et al. model [2003]	Liang & Fragomeni [2009]
		$P_{u,num}$(kN)	$P_{u,num}/P_{u,exp}$	$P_{u,num}/P_{u,exp}$	$P_{u,num}/P_{u,exp}$	$P_{u,num}/P_{u,exp}$
CC8-C-8	7304	7768.16	1.064	1.100	1.080	1.021
CC8-D-2	8475	8886.37	1.049	1.034	1.007	1.007
CC8-D-4-1	9668	9997.66	1.034	1.082	0.996	0.996
CC8-D-4-2	9835	9997.66	1.017	1.063	0.979	0.979
CC8-D-8	13776	13076.2	0.949	1.083	0.923	0.923
CU-040	2016.9	1979.91	0.982	1.085	0.983	1.006
CU-070	3025.2	2843.04	0.940	1.119	0.987	0.987
C3	948	913.343	0.963	0.994	1.030	0.926
C8	1787	1685.78	0.943	0.972	0.963	0.916
C9	1413	1361.33	0.963	0.998	0.984	0.926
C11	1067	1142.37	1.071	1.125	1.058	1.039
C14	1359	1472.54	1.084	1.130	1.074	1.061
Mean			**1.015**	**1.065**	**1.039**	**0.985**
Standard deviation (SD)			**0.0492**	**0.0717**	**0.0849**	**0.0465**
Variance			**0.0024**	**0.0051**	**0.0070**	**0.0021**

APPENDIX B: Visual Basic for Application (VBA): User defined function Codes

User-defined functions for calculating the area of concrete layers

```
Function ACLcir(D, t, yl, yu)
Xl = yl / (D / 2 - t)
Xu = yu / (D / 2 - t)
ql = (D / 2 - t) ^ 2 - yl ^ 2
qu = (D / 2 - t) ^ 2 - yu ^ 2
If yl >= (D / 2 - t) Or yu <= -(D / 2 - t) Then
ACLcir = 0
Else
ACLcir = ((D / 2 - t) ^ 2) * (Arcsin(Xu) - Arcsin(Xl)) + yu * Sqr(qu) - yl * Sqr(ql)
End If
End Function
```

User-defined functions for calculating the centroid of concrete layers

```
Function ZCLcir(D, t, yl, yu)
ql = (D / 2 - t) ^ 2 - yl ^ 2
qu = (D / 2 - t) ^ 2 - yu ^ 2
If yl >= (D / 2 - t) Or yu <= -(D / 2 - t) Then
ZCLcir = 0
Else
ZCLcir = 2 * (ql ^ 1.5 - qu ^ 1.5) / (3 * ACLcir(D, t, yl, yu))
End If
End Function
```

User-defined functions for calculating the area of steel layers

```
Function ASLcir(D, t, yl, yu)
Zl = yl / (D / 2)
Zu = yu / (D / 2)
pl = (D / 2) ^ 2 - yl ^ 2
pu = (D / 2) ^ 2 - yu ^ 2
Atotal = ((D / 2) ^ 2) * (Arcsin(Zu) - Arcsin(Zl)) + yu * Sqr(pu) - yl * Sqr(pl)
If yl >= (D / 2 - t) Or yu <= -(D / 2 - t) Then
ASLcir = Atotal
Else
ASLcir = Atotal - ACLcir(D, t, yl, yu)
End If
End Function
```

User-defined functions for calculating the centroid of steel layers

```
Function ZSLcir(D, t, yl, yu)
ql = (D / 2 - t) ^ 2 - yl ^ 2
qu = (D / 2 - t) ^ 2 - yu ^ 2
pl = (D / 2) ^ 2 - yl ^ 2
pu = (D / 2) ^ 2 - yu ^ 2
If yl >= (D / 2 - t) Or yu <= -(D / 2 - t) Then
ZSLcir = 2 * (pl ^ 1.5 - pu ^ 1.5) / (3 * ASLcir(D, t, yl, yu))
Else
ZSLcir = 2 * (qu ^ 1.5 - ql ^ 1.5 + pl ^ 1.5 - pu ^ 1.5) / (3 * ASLcir(D, t, yl, yu))
End If
End Function
```

User defined functions for calculating stress-strain relation of concrete

```
Function ConSTRScir(D, t, L, fc, fy, ec, phi)
If (1.85 * (D - 2 * t) ^ -0.135) <= 0.85 Then
gamma = 0.85
Else
If (1.85 * (D - 2 * t) ^ -0.135) >= 1 Then
gamma = 1
Else
gamma = 1.85 * (D - 2 * t) ^ -0.135
End If
End If
Pi = 4 * Atn(1)
Act = (Pi * (D - 2 * t) ^ 2) / 4
Ast = ((Pi * D ^ 2) / 4) - Act
roh = Ast / Act
moel = 22000 * ((gamma * fc + 8) / 10) ^ 0.3
a = moel
nn = 210000 / a
alph = 0.017 + 0.255 * (roh * nn) - 0.106 * (roh * nn) ^ 2 + 0.016 * (roh * nn) ^ 3
fct = 1.4 * ((fc - 8) / 10) ^ (2 / 3)
ecr = fct / moel
If gamma * fc <= 28 Then
ec1 = 0.002
Else
If gamma * fc > 82 Then
ec1 = 0.003
```

```
Else
ec1 = 0.002 + (gamma * fc - 28) / 54000
End If
End If
ve1 = 0.881 * 10 ^ -6 * (D / t) ^ 3 - 2.58 * 10 ^ -4 * (D / t) ^ 2 + 1.953 * 10 ^ -2 * (D / t) +
0.4011
ve = 0.2312 + 0.3582 * ve1 - 0.1524 * (fc / fy) + 4.843 * ve1 * (fc / fy) - 9.169 * (fc / fy) ^ 2
If D / t > 47 Then
fr_avg = (0.006241 - 0.0000357 * (D / t)) * fy
Else
fr_avg = 0.7 * (ve - 0.5) * 2 * t * fy / (D - 2 * t)
End If
redfct = Exp(-15 * phi)
fr_eff = redfct * fr_avg
If L / D < 10 Then
fcc = gamma * fc + 4.1 * fr_eff
Else
fcc = gamma * fc
End If
ecc = ec1 * (1 + 20.5 * fr_eff / (gamma * fc))
v = a * ecc / fcc
w = 0.5 - 0.00171 * fc + 2.39 * Sqr(fr_eff)
x = ec / ecc
n = v * x + w * (x ^ 2)
M = 1 + (v - 2) * x + (w + 1) * (x ^ 2)
If D / t <= 40 Then
beta = 1
Else
beta = 0.0000339 * (D / t) ^ 2 - 0.010085 * (D / t) + 1.3491
End If
eucc = 0.02
If ec < 0 Then
   If ec >= ecr Then
   ConSTRScir = a * ec
   Else
   ConSTRScir = -fct * Exp(-alph * Abs(ec / ecr))
   End If
Else
If ec <= ecc Then
ConSTRScir = fcc * n / M
```

```
Else
If ec <= eucc Then
ConSTRScir = beta * fcc + ((0.02 - ec) / (0.02 - ecc)) * (fcc - beta * fcc)
Else
ConSTRScir = beta * fcc
End If
End If
End If
End Function
```

User defined functions for calculating stress-strain relation of steel tube

```
Function StlSTRScir(D, t, L, fc, fy, es, phi)
Const SMoel = 210000
Ks = -SMoel / 30
Esh = SMoel / 100
ve1 = 0.881 * 10 ^ -6 * (D / t) ^ 3 - 2.58 * 10 ^ -4 * (D / t) ^ 2 + 1.953 * 10 ^ -2 * (D / t) +
0.4011
ve = 0.2312 + 0.3582 * ve1 - 0.1524 * (fc / fy) + 4.843 * ve1 * (fc / fy) - 9.169 * (fc / fy) ^ 2
If D / t <= 47 Then
fr_avg = 0.7 * (ve - 0.5) * 2 * t * fy / (D - 2 * t)
Else
If D / t <= 150 Then
fr_avg = (0.006241 - 0.0000357 * (D / t)) * fy
Else
fr_avg = 0
End If
End If
hoopstrs = fr_avg * (D - 2 * t) / (2 * t)
If L / D < 10 Then
fyt = 0.5 * (hoopstrs - Sqr(4 * fy ^ 2 - 3 * hoopstrs ^ 2))
fyc = 0.5 * (hoopstrs + Sqr(4 * fy ^ 2 - 3 * hoopstrs ^ 2))
Else
fyt = -fy
fyc = fy
End If
If es < 0 Then
fsy = fyt
Else
fsy = fyc
End If
```

```
esy = Abs(fsy / SMoel)
eult = 120 * esy
If fy <= 460 Then
fsu = 1.1 * fy
Else
fsu = 1.05 * fy
End If
elb = 0.2139 * ((D / t) ^ (-1.41)) * (esy ^ (-0.41))
R = D * esy / t
If elb <= esy Then
Flb = SMoel * elb
Else
Flb = fsy + Esh * (elb - esy)
End If
If Flb >= 0.17 * Flb / R Then
Frs = 0.17 * Flb / R
Else
Frs = Flb
End If
If es >= 0 Then
   If elb <= esy Then
      If es <= elb Then
      StlSTRScir = SMoel * es
      Else
      StlSTRScir = Flb + Ks * (es - elb)
         If (Flb + Ks * (es - elb)) <= Frs Then
         StlSTRScir = Frs
         End If
      End If
   Else
      If es <= esy Then
      StlSTRScir = SMoel * es
      Else
         If es <= elb Then
         StlSTRScir = fsy + Esh * (es - esy)
            If (fsy + Esh * (es - esy)) >= fsu Then
            StlSTRScir = fsu
            End If
         Else
            If Flb < fsu Then
```

```
            StlSTRScir = Flb + Ks * (es - elb)
               If (Flb + Ks * (es - elb)) <= Frs Then
               StlSTRScir = Frs
               End If
            Else
            StlSTRScir = fsu
               If Flb >= fsu And Frs <= fsu Then
               StlSTRScir = fsu + Ks * (es - elb)
                  If (fsu + Ks * (es - elb)) <= Frs Then
                  StlSTRScir = Frs
                  End If
               End If
            End If
         End If
      End If
   End If
Else
   If Abs(es) <= esy Then
   StlSTRScir = SMoel * es
   Else
   StlSTRScir = fsy + Esh * (es + esy)
      If Abs(fsy + Esh * (es + esy)) >= fsu Then
      StlSTRScir = -fsu
      End If
   End If
End If
End Function
```

User defined functions for integrating total internal axial force response of the section

```
Function F_int(D, t, L, fc, fy, eo, phi)
Dim n As Integer
ncl = CInt(CInt(D / (1 + D / 350)) / 2) * 2
yl = -D / 2
For n = 1 To ncl + 8
If n <= 4 Or n > ncl + 4 Then
   Delta = t / 4
Else
   Delta = (D - 2 * t) / ncl
End If
If n = ncl + 4 Then
```

```
yu = (D - 2 * t) / 2
Else
If n = ncl + 8 Then
yu = D / 2
Else
yu = yl + DeltaEnd If
End If
Acn = ACLcir(D, t, yl, yu)
Zcn = ZCLcir(D, t, yl, yu)
Astn = ASLcir(D, t, yl, yu)
Zstn = ZSLcir(D, t, yl, yu)
esn = eo + phi * Zstn
SIGstn = StlSTRScir(D, t, L, fc, fy, esn, phi)
Fstn = Astn * SIGstn / 1000
ecn = eo + phi * Zcn
SIGctn = ConSTRScir(D, t, L, fc, fy, ecn, phi)
Fctn = Acn * SIGctn / 1000
Fintn = Fctn + Fstn
F_int = F_int + Fintn
If n = 5 Then
yl = -(D - 2 * t) / 2
Else
yl = yu
End If
Next
End Function
```

User defined functions for integrating total internal moment response of the section

```
Function M_int(D, t, L, fc, fy, eo, phi)
Dim n As Integer
ncl = CInt(CInt(D / (1 + D / 350)) / 2) * 2
yl = -D / 2
For n = 1 To ncl + 8
If n <= 4 Or n > ncl + 4 Then
   Delta = t / 4
Else
   Delta = (D - 2 * t) / ncl
End If
If n = ncl + 4 Then
yu = (D - 2 * t) / 2
```

```
Else
If n = ncl + 8 Then
yu = D / 2
Else
yu = yl + DeltaEnd If
End If
Acn = ACLcir(D, t, yl, yu)
Zcn = ZCLcir(D, t, yl, yu)
Astn = ASLcir(D, t, yl, yu)
Zstn = ZSLcir(D, t, yl, yu)
esn = eo + phi * Zstn
SIGstn = StlSTRScir(D, t, L, fc, fy, esn, phi)
Fstn = Astn * SIGstn / 1000
Mstn = Fstn * Zstn / 1000
ecn = eo + phi * Zcn
SIGctn = ConSTRScir(D, t, L, fc, fy, ecn, phi)
Fctn = Acn * SIGctn / 1000
Mctn = Fctn * Zcn / 1000
Mintn = Mctn + Mstn
M_int = M_int + Mintn
If n = 5 Then
yl = -(D - 2 * t) / 2
Else
yl = yu
End If
Next
End Function
```

User defined functions for cross section equilibrium secant method

```
Function Sct_dnXS(D, t, L, fc, fy, phi, Pex) As Double
Dim n As Integer, I As Integer
n = 20
I = 1
dn0 = 0
dn1 = 20 * D
   Do
      eo0 = phi * (dn0 - D / 2)
      eo1 = phi * (dn1 - D / 2)
      F0 = F_int(D, t, L, fc, fy, eo0, phi)
      f1 = F_int(D, t, L, fc, fy, eo1, phi)
```

```
    dF0 = Pex - F0
    dF1 = Pex - f1
    dn = dn1 - (dn1 - dn0) * dF1 / (dF1 - dF0)
    eo = phi * (dn - D / 2)
    f = F_int(D, t, L, fc, fy, eo, phi)
    dF = Pex - f
    If Abs(dF) < 0.0001 Then
       Sct_dnXS = dn
       Exit Function
    End If
    I = I + 1
    If dF < 0 And dF1 < 0 And dF0 > 0 Then
       dn0 = dn0
       dn1 = dn
    Else
    If dF > 0 And dF1 < 0 And dF0 > 0 Then
       dn0 = dn
       dn1 = dn1
    End If
    End If
  Loop Until I = n
  Sct_dnXS = 0
End Function
```

User defined functions for beam-column member equilibrium secant method

```
Function Sct_dnL(D, t, L, fc, fy, e, um) As Double
Dim n As Integer, I As Integer
n = 20
I = 1
dn0 = 0
dn1 = 20 * D
  Do
    u0 = L / 1000
    Pi = 4 * Atn(1)
    phi = um * (Pi / L) ^ 2
    eo0 = phi * (dn0 - D / 2)
    eo1 = phi * (dn1 - D / 2)
    F0 = F_int(D, t, L, fc, fy, eo0, phi)
    f1 = F_int(D, t, L, fc, fy, eo1, phi)
    M_ext0 = F0 * (u0 + um + e) / 1000
```

```
        M_ext1 = f1 * (u0 + um + e) / 1000
        M0 = M_int(D, t, L, fc, fy, eo0, phi)
        M1 = M_int(D, t, L, fc, fy, eo1, phi)
        dM0 = M_ext0 - M0
        dM1 = M_ext1 - M1
        dn = dn1 - (dn1 - dn0) * dM1 / (dM1 - dM0)
        eo = phi * (dn - D / 2)
        f = F_int(D, t, L, fc, fy, eo, phi)
        M_ext = f * (u0 + um + e) / 1000
        M = M_int(D, t, L, fc, fy, eo, phi)
        dM = M_ext - M
        If Abs(dM) < 0.0001 Then
            Sct_dnL = dn
            Exit Function
        End If
        I = I + 1
        If dM < 0 Then
            dn0 = dn
            dn1 = dn1
        Else
        If dM > 0 Then
            dn0 = dn0
            dn1 = dn
        End If
        End If
    Loop Until I = n
    Sct_dnL = 0
End Function
```

APPENDIX C: Worked Example

Investigate the capacity of circular concrete filled steel tube column made of CHS 400 × 10, S460 steel with C40/50 concrete subjected to pure compression according to EC4 with effective lengths of:

a) 3m
b) 6m
c) 8m
d) 10m

And compare the results with the values from numerical model

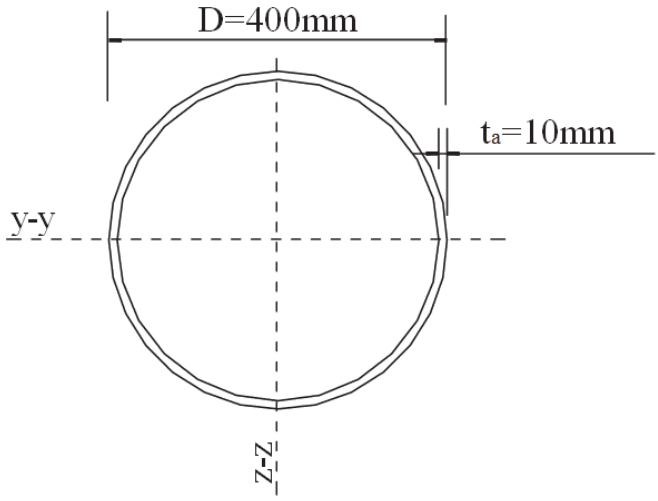

A. With 3m effective length

Material properties

Concrete

C40/50, $f_{ck} = 40\text{N/mm}^2$

$f_{cd} = f_{ck}/\gamma_c = 40/1.5 = 26.7\text{N/ mm}^2$

$f_{cm} = f_{ck} + 8 = 40 + 8 = 48\text{ N/ mm}^2$

$E_{cm} = 22\,(f_{cm}/10)^{0.3} = 22 \times (48/10)^{0.3} = 35.2\text{GPa}$

Steel tube

Grade S460, $f_y = 460\text{N/mm}^2$

$f_{yd} = f_y/\gamma_a = 460/1.1 = 418.2\text{N/ mm}^2$

E_a = 210GPa

Characteristics of the Cross section

Concrete core

$$A_c = (\pi/4)(D - 2t)^2 = (\pi/4)(400 - 2\times 10)^2 = 113{,}411.5\ \text{mm}^2$$

$$I_c = (\pi/64)(D - 2t)^4 = (\pi/64)\left(400 - 2\times 10\right)^4 \times 10^{-4} = 102{,}353.9\ \text{cm4}$$

$$W_{pc} = \frac{(D-2t)^3}{6} = \frac{(400-2\times 10)^3}{6} = 9145333.3\text{mm}^3$$

$$\text{h}_n = \frac{A_c f_{cd}}{2Df_{cd}+4t(2f_{yd}-f_{cd})} = \frac{113411.5\times 26.7}{2\times 400\times 26.7+4\times 10\times(2\times 418.2-26.7)} = 56.34mm$$

$$W_{pc,n} = (D-2t)\text{h}_n{}^2 = (400-2\times 10)\times 56.34^2 = 1206194.33\text{mm}^3$$

Steel tube

$$A_a = (\pi/4)[D^2 - (D - 2t)^2] = (\pi/4)[400^2 - (400 - 2\times 10)^2] = 12{,}252.2\ \text{mm}^2$$

$$I_a = (\pi/64)\left[D^4 - (D - 2t)^4\right] = (\pi/64)\left[400^4 - \left(400 - 2\times 10\right)^4\right]\times 10^{-4}$$

$$= 23{,}309.8\ \text{cm}^4$$

$$W_{pa} = \frac{D^3}{6} - W_{pc} = \frac{(400)^3}{6} - 9145333.3 = 1521333.4\text{mm}^3$$

$$W_{pa,n} = D\text{h}_n{}^2 - W_{pc,n} = 400\times 56.34^2 - 1206194.33 = 63483.9\text{mm}^3$$

Check for local buckling

$$D/t = 400/10 = 40 < 90\times 235/f_y = 90\times(235/460) = 45.98$$

Resistance against local buckling is adequate!

Characteristic plastic resistance of cross-section

$$N_{pl,Rk} = A_a f_y + A_c f_{ck} = (12252.2\times 460 + 113411.5\times 40)\times 10^{-3}$$

$$= 10{,}172.5\ \text{kN}$$

$$M_{pl,Rk} = (W_{pa} - W_{pa,n})f_y + 0.5(W_{pc} - W_{pc,n})f_{ck} = 670.6 + 317.6 = 988.2kNm$$

Design plastic resistance of cross-section

$$N_{pl,Rd} = A_a f_{yd} + A_c f_{cd} = (12252.2\times 418.2 + 113411.5\times 26.7)\times 10^{-3}$$

$$= 8{,}151.9\ \text{kN}$$

$$M_{pl,Rd} = (W_{pa} - W_{pa,n})f_{yd} + 0.5(W_{pc} - W_{pc,n})f_{cd} = 609.64 + 211.73 = 821.37kNm$$

Steel contribution ratio

$$0.2 < \delta = \frac{A_a f_{yd}}{N_{pl,Rd}} = 12252.2 \times 418.2 \times 10^{-3}/8{,}151.9 = 0.63 < 0.9$$

Effective flexural and axial stiffness of cross-section

$$(\mathrm{EI})_{eff} = E_a I_a + 0.6 E_{cm} I_c$$

$$= (210 \times 10^3 \times 23309.8 \times 10^4 + 0.6 \times 35.2 \times 10^3 \times 102353.9 \times 10^4) \times 10^{-3}$$

$$= 7.056 \times 10^{10} \mathrm{kNmm}^2$$

Elastic critical Euler buckling resistance

$$N_{cr} = \frac{\pi^2 (\mathrm{EI})_{eff}}{\mathrm{L}_{eff}{}^2} = \frac{\pi^2 \times 7.056 \times 10^{10}}{3000^2} = 77377.7\mathrm{kN}$$

Check for Long-term effect (creep and shrinkage)

$$\overline{\lambda} = \sqrt{\frac{N_{pl,Rk}}{N_{cr}}} = \sqrt{\frac{10{,}172.5}{77377.7}} = 0.36$$

$$\overline{\lambda}_{lim} = \frac{0.8}{1-\delta} = \frac{0.8}{1-0.63} = 2.16$$

Since $\overline{\lambda} < \overline{\lambda}_{lim}$ no need to take long-term effects to account

Confinement coefficients

Since the λ is less than 0.5 and the load eccentricity is equal to 0 (axially loaded column), the confinement effect may be considered for the circular CFST column.

$$\eta_a = \eta_{ao} = \min\left[0.25\left(3 + 2\overline{\lambda}\right), 1.0\right] = \min\left[0.93, 1.0\right] = 0.93$$

$$\eta_c = \eta_{co} = \max\left[4.9 - 18.5\overline{\lambda} + 17\overline{\lambda}^2, 0\right] = \max\left[0.44, 0\right] = 0.44$$

Design plastic resistance of cross-section

$$N_{pl,Rd} = \eta_a A_a f_{yd} + A_c f_{cd}\left(1 + \eta_c \frac{t}{D}\frac{f_y}{f_{ck}}\right)$$

$$= \left(0.93 \times 12252.2 \times 418.2 + 113411.5 \times 26.7 \times \left(1 + 0.44 \times \frac{10}{400} \times \frac{460}{40}\right)\right) \times 10^{-3}$$

$$= 8{,}176.34 \text{ kN}$$

Imperfection factor

The buckling curve is taken as "a" and thus the imperfection factor α is determined as 0.21 according to EC4.

Buckling reduction factor

$$\Phi = 0.5 \times \left[1 + \alpha\left(\overline{\lambda} - 0.2\right) + \overline{\lambda}^2\right] = 0.5 \times \left[1 + 0.21 \times \left(0.36 - 0.2\right) + 0.36^2\right]$$

$$= 0.582$$

$$\chi = \frac{1}{\Phi + \sqrt{\Phi^2 - \overline{\lambda}^2}} = \frac{1}{0.582 + \sqrt{0.582^2 - 0.36^2}} = 0.96$$

Buckling resistance

$$N_{b,Rk} = \chi N_{pl,Rk} = 0.96 \times 10{,}172.5 = 9765.6kN$$

$$N_{b,Rd} = \chi N_{pl,Rd} = 0.96 \times 8{,}176.34 = 7849.3\text{kN}$$

B. With 6m effective length

Elastic critical Euler buckling resistance

$$N_{cr} = \frac{\pi^2 (\text{EI})_{eff}}{\text{L}_{eff}{}^2} = \frac{\pi^2 \times 7.056 \times 10^{10}}{6000^2} = 19346.54\text{kN}$$

$$\overline{\lambda} = \sqrt{\frac{N_{pl,Rk}}{N_{cr}}} = \sqrt{\frac{10{,}172.5}{19346.54}} = 0.72$$

$$\overline{\lambda}_{lim} = \frac{0.8}{1 - \delta} = \frac{0.8}{1 - 0.63} = 2.16$$

Since $\overline{\lambda} < \overline{\lambda}_{lim}$ no need to take long-term effects to account and also for $\overline{\lambda}$ is greater than 0.5, the confinement effect will not be considered.

Imperfection factor

The buckling curve is taken as "a" and thus the imperfection factor α is determined as 0.21 according to EC4.

Buckling reduction factor

$$\Phi = 0.5 \times \left[1 + \alpha\left(\overline{\lambda} - 0.2\right) + \overline{\lambda}^2\right] = 0.5 \times \left[1 + 0.21 \times \left(0.72 - 0.2\right) + 0.72^2\right]$$

$$= 0.814$$

$$\chi = \frac{1}{\Phi + \sqrt{\Phi^2 - \overline{\lambda}^2}} = \frac{1}{0.814 + \sqrt{0.814^2 - 0.72^2}} = 0.84$$

Buckling resistance

$$N_{b,Rk} = \chi N_{pl,Rk} = 0.84 \times 10172.5 = 8544.9kN$$

$$N_{b,Rd} = \chi N_{pl,Rd} = 0.84 \times 8{,}151.9 = 6847.6\text{kN}$$

C. With 8m effective length

Elastic critical Euler buckling resistance

$$N_{cr} = \frac{\pi^2 (\text{EI})_{eff}}{\text{L}_{eff}{}^2} = \frac{\pi^2 \times 7.056 \times 10^{10}}{8000^2} = 10882.43\text{kN}$$

$$\overline{\lambda} = \sqrt{\frac{N_{pl,Rk}}{N_{cr}}} = \sqrt{\frac{10{,}172.5}{10882.43}} = 0.967$$

Since $\overline{\lambda} < \overline{\lambda}_{lim}$ no need to take long-term effects to account and also for $\overline{\lambda}$ is greater than 0.5, the confinement effect will not be considered.

Imperfection factor

The buckling curve is taken as "a" and thus the imperfection factor α is determined as 0.21 according to EC4.

Buckling reduction factor

$$\Phi = 0.5 \times \left[1 + \alpha\left(\overline{\lambda} - 0.2\right) + \overline{\lambda}^2\right] = 0.5 \times \left[1 + 0.21 \times \left(0.967 - 0.2\right) + 0.967^2\right]$$

$$= 1.05$$

$$\chi = \frac{1}{\Phi + \sqrt{\Phi^2 - \overline{\lambda}^2}} = \frac{1}{1.05 + \sqrt{1.05^2 - 0.967^2}} = 0.685$$

Buckling resistance

$$N_{b,Rk} = \chi N_{pl,Rk} = 0.685 \times 10172.5 = 6968.16kN$$

$$N_{b,Rd} = \chi N_{pl,Rd} = 0.685 \times 8{,}151.9 = 5584.05\text{kN}$$

D. With 10m effective length

Elastic critical Euler buckling resistance

$$N_{cr} = \frac{\pi^2 (\text{EI})_{eff}}{\text{L}_{eff}{}^2} = \frac{\pi^2 \times 7.056 \times 10^{10}}{10000^2} = 6964.76\text{kN}$$

$$\overline{\lambda} = \sqrt{\frac{N_{pl,Rk}}{N_{cr}}} = \sqrt{\frac{10{,}172.5}{6964.76}} = 1.21$$

Since $\overline{\lambda} < \overline{\lambda}_{lim}$ no need to take long-term effects to account and also for $\overline{\lambda}$ is greater than 0.5, the confinement effect will not be considered.

Imperfection factor

The buckling curve is taken as "a" and thus the imperfection factor α is determined as 0.21 according to EC4.

Buckling reduction factor

$$\Phi = 0.5 \times \left[1 + \alpha\left(\overline{\lambda} - 0.2\right) + \overline{\lambda}^2\right] = 0.5 \times \left[1 + 0.21 \times \left(1.21 - 0.2\right) + 1.21^2\right]$$

$$= 1.34$$

$$\chi = \frac{1}{\Phi + \sqrt{\Phi^2 - \overline{\lambda}^2}} = \frac{1}{1.34 + \sqrt{1.34^2 - 1.21^2}} = 0.522$$

Buckling resistance

$$N_{b,Rk} = \chi N_{pl,Rk} = 0.522 \times 10172.5 = 5310.045kN$$

$$N_{b,Rd} = \chi N_{pl,Rd} = 0.522 \times 8{,}151.9 = 4255.29\text{kN}$$

Comparison with the developed numerical tool results

Cross section capacity

$$\mathrm{P_{Num}}/N_{pl,Rk} = 14098.7/10172.5 = 1.38$$

$$\mathrm{M_{Num}}/M_{pl,Rk} = 940/988.2 = 0.95$$

Member buckling capacity

Length (m)	$N_{b,Rk}$ (kN)	$\mathrm{P_{Num}}$ (kN)	$\mathrm{P_{Num}}/N_{b,Rk}$
3	9765.6	12412.66	1.27
6	8544.9	8647.063	1.012
8	6968.16	7021.247	1.008
10	5310.045	5369.578	1.011

It is visible from the analysis that the confinement effect was more significant in short columns than slender ones as values from numerical results include confinement effects.